This file is part of the following work:

Hoogenboom, Mia O. (2008) *Physiological models of performance for scleractinian corals.* **PhD Thesis, James Cook University.**

Access to this file is available from:

https://doi.org/10.25903/evq8%2Db235

Physiological models of performance

for scleractinian corals

Mia Odell Hoogenboom

September 2008

For the degree of Doctor of Philosophy
in the School of Marine and Tropical Biology
James Cook University

STATEMENT OF ACCESS

I, the undersigned, the author of this thesis, understand that James Cook University will make this thesis available for use within the University Library and via the Australian Digital Theses network (unless granted any exemption) for use elsewhere.

I understand that, as an unpublished work, a thesis has significant protection under the Copyright Act and;

I wish this work to be embargoed until September 2009.

_____   <u>04-09-2008</u>
Signature   Date

ELECTRONIC COPY OF THESIS

I, the undersigned, the author of this work, declare that the electronic copy of this thesis provided to the James Cook University Library is an accurate copy of the print thesis submitted, within the limits of the technology available.

_____ 04-09-2008

Signature   Date

STATEMENT OF SOURCES

I declare that this thesis is my own work and has not been submitted in any other form for another degree or diploma at any university or other institution of tertiary education. Information derived from the published or unpublished work of others has been acknowledged in the text and a list of references is given.

_____   04-09-2008
Signature   Date

ACKNOWLEDGEMENTS

respirometry chambers. I would also like to thank Claudia and Greg for various equipment loans, and Bette Willis for letting me take up so much space in her lab. Finally, thanks to Wayne Mallet and the staff of JCU's High Performance Computing team for providing an excellent platform.

I am very grateful to all of the people who have been members of the Theoretical Ecology Lab over the years. Thankyou to Maria, Ailsa, Matt, Loic and Andrew for their honest and constructive feedback on all aspects of my research. Also, thanks to Maria for being the best office-mate ever!

To my partner Duncan, thank you for your tireless support and encouragement, and for being there for me through the ups and downs of my project. Finally, to Mum and Dad, thank you for always believing in me, and for giving me every opportunity to reach my goals.

TABLE OF CONTENTS

LIST OF FIGURES

Chapter 5

LIST OF TABLES

ABSTRACT

A fundamental objective of ecology is to evaluate the conditions that permit different species to survive and reproduce, that is, to identify each species' 'niche'. The overarching aim of this thesis was to identify and quantify the primary processes that influence the distribution and abundance of reef-building, scleractinian corals. My general approach was to develop and calibrate process-based models that link physiology to environmental conditions, and quantify ecological performance as a function of physiology.

Light intensity is a fundamental determinant of coral performance. For several photosynthetic taxa exposure to high light levels causes a decline in daily carbon gain. In this thesis I first investigated whether this phenomenon (i.e. photoinhibition) had energetic consequences for coral symbioses. Surprisingly, results demonstrated that costs of photoinhibition are negligible under short-term exposure to high irradiance (Chapter 2). I subsequently investigated whether costs of photoinhibition manifest over a longer time-period due to changes in the photosynthetic apparatus that arise during photoacclimation to high light intensities (Chapter 3). Analyses revealed that repeated exposure to high light intensity causes changes in the photosynthetic machinery such that high-light habitats do not provide maximal energy acquisition. In fact, I found evidence of a strong reduction in energy available for growth and reproduction for corals growing under high light.

Corals potentially avoid costs of excessive light exposure by altering colony morphology. Previously, no framework has been available that allowed comparison of energy acquisition for multiple, complex coral morphologies, in response to varying light conditions, while taking into account the flexibility in coral photophysiology. Using a novel, three-dimensional geometric model of light capture

in combination with a comprehensive photosynthesis dataset, in Chapter 4 I demonstrate that morphological plasticity maximizes the amount of energy corals have available for growth and reproduction. In addition, results showed that variation in morphology is most important at niche boundaries whereas physiological flexibility is important in intermediate habitats.

In addition to light intensity, water flow velocity varies markedly between reef habitats and has a strong influence on coral metabolism. In this thesis, I built on existing models of gas exchange to incorporate the effects of light intensity, flow velocity and colony size into a single model (Chapter 5). Analysis of this model showed that the branching coral *Acropora nasuta* has a positive energy balance over a wider range of conditions than both a massive (*Leptoria phrygia*) and a foliose species (*Montipora foliosa*). Moreover, colony size was revealed as having a strong influence on niche width: large colonies of all three species had a positive energy balance over a broader range of conditions than small colonies.

The overarching aim of my thesis was to evaluate the performance of corals in response to environmental gradients. This work quantifies the mechanisms through which light and flow influence coral physiology. Model predictions were strongly correlated with observed tissue biomass and reproductive output. In addition, an optimality model based on morphology-specific energy acquisition as a function of the ambient light-regime, adequately captured observed variation in colony shape across a depth gradient. Overall, this thesis provides new insight into the processes underlying the habitat distributions of reef-building corals, achieved by quantifying environmental effects on physiology and integrating these effects into an energy-budget framework.

1   GENERAL INTRODUCTION

A fundamental objective of ecology is to identify the conditions that permit survival of different species, that is, to identify each species' 'niche'. Although the term niche carries many different meanings (e.g. Whittaker et al. 1973; Pulliam 2000), the 'fundamental niche' is conventionally defined as the range of conditions under which an organism can survive and reproduce in the absence of biotic interactions (e.g. Hutchinson 1957). Over time, methods for measuring the niche have evolved from a conceptual 'hypervolume' (Hutchinson 1957), to the use of statistical methods to identify correlates of species occurrence (e.g. Austin et al. 1990; Wright et al. 2006). An alternative approach is to describe the niche based on the processes that determine how organisms perform under specific environmental conditions (e.g. Kearney & Porter 2004). In turn, quantifying how the environment influences organism performance allows insight into the processes that influence population demography and species' distribution and abundance.

Coral reefs are spatially very complex habitats. Typically, reef environments are divided into several zones (Figure 1.1) across which the physical environment varies markedly. In general, the reef crest is the habitat with the highest energy characterised by high light intensity and strong wave activity (e.g. Veron 2000). Moving away from the crest, either toward lagoon habitats or into deeper water, water flow generally declines (e.g. Helmuth et al. 1997a). Light intensity also declines with depth below the water surface (Mobley 1994), and depth-related changes in light spectrum (e.g. Dustan 1982) together with crevices and overhangs in the reef matrix further enhance spatial variation in light availability (e.g. Anthony & Hoegh-Guldberg 2003a). The net result of these changes is the creation of a complex mosaic of habitats with very different physical environments.

In concert with changes in the physical environment, the composition of the coral community varies between zones (e.g. Done 1982; Torruco et al. 2003). Generally, upper reef slopes have the highest species diversity (e.g. DeVantier et al. 2006; Karlson et al. 2004), and are dominated by branching corals from the genus *Acropora* (Done 1982; Veron 2000). In habitats with lower wave exposure, staghorn *Acropora* become more abundant, together with massive and/or branching corals from the genera *Porites* and *Galaxea* (Done 1982). On reef flats, mound-shaped corals from the family Faviidae are generally most abundant, whereas *Goniopora* (Poritiidae) and *Turbinaria* (Dendrophyllidae) tend to dominate under conditions of high turbidity (Veron 2000). Finally, foliose or laminar species such as *Montipora*, *Pachyseris* and *Leptoseris* are most abundant in deep waters.
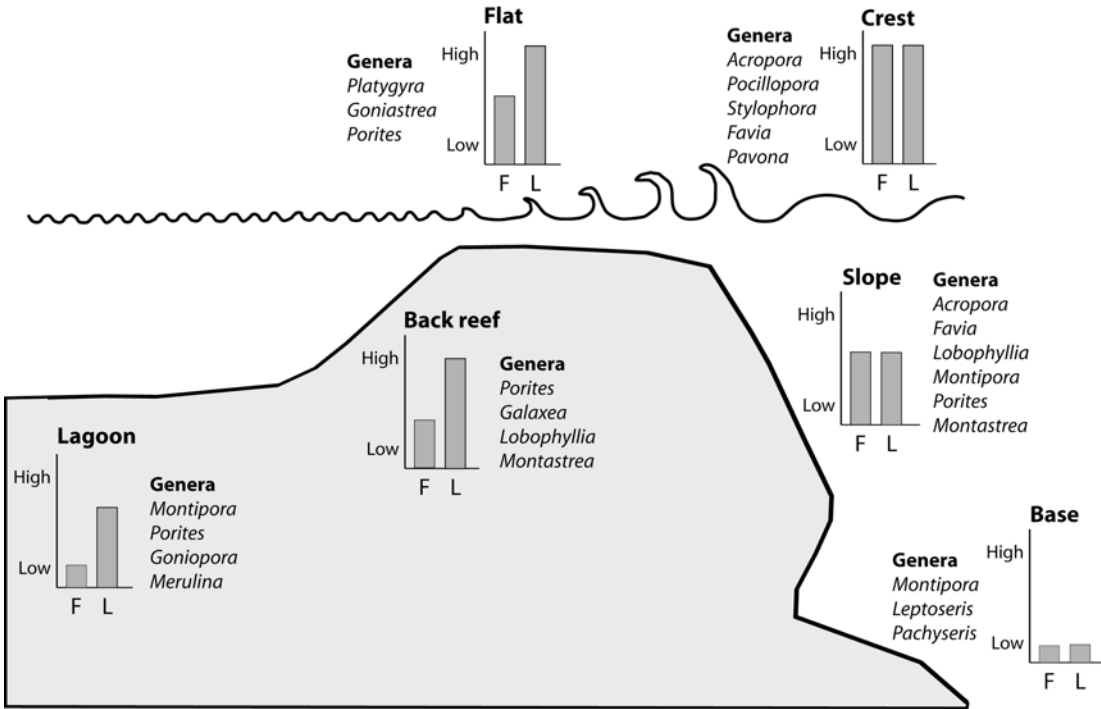
Figure 1.1: Environmental conditions and distribution of key coral genera across a reef. Physical environmental parameters, such as water flow (F) and light intensity (L), vary between lagoonal habitats, reef crests and the reef base. The composition of the coral community also varies strongly across this gradient. Genus distributions are taken from habitat data in Veron (2000).

In addition to changes in community composition, many coral species show distinct variation in colony morphology in response to environmental variation (i.e. phenotypic plasticity, Bradshaw 1965). For corals, several morphological characteristics may vary, including corallite structure (Foster 1979; Bruno & Edmunds 1997; Todd et al 2004), branch density and thickness (Helmuth et al. 1997b; Bruno & Edmunds 1998), budding of sub-branches (Oliver et al. 1983; Muko et al. 2000), or the direction of colony growth (Dustan 1975; Willis 1985). Although corals vary greatly in overall colony architecture, plasticity generally results in an increase in colony 'openness' with depth (e.g. wider spaced branches or a more horizontal growth direction). The consensus view in the literature is that such variation in colony morphology is correlated with gradients of light intensity and water flow velocity (e.g. Graus & McIntyre 1982; Bruno & Edmunds 1997, 1998).

The physical environment influences the habitat distributions of all corals, and the expression of colony morphology for particular species (e.g. Connell 1973). Previous studies have generally used experiments and/or field observations to quantify how particular environmental variables influence different species (e.g. Hughes & Jackson 1985; Sebens et al. 2003). One limitation of this approach is that, although it allows enumeration of species-specific effects, it does not provide insight into the underlying mechanisms driving such effects. Without an understanding of why particular species respond in the ways observed, empirical measurements cannot be reliably translated into general predictions about environmental effects on coral performance. An alternative approach that circumvents this limitation is to explore species' habitat distributions using mechanistic models derived from physiological first principles. That is, using models that link ecological performance to physiology, and relate physiology to environmental conditions. Mechanistic approaches to niche studies are beneficial because they explicitly identify drivers of species'

distributions, and allow greater confidence when extrapolating niche properties to conditions not included in multivariate datasets (Pulliam 2000; Kearney 2006). Therefore, the overarching aim of my thesis research was to develop and calibrate process-based models that express coral performance as an explicit function of environmental conditions. In this work I focus on quantifying variation along environmental gradients that might typically be observed on coral reefs.

In this chapter I review the literature describing how environmental conditions influence the performance of scleractinian corals. Firstly, I discuss the importance of physiology and energy balance in determining the threshold conditions for species survival (Section 1.1). Secondly, I give a brief synopsis of documented patterns of within- and between-species variation in several measures of coral performance (growth, tissue composition and reproductive output, Section 1.2). Third, I identify the dominant environmental gradients on coral reefs (Section 1.3) and summarize how these gradients influence coral physiology and energy balance (Section 1.4). Subsequently, I discuss the role of colony morphology in mediating how the environment influences coral performance (Section 1.5). Finally, I identify key unresolved questions that form the basis of my thesis (Section 1.6).

1.1 Energetics and the niche

The functional response of physiological energetics to environmental variables is a fundamental determinant of organism performance and niche characteristics for all species. Essentially, survival under a particular set of environmental conditions requires, at a minimum, sufficient energy uptake to meet cellular maintenance costs (Leibold 1995; Kooijman 2000; Kearney 2006). Therefore, at its most basic level, the niche may be described by identifying thresholds along environmental gradients above which a positive energy balance is

possible (e.g. Anthony & Connolly 2004). Above these environmental thresholds –

that is, within the niche – variation in energy balance may drive variation in rates of

growth and reproduction. A greater energy surplus (i.e. energy remaining once

maintenance costs have been accounted for), may translate to more rapid growth, or

to greater reproductive output (e.g. Kooijman 2000). For corals, the importance of

energy balance as a determinant of performance is confirmed by strong evidence of

trade-offs in energy allocation. Reproduction reduces growth for several species

(Kojis and Quinn 1981, 1985; Heyward & Collins 1985; Ward 1995a), and tissue

damage leads to reduced growth and/or reproduction (Kojis & Quinn 1985; van

Veghel & Bak 1994; Zakai et al. 2000; Oren et al. 2001). Patterns of energy

allocation have important implications for the capacity of a species to colonise new

habitats, for a species' competitive ability, or, finally, for a species' ability to tolerate

conditions of stress. However, maximising any one of these processes is contingent

upon having an energy surplus. Understanding how energy balance varies along

environmental gradients provides a useful framework for defining the niche, and for

quantifying and comparing the relative performance of different species.

1.2   Performance of corals: variation within- and between-species

Scleractinian corals display pronounced life-history variation (e.g. Jackson

1979; Veron 2000). Not only are there marked differences in polyp and colony

morphology between species, these differences have implications for colony growth,

tissue biomass, and reproductive output. In the following section I summarise inter-

specific variation in growth, tissue composition and reproduction, and discuss how

environmental conditions influence these processes.

1.2.1   Colony growth

For corals, colony morphology is correlated with growth rates. On average, branching and foliose corals grow 5 and 3 times faster, respectively, than massive corals (linear or radial extension, Table 1.1). In addition to effects of morphology, coral growth rates generally decrease with depth below the water surface (Guzman & Cortes 1989; Custodio & Yap 1997). However, these effects are often weak (Gladefelter et al. 1978; Hughes & Jackson 1985), and there is no clear evidence as to which environmental variable is the major driver of these patterns. For example, Gladefelter et al (1978) found that water temperature had a measurable influence on colony growth, but only for 2 of 5 species investigated. Guzman & Cortes (1989) demonstrated seasonal effects on growth of 2 coral species and hypothesised that some combination of rainfall, salinity, temperature, sunlight and particulate matter concentration was responsible for this effect.

In summary, experiments and field observations indicate that environmental conditions influence how rapidly colonies of some coral species are able to grow. However, empirical approaches have had limited success in identifying why particular conditions influence some species but not others. Answering this question requires a framework that characterises what it is that causes species to respond in certain ways. Process-based models are one such framework that can be used to establish a mechanistic link between coral performance and environmental gradients, potentially enabling a better understanding of variation in colony growth.

1.2.2   Tissue composition

As a general rule, branching corals such as *Acropora*, *Montipora* and *Pocillopora* have low tissue mass (2-10 mg cm^{-2}, Davies 1984; Leuzinger et al. 2003) compared to that of massive corals from the families Mussidae, Faviidae and

Table 1.1: Growth rates of scleractinian corals, measured as linear/radial extension

Branching		Irregular branching/Foliose		Massive	
Species	**Growth (cm y^{-1})**	**Species**	**Growth (cm y^{-1})**	**Species**	**Growth (cm y^{-1})**
Acropora formosa[1]	15.5	*Hydnophora rigida*[1]	7.1	*Cyphastrea serailia*[2]	0.3
A. pulchra[1]	18.1	*Montipora foliosa*[1]	3.3	*Favia pallida*[2]	0.3
A. yongei[2]	4.9	*M. undata*[1]	2.6	*Gardineroseris planulata*[6]	1.0
A. hyacinthus[3]	4.3	*Pocillopora verrucosa*[4]	3.7	*Goniastrea australiensis*[2]	0.3
A.brueggemanni[1]	7.5	*P. verrucosa*[3]	2.5	*Montastrea curta*[2]	0.3
A. cerealis[4]	4.7	*Pocillopora damicornis*[4]	2.6	*Pavona clavus*[6]	1.0
A. cytherea[3]	5.8	*P. damicornis*[6]	3.5	*P. minuta*[7]	1.0-1.4
A.divaricata[3]	4.2	*P.damicornis*[2]	1.6	*P. varians*[6]	0.4
A. humilis[3]	1.9	*P.damicornis*[6]	3.0	*Porites heronensis*[2]	1.1
A. nasuta[4]	4.8			*P. lichen*[3]	1.6
Montipora digitata[5]	3.1			*P. lobata*[6]	1.2
Seriatopora hystrix[4]	2.2			*P. lobata*[3],[7]	1.2-1.5
S. hystrix[2]	1.7			*P. lutea*[3]	1.1
S. hystrix[1]	3.8			*P. nigrescens*[3]	1.8
Stylophora pistillata[1]	3.5			*Psammocora superficialis*[6]	0.6

References: (1) Gomez et al. 1985, (2) Harriott 1999, (3) Clark & Edwards 1995, (4) Stimson 1985, (5) Heyward & Collins 1985, (6) Guzman & Cortes 1989, (7) Glynn et al. 1996.

Poritidae (approximately 20 mg cm^{-2}, Edmunds & Davies 1986; Leuzinger et al. 2003; Rodrigues & Grotolli 2007). For most species, lipids make up the greatest proportion of tissue, accounting for up to 75% of biomass (Figure 1.2). Proteins are the second largest component of tissue mass (36% on average) while carbohydrates contribute only a small proportion of tissue mass (averaging 6%, Figure 1.2).

For some coral species, seasonal fluctuations in lipid and protein have been documented. Lipid concentrations may vary 2-fold over the year (Stimson 1987), and there is evidence for one species that total lipid content is correlated with light intensity and water temperature (*Goniastrea aspera*, Oku et al 2003). For other corals, lipid composition varies with proximity to the coast, with higher lipid content observed in inshore environments (Anthony 2006). Protein content also varies seasonally (Fitt et al. 2000), and changes in temperature and water clarity have been implicated as the environmental drivers of these patterns for temperate corals (Rossi & Tsounis 2007).

Investigations of variation in tissue composition have generally focused on differences between species (e.g. Leuzinger et al. 2003). Where the effects of

environmental gradients on variation in tissue quality within species have been

studied, results have generally been species-specific. This indicates that experimental

approaches have limited capacity to identify general trends underlying variation in

coral tissue quality. In contrast, process-based models provide a framework to link

species performance to environmental conditions, and to project how species may

respond under varying environmental predictions and forecasts.
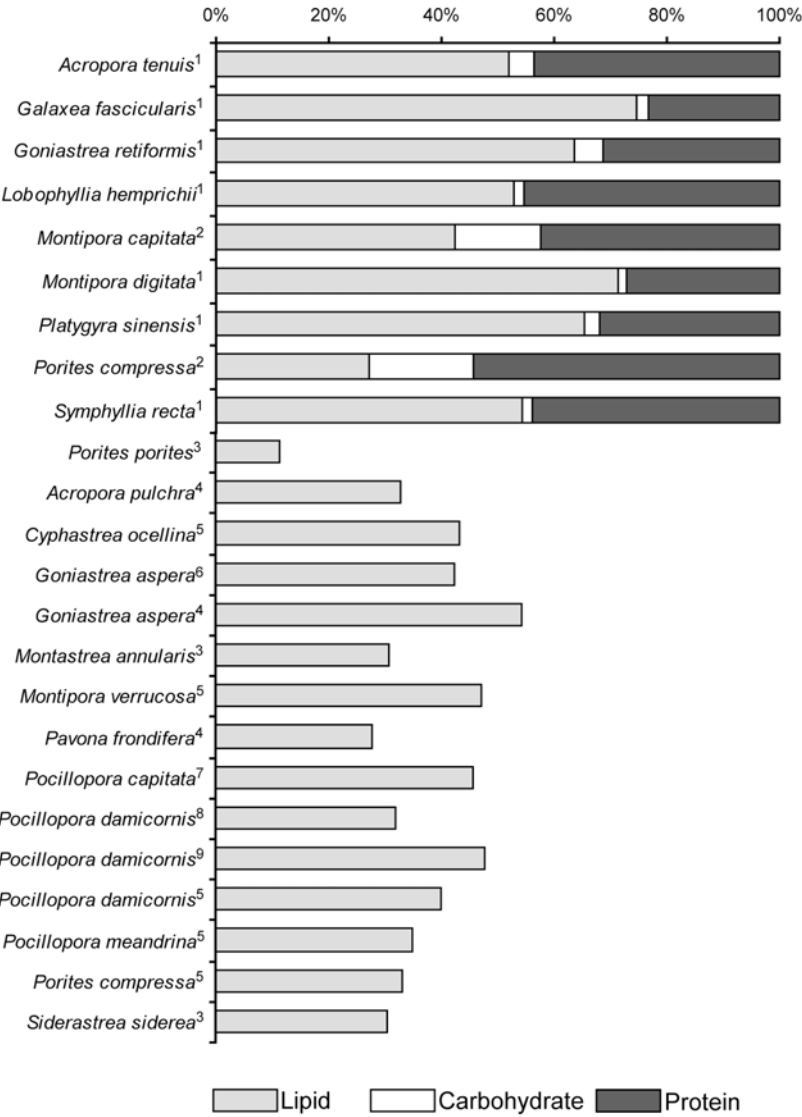
Figure 1.2: Tissue composition of scleractinian corals. Bars represent the proportion of total tissue biomass that is composed of lipids, carbohydrates and proteins. Numbers refer to: 1) Leuzinger et al. 2003, 2) Rodrigues & Grottoli 2007, 3) Harland et al. 1992, 4) Bachok et al. 2006, 5) Stimson 1987, 6) Oku et al. 2003, 7) Patton et al. 1977, 8) Ward 1995b 9) Ward 1995a.

1.2.3 Reproductive output

Reef-building corals display a diversity of reproductive modes, with sexual reproduction occurring through the release of externally fertilised eggs and/or brooded larvae (reviewed by Fadallah 1983). For broadcast-spawning corals, the size of eggs and the number of eggs produced per polyp varies greatly between species (Table 1.2). In addition, differences in polyp density mean that reproductive output per unit area varies more than 30-fold between species (e.g. 100 – 200 cm^{-2} for *Acropora* c.f. 4000 cm^{-2} for *Porites*, Table 1.2).

In light of the observed trade-off between coral growth and reproduction (e.g. Heyward & Collins 1985; Ward 1995a), an increase in reproductive output may be expected to accompany general declines in growth with water depth. However, data for *Montastrea faveolata* in the Caribbean indicates that reproduction is consistent across depths (Villinski 2003). Work by Wallace (1985) also suggests that depth has negligible effects on reproduction in several species from the genus *Acropora*. To identify the processes that drive these patterns, we must first understand how environmental conditions vary between reef habitats, and how variation in the environment influences energy balance. These questions are the focus of the remainder of this chapter.

1.3 Environmental variation on coral reefs

Light intensity and water flow velocity are key environmental gradients that vary between coral reef habitats (Denny 1988; Kirk 1994). In shallow habitats, maximum light intensities can be in excess of 2000 μmol photons m^{-2} s^{-1} (Kirk 1994; Jones & Hoegh-Guldberg 2001). Moving into deeper waters, light intensity decreases exponentially (e.g. Falkowski & Raven 1997), at a rate that is dependent upon the concentration of particulate matter in the water column (e.g. Mobley 1994).

Table 1.2: Reproductive output of scleractinian corals.

Species	Egg size (μm)	Egg number
Acropora aspera	300-350[1]	10-15[1p]
Acropora cytherea	558[2], 749[3]	4.5[2p]
Acropora digitifera	600-700[4]	-
Acropora florida	584[5]	6-14[5p], 209[10a]
Acropora formosa	558[2]	-
Acropora gemmifera	517-620[6]	4.5-6.4[6p]
Acropora granulosa	534[5]	12.8[5p], 116[10a]
Acropora humilis	395[7], 714[3]	27[7p], 7.3[3p]
Acropora hyacinthus	622[5], 553[8], 375[7]	6.1[5p], 4.5-6.4[6p], 20[7p]
Acropora cuneata	325[7], 255[9], 1462[10]	4-12[7p]
Acropora palifera	325[7], 249[9], 1020-1450[10]	4-12[7p], 4-7[17p]
Acropora longicyathus	591[5]	11.7[5p], 190[10a]
Acropora loripes	560[5]	11.8[5p], 156[10a]
Acropora microphthalma	502[2]	-
Acropora millepora	541[8]	4.5-6.4[6p]
Acropora nana	517-620[6]	4.5-6.4[6p]
Acropora nobilis	571[5]	7.7[5p], 261[10a]
Acropora sarmentosa	652[5]	10.2[5p], 169[10a]
Acropora valida	633[5], 643[3]	5.6[5p], 7.3[3p]
Cyphastrea microphthalma	290[7]	105[7p]
Favia favus	395[7], 500[10]	700[7p], 764[10a]
Favia pallida	343[2]	-
Favites abdita	363-424[11]	-
Favites halicora	401[8]	-
Favites pentagona	240[7]	355[7p]
Galaxea fasicularis	395[7], 389[2]	2160[7p]
Goniastrea aspera	350[7], 360[12], 340[2]	200-350[12p], 935[10a]
Goniastrea australiensis	430-530[11]	-
Goniastrea favulus	510[7], 420[12], 430[10]	53-148[12p], 368[10a]
Goniastrea reniformis	371[8], 315[7]	600[7p], 46[6p]
Leptoria phrygia	391-440[11]	-
Lobophyllia corymbosa	600[7], 750[10]	2800[7p], 178[10a]
Lobophyllia hemprichii	290[7]	2450[7p]
Merulina ampliata	214[13]	166[13p]
Montipora digitata	337[8], 410[10], 383[14], 312[2]	250[10a]
Pavona varians	50[7], 105[15]	18[7p], 161[15]
Platygyra sinensis	405[12]	46-104[12p], 350[10a]
Pocillopora damicornis	30-100[7]	18-24[7p]
Pocillopora eydouxi	136[14], 148[16]	144[16p]
Pocillopora meandrina	30[7]	108-120[7p]
Pocillopora verrucosa	130-150[7], 128-147[16]	360-540[7p]
Porites australiensis	150[7]	72[7p], 1146[10a]
Porites lobata	120-170[7]	36-75[7p], 4000[10a]
Porites lutea	160 – 180[7]	60-72[7p], 1146[10a]
Symphyllia recta	240-415[11]	-
Turbinaria mesenterina	353[10]	1452[10a]

Notes: subscript p and a in citations for egg number refer to eggs per polyp (p) and eggs per unit surface area(a). Sizes of planulae are underlined to differentiate from egg sizes.

References: (1) Ward & Harrison 2000, (2) Heyward et al. 1987, (3) Kenyon 1992, (4) Gilmour 1999, (5) Wallace 1985, (6) Hall & Hughes 1996, (7) Shlesinger et al. 1998, (8) Baird et al 2001, (9) Kojis 1986, (10) Harrison & Wallace 1990, (11) Fadallah 1983, (12) Glynn et al. 1996, (13) Fan & Dai 1998, (14) Hirose et al. 2001, (15) Glynn et al. 2000, (16) Kinzie 1993, (17) Kojis & Quinn 1984.

On reefs, a decline in water flow is also generally observed as depth increases, with flow velocities typically ranging from approximately 30 to 50 cm s^{-1} at exposed reef crests to 5cm s^{-1} in deep waters (Sebens & Johnson 1991; Helmuth et al. 1997a; Fulton & Bellwood 2005). In addition, water flow is reduced in lagoon and back-reef habitats (e.g. Helmuth et al. 1997a; Fulton & Bellwood 2005). This means that, when considering the performance of corals across a range of reef habitats, light intensity and water flow do not necessarily co-vary in a consistent fashion. Instead, all combinations of light and flow conditions may be observed.

In addition to light and flow, other physical factors vary within reefs. Water temperature and sedimentation are two additional environmental variables that are known to influence coral physiology (e.g. Edmunds 2005; Anthony 2006). Both of these variables may be influenced by depth: settlement of sediment increases with depth during certain weather conditions (Wolanski et al. 2005), and temperature generally decreases over a depth range of 30 to 50 m (e.g. Leichter et al. 1996; Bak et al. 2005). However, sedimentation and temperature appear to vary more strongly within than between locations on a reef, and generally show greater variation at spatial scales larger than within reefs (e.g. along an inshore to offshore gradient). For example, Anthony & Fabricius (2000) reported a difference in particle concentration of 12% between reef-flat and reef-slope habitats, while Larcombe et al. (1995) reported 20-fold differences in sediment loads between inshore and offshore reefs. With respect to temperature, Baird & Marshall (2002) reported a maximum temperature difference of approximately 0.5ºC between sites on the windward and leeward sides of adjacent islands, compared with a fluctuation of 4.0ºC over a 3-month time period. Similarly, Leichter et al. (2006) reported a maximum difference of approximately 1.3ºC in mean annual temperature between 6 sites in the Caribbean, compared to a range within sites of 5 - 10ºC over the year. The high variability of

temperature and sedimentation within sites, and the small magnitude of the differences between sites, suggests that these factors are unlikely to be the primary drivers of variation in coral performance within reefs.

My thesis research focuses on light intensity and water flow as the key drivers of spatial variation in performance of different coral species. Both of these factors vary strongly within reefs. In addition, light and flow have a fundamental, and potentially very strong, influence on energy acquisition of corals. As discussed in the following section, light influences energy balance through its effect on photosynthesis and photoinhibition, and flow via its effects on both photosynthesis and respiration together with delivery of particles for heterotrophic feeding (Falkowski & Raven 1997; Denny 1998; Sebens et al. 1998).

1.4   Influence of light and flow on coral energetics

Reef-building corals acquire the majority of their energy (carbon) through photosynthesis of their symbiotic dinoflagellates (Muscatine & Porter 1977; Muscatine et al. 1981). Therefore, light intensity is a fundamental determinant of energy acquisition for corals. Not only do rates of photosynthesis vary in response to changes in light intensity over diurnal cycles, the overall capacity for photosynthesis also differs according to the light levels under which corals are grown (i.e. photoacclimation, Chalker et al. 1983; Falkowski & Raven 1997).

In general, maximum rates of photosynthesis occur at high light intensities. However, exposure to excessive light results in impairment of the photosynthetic apparatus, or a reduction in the efficiency with which absorbed light is utilized for photosynthesis (i.e. photoinhibition, Long et al. 1994). For plants and phytoplankton, such effects cause photosynthesis to decline at very high light levels, and this translates into lower energy acquisition (Platt et al. 1980; Ogren and Sjostrom 1990;

Pahl-Wostl 1992). There has been considerable conjecture about the potential for costs of excessive light exposure to influence the depth distributions of corals (e.g. Connell 1973; Oliver et al. 1983; Muko et al. 2000). However, whether such costs are sufficiently large to exclude species from shallow habitats has not been resolved.

A review of data available in the literature suggests that daily carbon acquisition per unit colony surface area varies by an order or magnitude between species (Table 1.3). However, there is also evidence of order of magnitude variation within species, depending upon the conditions under which colonies are grown (e.g. *Stylophora pistillata*, Table 1.3). Such high within-species variability means that it is not possible to discern the true differences between species. Moreover, daily maintenance costs (measured as baseline rates of respiration), vary up to 3-fold within species (Table 1.3). The net result of this is that ratios of carbon acquired through photosynthesis to carbon used in maintenance metabolism (P:R ratio) range from less than 1 (energy deficit) to more than 8 (substantial energy surplus). In other words, there appears to be substantial variation in the energy that coral colonies have available for growth and reproduction. Nevertheless, from literature data alone, it is not possible to quantify the relative contributions that environmental effects, versus species identity, make to differences in energy balance.

There is little consensus in the literature as to how energy acquisition of different coral species varies along environmental gradients. For some species, a consistent level of productivity has been observed across a depth range (Titlyanov 1991a). In other studies, an energy deficit in deep water was associated with limited light availability (Muscatine et al. 1981, 1984; Mass et al. 2007). Given the obvious changes in light availability with depth, and between coastal and oceanic environments, on coral reefs, it is remarkable that some corals maintain equivalent energy acquisition in all habitats. For coral symbioses, as for other photosynthetic

organisms, there is considerable flexibility in the arrangement of the photosynthetic machinery of symbionts (e.g. Iglesias-Prieto & Trench 1994). It is generally thought that adjusting the photosynthetic machinery to suit local light conditions (i.e. 'photoacclimation', Falkowski & Raven 1997) maximises energy acquisition. Several studies have quantified variation in properties of the photosynthetic apparatus in response to changes in the light intensity under which corals are grown (e.g. Chalker et al. 1983; Anthony & Hoegh-Guldberg 2003b). However, precisely how these changes affect energy balance, and how well adjustment of photophysiology compensates for changes in light availability, remains unknown. Understanding how different processes of photoacclimation interact to influence photosynthesis under a specific light regime is critical to defining the range of light conditions under which survival, growth and reproduction of particular coral species is possible.

Water flow also affects rates of photosynthesis, via its influence on the exchange of photosynthetic gases. Generally, both carbon fixation and maintenance metabolism increase with flow (Patterson et al. 1991; Reidenbach et al. 2006). However, there is also evidence that changes in flow have negligible effects on net photosynthesis (Sebens et al. 2003), or that both photosynthesis and respiration are equally affected such that the net effect of varying flow on energy balance is negligible (Rex et al. 1995). Furthermore, there is some indication that adjustment of biochemistry in response to water flow (akin to photoacclimation) may mediate the influence of flow variation on colony energetics (Lesser et al. 1994). Overall, there is little consensus in the literature as to how flow influences the performance of coral colonies. In addition, it is unclear how flow interacts with light to determine energy balance of different coral species in particular habitats. Understanding how and why performance of different coral species varies across reef habitats, requires knowledge

of the processes through which light and flow interact to influence physiology and

energy balance.

Table 1.3: Summary of literature estimates of daily carbon acquisition from symbiont photosynthesis for scleractinian corals.

Species	P (μg C cm^{-2} d^{-1})	R (μg C cm^{-2} d^{-1})	P:R	Conditions
Acropora cervicornis[1]	250	-	-	1m
Acropora cervicornis[1]	374	-	-	10m
Acropora palmata[2]	780	820.8	1.0	
Acropora palmata[1]	672	-	-	1m
Acropora palmata[1]	350	-	-	10m
Acropora pulchra[3]	226	-	-	Nitrogen enrichment.
Acropora sp.[4]	256	123	2.1	
Agaricia agaricites[1]	404	-	-	1m
Agaricia agaricites[1]	288	-	-	10m
Agaricia tenuifolia[5]	209	-	-	Water flow varied.
Goniastrea retiformis[6]	1001	564	1.8	Sediment & shading.
Montastrea annularis[7]	410	203	2.0	
Montastrea annularis[1]	595	-	-	1m
Montastrea annularis[1]	513	-	-	10m
Montastrea cavernosa[1]	261	-	-	1m
Montastrea cavernosa[1]	225	-	-	10m
Montastrea cavernosa[8]	253	65	3.9	
Montastrea faveolata[8]	448	129	3.5	
Montipora capitata[9]	454	138	3.3	
Montipora monasteriata[10]	912	264	3.5	
Montipora verrucosa[11]	262	242	1.1	'ideal day'
Pocillopora eydouxi[12]	375	111	1.7	
Pocillopora damicornis[11]	169	189	0.9	'ideal day'
Pocillopora verrucosa[13]	191	-	-	
Porites astreioides[1]	437	-	-	1m
Porites astreioides[1]	382	-	-	10m
Porites compressa[9]	1257	415	3.0	
Porites cylindrica[6]	1028	442	2.3	Sediment & shading.
Porites lobata[11]	195	202	1.0	'ideal day'
Porites porites[14]	666	192	3.5	Stressed conditions.
Porites porites[15]	855	327	2.6	Normal conditions.
Porites porites[7]	459	299	1.5	
Stylophora pistillata[16]	2948	334	8.8	light adapted
Stylophora pistillata[16]	621	182	3.4	shade-adapted
Stylophora pistillata[4]	112	111	1.0	
Siderastrea siderea[17]	390	278	1.4	Salinity experiment.
Turbinaria mesenterina[18]	372	-	-	Diff. light levels.

Notes: P = photosynthesis, R = respiration. Values have been converted from original estimates based on: photosynthesis at maximum rate for 8 hours over the day, photosynthesis and respiration quotients of 1.1 and 0.8 respectively (Muscatine et al. 1981), and conversion from μl to μg O2 using 1.43 μg O2 μl^{-1}.

References: (1) Wyman et al. 1987, (2) Bythell 1988, (3) Tanaka et al. 2007, (4) Reynaud-Vaganay et al. 2001, (5) Sebens et al. 2003, (6) Anthony & Fabricius 2000, (7) Marubini & Davies 1996, (8) Lesser et al. 2000, (9) Rodrigues & Grottoli 2007, (10) Anthony & Hoegh-Guldberg 2003a, (11) Davies 1991, (12) Davies 1984, (13) Titlyanov 1991b, (14) Edmunds & Davies 1989, (15) Edmunds & Davies 1986, (16) Muscatine et al. 1984, (17) Muthiga & Szamant 1987, (18) Anthony & Hoegh-Guldberg 2003b.

1.5 Colony morphology and performance

Coral colonies form three-dimensional structures that, by virtue of their shape, stratify the light and flow environments within the colony. Due to self-shading, light intensity decreases with depth into a coral colony at a rate that is influenced by morphology (Titlyanov 1991b; Helmuth et al. 1997b; Anthony et al. 2005). Similarly, flow declines with distance from the front edge of a colony so that regions of stagnant water may form in the colony interior (Chamberlain and Graus 1975). Due to these effects, morphology is an important mediator of colony oxygen and carbon dioxide exchange and thereby metabolism (Lesser et al. 1994; Bruno and Edmunds 1998). Indeed, the dominant hypothesis that has been proposed to explain plasticity in corals contends that changes in morphology compensate for changes in light intensity and flow velocity along depth gradients (Gleason 1992; Anthony et al. 2005; Kaandorp & Sloot 2001).

Despite being recognised as organisms that show a high degree of phenotypic plasticity (Veron 2000), the influence of colony morphology on energy acquisition of corals is not well understood. This is because a mechanistic framework linking colony shape, variation in environmental conditions, and energy acquisition has not been available. In earlier work, I developed a geometric model to predict light acquisition over the surface of simple colony morphologies (Hoogenboom 2003). The results of that study showed that simple, flat morphologies always had higher energy acquisition than other alternative colony shapes. However, my previous research did not incorporate potential costs associated with exposure to very high light intensities. Therefore, in this thesis, I explicitly account for changes in the relationship between light and photosynthesis due to photoacclimation of colonies to a range of light conditions comparable to those experienced in the field. I also extend

the light model to more realistic colony morphologies. Together, these improvements allow a rigorous analysis of the energetic implications of variations in colony morphology.

1.6   Thesis overview

Although the literature indicates a general decline in carbon acquisition with depth for some coral species (e.g. Muscatine et al. 1984; Mass et al. 2007), mechanistic relationships between energy acquisition and environmental gradients on reefs have not been developed. An understanding of these relationships is critical if hypotheses regarding the effects of environmental gradients on species performance are to be addressed. This chapter has identified four central areas where research into the links between physiology, ecology and environment should be targeted.

Many coral species occur in habitats with very high light intensities. However, energetic costs associated with excess light absorption leading to the inhibition of photosynthetic rate (photoinhibition), and how these costs influence the light niche, have not been quantified. There is evidence in the literature that efficiency of photosynthesis declines at very high light intensities (e.g. Winters et al. 2003) and that the toxic effects of light at high temperatures cause coral bleaching (Jones et al. 1998). However, it is not known how these effects translate to energetics of coral colonies. Quantifying the energetic costs of photoinhibition is the primary aim of Chapter 2 of this thesis.

The capacity for photoacclimation to extend the width of the light niche has been inferred in many studies of photosynthesis (e.g. Anderson et al. 1995) but never quantified. Differences in photoacclimation strategies have also been highlighted as a potential mechanism that may promote coexistence of phytoplankton species (Richardson et al. 1983). However, the interacting effects of different mechanisms of

photoacclimation on energetics are not known. In Chapter 3, I quantify how the physiological processes that moderate photosynthesis vary with changes in the irradiance under which corals are grown. I then combine these functional relationships in a mechanistic model to characterise the light niche, and quantify the sensitivity of niche boundaries to variation in different photoacclimation strategies.

Many species of reef-building corals demonstrate pronounced phenotypic plasticity in response to environmental variation. Colony morphology strongly influences energetics, and maximization of energy acquisition through changes in colony shape is the dominant hypothesis that purports to explain plasticity in corals. However, a rigorous demonstration of this phenomenon requires a mechanistic link between physiology, colony shape and environmental variation. In Chapter 4, I use a 3-dimensional geometric model of light capture by complex colony morphologies, together with data describing variation in photophysiology in response to growth irradiance, to investigate the energetic implications of phenotypic plasticity in species of foliose coral.

In addition to light intensity, water flow influences metabolic rates and shows strong spatial variation on coral reefs. In Chapter 5, I modify and calibrate mass-transfer models of gas exchange originally developed for engineering applications (see Patterson et al. 1991) in order to quantify energy acquisition of corals as a function of light intensity and flow velocity. This model integrates the effects of, and allows a mechanistic quantification of the interaction between, these two environmental gradients. I then apply this model to identify the light and flow thresholds for survival of 3 coral species that are common on the Great Barrier Reef.

The general aim of the research presented in this thesis was to develop and calibrate models that link physiological processes with ecological patterns. In the

broader context of general ecological theory, such models are beneficial because they allow a mechanistic understanding of the factors that delineate the fundamental niche for different species, and influence the performance of individuals within the niche. In the final chapter of my thesis, I summarise the key findings of my research and discuss the robustness of my results to other aspects of coral physiology and biology.

1.7 Publication details

Chapter 2 of my thesis was published in *Marine Ecology Progress Series* in 2006 (Hoogenboom et al. 2006). Chapter 4 was published in *Ecology* in 2008 (Hoogenboom et al. 2008) and Chapter 5 has been accepted for publication in *Ecology* (Hoogenboom & Connolly, In Press). I am in the final stages of preparing Chapter 3 for submission to *Marine Ecology Progress Series*. In addition, I am preparing a review article that summarises patterns of energy acquisition and allocation for scleractinian corals, and incorporates much of the synthesis of literature data presented in this chapter.

2 ENERGETIC COSTS OF PHOTOINHIBITION AT DIURNAL TIMESCALES

2.1 Summary

Photoinhibition may constitute an energetic cost for photosynthetic organisms through damage to the photosynthetic apparatus or increased metabolism due to damage avoidance and repair. For several species of scleractinian corals, studies using fluorescence have a revealed a significant reduction in photochemical efficiency of symbiotic dinoflagellates within coral tissue in response to excess light absorption. However, for corals it is unclear whether photoinhibition has a negative impact on energy budgets. In this chapter, I simultaneously quantified the effect of exposure to excessive light on net rates of photosynthesis and on fluorescence-derived photochemistry. In a laboratory setting, colonies of the reef-building coral *Turbinaria mesenterina* were acclimatized to three different irradiance regimes. The corals were then exposed to a potentially photoinhibitory diurnal irradiance cycle and assayed for rates of photosynthesis and photochemical yields. Results indicated that daily costs of photoinhibition are negligible under field conditions. Reduced net rates of photosynthesis in the afternoon compared with the morning were predominantly due to enhanced rates of dark respiration in the afternoon. However, photoacclimation to high light levels reduced daily energy acquisition in the long term, primarily due to decreased chlorophyll concentrations. Therefore, although changes in the photosynthetic activity in symbiotic dinoflagellates over a diurnal irradiance cycle do not cause a measurable decline in net oxygen evolution for coral colonies, repeated exposure to excessive irradiance can reduce energy acquisition per

unit surface area, and hence influence the upper limit of the depth distribution of scleractinian corals.

2.2 Introduction

The saturating relationship between photosynthesis and irradiance is well established (Falkowski & Raven 1997). At high irradiances, excess light absorption can damage the photosynthetic apparatus or, alternatively, induce processes that dissipate energy before damage can occur (Demmig-Adams & Adams 1992). This phenomenon, photoinhibition, has been shown to result in a $6 - 25\%$ decline in daily carbon gain of higher plants and phytoplankton (Ogren & Sjostrom 1990; Pahl-Wostl 1992; Werner et al. 2001), leading to reduced growth rates (Laing et al. 1995). For numerous scleractinian coral species, a marked reduction in the efficiency of light use for photochemistry by zooxanthellae, the symbiotic dinoflagellates within coral tissue, is apparent under high light conditions. (e.g. Brown et al. 1999; Jones & Hoegh-Guldberg 2001; Winters et al. 2003). Furthermore, when isolated from their coral host, zooxanthellae exhibit reduced rates of photosynthesis at high light levels (Shick et al. 1995; Goiran et al. 1996: but see Iglesias-Prieto & Trench 1994). Correspondingly, avoidance of excess light has been noted as a determinant of coral colony morphology, with colonies of many species generating self-shading morphologies in high-light habitats (Oliver et al. 1983; Titlyanov 1991b; Muko et al. 2000). Despite this, the impact of photoinhibition on net rates of photosynthetic energy acquisition of the coral symbiosis is not well understood. If photoinhibition incurs significant costs for corals, it may exclude light-sensitive species from shallow habitats. Even in the presence of morphological strategies that reduce light absorption, or potential changes to the composition of the symbiont population

toward light-tolerant clades (e.g. Iglesias-Prieto et al. 2004), costs of photoinhibition potentially demarcate an upper bound of the depth distribution of reef-building corals.

Using O_2 or CO_2 flux measurements (respirometry), photoinhibition has traditionally been detected as a decline in the light-saturated photosynthetic rate (e.g. Platt et al. 1980). An alternative method for assaying photosynthesis is fluorometry, which allows estimates of photosynthetic activity to be obtained from the fluorescent properties of chlorophyll *in vivo* (Maxwell & Johnson 2000). Using fluorescence, photoinhibition is typically inferred from a decline in photochemical efficiency during and/or after exposure to high irradiance. Such a decline may be due to reversible processes such as increased dissipation of absorbed light as heat ('dynamic' photoinhibition), or to damage to photosynthetic units requiring *de novo* synthesis of protein for repair ('chronic' photoinhibition: Hoegh-Guldberg & Jones 1999; Gorbunov et al. 2001). For corals, changes in photochemical yield of zooxanthellae over a diurnal irradiance cycle are generally attributed to dynamic photoinhibition (Hoegh-Guldberg & Jones 1999; Lesser & Gorbunov 2001; Winters et al. 2003). However, chronic photoinhibition has also been reported, with up to 30% of photosynthetic reaction centers damaged by exposure to full sunlight in shallow waters (see Gorbunov et al. 2001). Nevertheless, there is no evidence to indicate whether such changes in photochemistry of zooxanthellae lead to reduced photosynthetic energy acquisition of the coral symbiosis. In fact, for some corals, rates of photosynthetic oxygen evolution are higher in the afternoon than in the morning (Levy et al. 2004), even though photoinhibition should be greater in the afternoon following exposure to high irradiance at midday. To determine the ecological significance of photoinhibition for reef-building corals, it must be

resolved whether excess light absorption entails an energetic cost, and, if so, whether this cost constitutes a significant proportion of daily photosynthetic energy acquisition.

The aim of this chapter was to resolve whether photoinhibition comprises a significant energetic cost for corals. I focused upon costs incurred by the coral/zooxanthellae symbiosis, the ecologically relevant unit of study for analyses of energy budgets for coral colonies. Costs of photoinhibition were quantified through changes in the parameters of the diurnal photosynthesis-irradiance (PE) relationship of corals. Given the influence of photoacclimation on the shape of the PE curve (e.g. Anthony & Hoegh-Guldberg 2003a), I calculated costs of photoinhibition for corals acclimated to three different light regimes and exposed to two different diurnal irradiance cycles. Photoinhibition, whether dynamic or chronic, may comprise an energetic cost by reducing the maximum rate of photosynthesis (P_{MAX}) at supra-saturating light levels (e.g. Platt et al. 1980). Alternatively, costs may arise from increased sub-saturation irradiance (E_K) following exposure to high irradiance, corresponding to lower efficiency of light utilization for photosynthesis (e.g. Kana et al. 2002). Finally, photoinhibition may cause elevated rates of respiration (R_{DARK}) due to increased biosynthesis for damage repair. In all cases, I expected that changes in photosynthesis parameters would be most pronounced for corals acclimated to lower light levels.

A secondary aim of this chapter was evaluate the functional relationship between fluorescence and oxygen respirometry as assays of photosynthesis in reef-building corals. Respirometry and fluorometry measure different aspects of the photosynthesis-irradiance relationship: the former captures net photosynthetic gas exchange averaged over a photosynthetic surface and the latter indicates gross

photosynthetic electron transport from a small area of that surface (e.g. Maxwell &
Johnson 2000). One of the key validations for the use of fluorescence as a measure of
photosynthesis is proportionality between the quantum yields (photosynthesis per
unit light absorbed) of oxygen evolution and photochemistry (e.g. Brown et al.
1999). Although a linear relationship between these variables has been established
experimentally for some plants (Genty et al. 1989; Maxwell et al. 1998), field-based
measurements often reveal a non-linear relationship (e.g. Seaton & Walker 1990;
Fryer et al. 1998). This non-linearity means that gross photochemical activity may
vary considerably without having any effect on net rates of photosynthesis. For
corals, the functional relationship between photosystem-II (PSII) photochemistry and
oxygen evolution is unknown. This is significant, because properties of the
coral/zooxanthella symbiosis may cause this relationship to diverge considerably
from that demonstrated for higher plants (e.g. due to respiration of coral tissue
independently of photosynthetic production by symbionts).

2.3 Materials and Methods

The foliose coral *Turbinaria mesenterina* (Dendrophyllidae) was used as a
study species in this study, because the self-shading colony morphology it generates
in high light habitats suggests sensitivity to excess light absorption (Willis 1985:
Anthony et al. 2005). 36 flat fragments (measuring approximately 10 cm by 10 cm)
were collected from deep (6 m average depth) and shallow (1 m average depth) sites
at Nelly Bay, Magnetic Island on 15 April 2004 (19°09S, 146°53E). Colonies were
transported to aquarium facilities at James Cook University, divided into groups and
allowed to photoacclimate to three different irradiance regimes: "High", "Medium"
and "Low" which corresponded to maximum daily irradiances of 570, 270 and 120

μmol photons m^{-2} s^{-1} respectively. The acclimation irradiances were representative of approximately 4, 7 & 10 m average depth below the water surface at the collection site (M. Hoogenboom, unpublished data). A minimum experimental depth of 4 m was used because previous attempts to photoacclimate flat fragments of the study species to higher light levels resulted in high mortality (K. Anthony, unpubl. data). This makes my results conservative with respect to the prevalence of photoinhibition under field conditions as all colonies were acclimated to relatively low light levels. Colonies were allowed 6 weeks for recovery and photoacclimation, which is ample for this species (Anthony & Hoegh-Guldberg 2003b). To avoid potential changes to photosynthetic properties of experimental colonies due to nutrient limitation, colonies were fed live rotifers (feeding density approximately 50 rotifers ml^{-1}). Water temperature was maintained between 26.5 and 28°C, approximating the modal temperature at the collection site (≈27°C, AIMS Cleveland Bay Weather Station Data).

2.3.1 Experimental setting

An array of six closed, clear-perspex incubation chambers (2.7 litre volume) coupled with calibrated Clark-type oxygen electrodes (Cheshire Systems, Australia) was used for the oxygen respirometry assays. The chambers were designed as flumes, equipped with pumps to maintain continuous water circulation at 5-6 cm s^{-1} (laminar flow), and were flushed for 4 minutes in every 20-minute measuring period to prevent oxygen super-saturation. To control for photosynthesis and respiration of microorganisms within the water, I regularly left one chamber empty during respirometry runs. In addition, chambers were cleaned at the end of each run to prevent biofilm formation. Oxygen concentrations were recorded every 20 seconds using a data logger (CR10X, Campbell Scientific Australia). 400W metal halide

lamps (Eye, Japan) suspended above the chambers and aquaria provided the light source for both diurnal photosynthesis measurements and the light acclimation treatments. These lights have a spectrum resembling natural sunlight with the ultraviolet component present. For the photosynthesis measurements, irradiance was varied over the course of the day by changing the elevation of the lamps every 20 minutes, during the flushing period. Light levels (downwelling PAR) were measured using a cosine-corrected Licor probe (Li-192S) attached to a Li-1000 data logger (Licor, Nebraska). The chambers were submerged in a 1000-litre water jacket with running seawater connected to a temperature control unit (C023, Carrier Systems Australia) to prevent changes in water temperature during the measurement period.

On each day of data collection, 5-6 colonies from a photoacclimation treatment were selected for oxygen evolution measurements. Photosynthesis versus irradiance curves (PE curves) were constructed over 10-hour diurnal cycles, with irradiance at time t, $E(t)$, varying approximately according to a cubic sine function $E(t) = E_{MAX} \sin^3(\pi t/\lambda)$ where t is time (hours since dawn), λ is day length (10 hours) and E_{MAX} is maximum daily irradiance. This function closely approximates diurnal irradiance variation under natural aquatic conditions (Marra 1978). Dark respiration was measured twice each day, at the beginning and end of each respirometry run. PE curves were measured on consecutive days with $E_{MAX} = 600$ μmol photons m^{-2} s^{-1} on day one and 1200 μmol photons m^{-2} s^{-1} on successive days. I used different diurnal irradiance cycles to assess whether costs of photoinhibition were influenced by the degree to which experimental irradiance exceeded the growth (acclimation) irradiance. For the corals acclimated to low light, measurements at $E_{MAX} = 1200$ μmol photons m^{-2} s^{-1} were repeated over three days to determine how photosynthetic properties may change through time under potentially photoinhibitory conditions. To

relate oxygen flux to colony tissue surface area, colonies were photographed together with a ruler using a digital camera (Canon G3). Surface areas were later determined using Image Tools (v3, UTHSCSA 2002).

At the same time as colonies were selected for O_2 evolution measurements, an identical set of colonies was selected for fluorescence measurements, and positioned outside the respirometry chambers. Irradiance at the surface of colonies inside and outside the chambers varied less than 5%. Fluorescence assays were carried out using a pulse-amplitude-modulated fluorometer (Mini-PAM, Walz, Germany, see Appendix A for settings) fitted with a 5mm fiber optic probe. At the end of each 20-minute illumination period, fluorescence was measured at the center of each colony. Apparent quantum yield of photochemistry ($\Delta F/F_m'$, dimensionless) was calculated as $\Delta F/F_m'=(F_m'-F)/F_m'$ (as per Genty *et al*. 1989), where F is steady state fluorescence in the light and F_m' is maximal fluorescence in the light. I also calculated a non-photochemical quenching coefficient as NPQ $= (F_m - F_m')/F_m'$ (after Maxwell & Johnson 2000). Yield measurements were converted to relative electron transport rates (*rETR*) using the formula $rETR = \Delta F/F_m' \times E \times 0.5$ where E is irradiance and 0.5 is a factor that accounts for the distribution of electrons between photosystems I & II (e.g. Hoegh-Guldberg & Jones 1999). This relative measure of the rate of electron transport was used because the light absorption characteristics of tissue are unknown for this species.

2.3.2 Chlorophyll concentration

Immediately after photosynthesis assays were completed, colonies were frozen at -40°C and later used to determine chlorophyll content. Colonies were broken into 2 fragments and photographed for surface area measurements (see above). Fragments were ground into a fine paste, and chlorophyll extracted in

darkness using cold acetone. To ensure that all chlorophyll was extracted from each

coral fragment, the initial overnight extraction (12hr) was followed by two one-hour

extractions. The combined volume of all three extractions was measured, and the

extract centrifuged. 10 replicate absorbance readings at 630nm and 663nm were

carried out for each fragment, and concentration of chlorophyll-*a* and -*c2* was

determined using the equations of Jeffrey & Humphrey (1975). Chlorophyll

concentrations were then normalized to fragment surface area.

2.3.3   Data Analysis

I fitted the hyperbolic tangent function (Eqn 1) to photosynthesis versus

irradiance data in order to estimate the parameters P_{MAX} (maximum rate of

photosynthesis, μmol O_2 cm^{-2} hr^{-1}) and E_K (sub-saturation irradiance, μmol photons

m^{-2} s^{-1}) using measured values of R_{DARK} (rate of respiration in darkness, μmol O_2 cm^{-2} hr^{-1}).

$$P(E) = P_{MAX} \tanh\left(\frac{E}{E_K}\right) - R_{DARK} \,, \qquad \qquad \text{Eqn 2.1}$$

This function was fitted to data using a Levenberg-Marquardt non-linear estimation

routine in *Statistica* (StatSoft Inc.). Firstly, I estimated P_{MAX} and E_K for the morning

part of the diurnal photosynthesis curve. As there was no evidence in the data of a

change in (net) P_{MAX} in the afternoon compared with the morning, I subsequently

used the fitted P_{MAX} value from the morning part of the PI curve to obtain an estimate

of E_K during the afternoon. This allowed me to detect whether exposure to light over

the course of the morning altered the shape of the PI curve during the afternoon.

Repeated-measures analysis of variance was used to investigate the effect of

photoacclimatory state and diurnal irradiance cycle on changes in photosynthesis

parameters over the day. Subsequently, I used the fitted parameters to calculate

photosynthetic oxygen evolution during mornings (5 h) and afternoons (5 h), based on the integral of Eqn 2.1. A numeric integration routine in MATLAB (MathWorks Inc) was used to evaluate this integral for each colony. The energetic cost of photoinhibition was then calculated as the proportional difference between total photosynthesis summed over the morning compared with the afternoon. Finally, I tested whether this cost was statistically significant using paired-samples t-tests. These costs therefore represent the reduction in net carbon acquisition due to exposure to excess irradiance over a daily timescale. I chose this method in place of commonly used photosynthesis/respiration ratios (e.g. Muscatine et al. 1981), as recent studies have demonstrated that rates of respiration over the day are not constant as assumed under the latter method (e.g. Kuhl et al. 1995; Al-Horani et al. 2003). To ascertain whether repeated exposure to excessive irradiance altered the photosynthetic properties of *Turbinaria mesenterina*, mean values of four key PE curve parameters were compared between days one and three of exposure using paired-samples t-tests.

Quantum yield of oxygen evolution (mol oxygen (mol photons)$^{-1}$) was obtained by dividing rates of photosynthesis (converted to appropriate units of μmol O_2 m^{-2} s^{-1} and corrected for dark respiration) by incident irradiance (μmol photons m^{-2} s^{-1}), as per Seaton & Walker (1990). Because dark respiration in corals is enhanced by light exposure (e.g. Edmunds & Davies 1988), I used linear interpolation between estimates of R_{DARK} for the morning and afternoon to convert measured net photosynthesis to estimates of gross photosynthesis. For comparison between fluorescence and respirometry assays of photosynthesis, data were normalized to chlorophyll concentration. This normalization was selected in order to avoid

confounding differences in photochemistry between light acclimation treatments with any differences in chlorophyll concentration.

2.4 Results

2.4.1 Net Photosynthesis and rETR

Photoinhibitory responses varied dramatically depending on whether respirometry or fluorescence assays of photosynthesis were used. In general, although *rETR* decreased under high irradiance in response to declining apparent photochemical yield (Figure 2.1A&B), light-saturated rates of photosynthesis remained constant for corals acclimated to all of the three light regimes, regardless of whether they were exposed to a daily irradiance cycle of E_{MAX} = 600 or 1200 μmol photons m^{-2} s^{-1} (Figure 2.1D-F). For all of the light-acclimation treatments, non-photochemical quenching (NPQ) was highest at midday, mirroring the decrease in photochemical yield (results not shown). The magnitude of NPQ was also related to photoacclimatory state, with corals acclimated to high light showing greater quenching capacity. Compared with rates of oxygen evolution, relative electron transport rates approached saturation more slowly, and were generally higher in the morning than the afternoon at the same irradiance. This effect was most apparent in mid-afternoon (under both diurnal irradiance cycles), with afternoon values returning to approximately the same level as morning values by late afternoon. In other words, effects of photoinhibition on electron transport rates were short-lived with photochemical activity returning to initial values by the end of the day despite exposure to light levels well above those to which corals were acclimated. Overall, there was no evidence that low photochemical efficiency at midday had any effect on
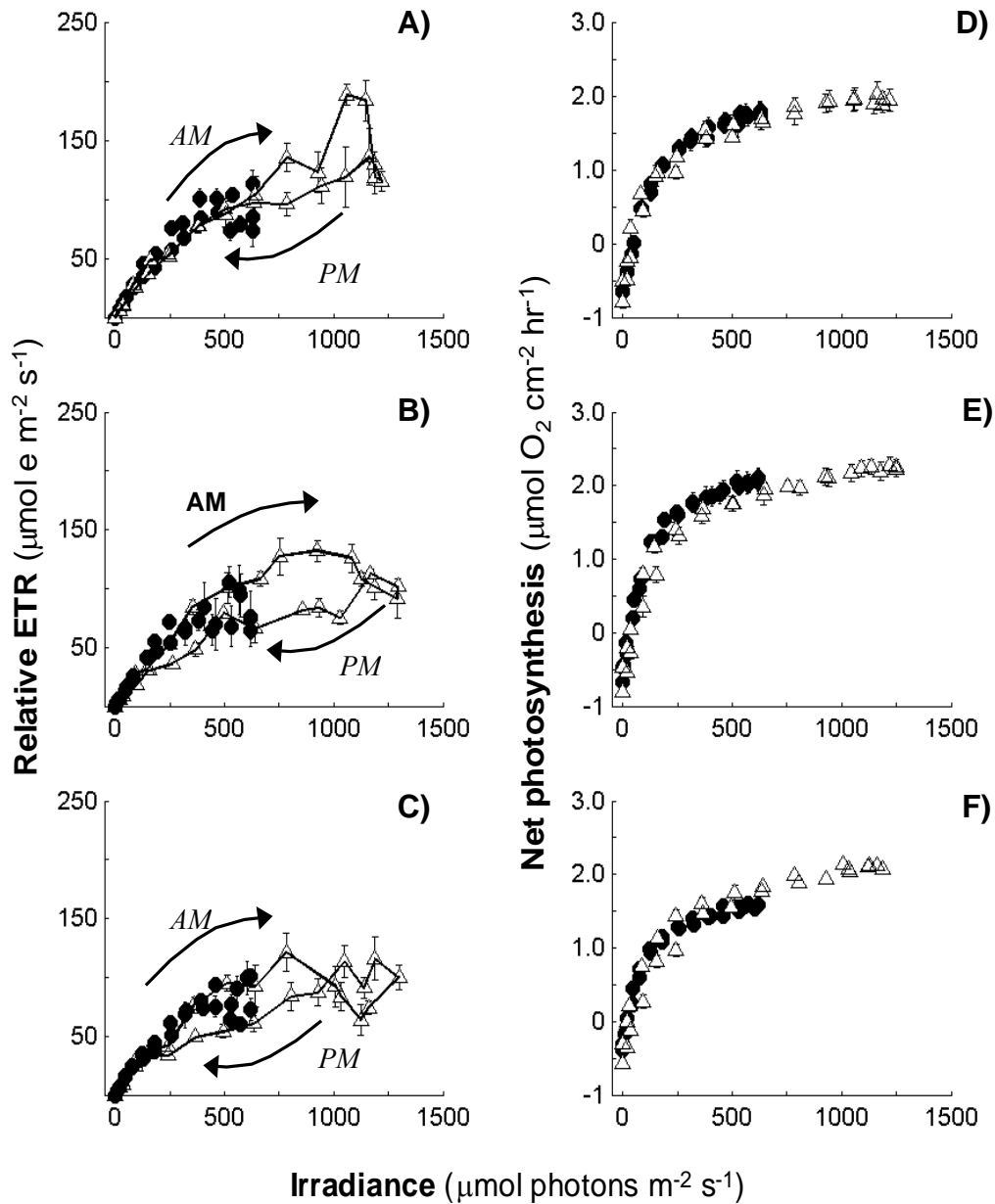
Figure 2.1: Diurnal photosynthesis and electron transport (*rETR*) versus irradiance for corals acclimated to three light regimes (high light: panels A&D; medium: B&E; and low: C&F), subjected to two daily irradiance cycles (filled circles, E_{MAX} = 600 μmol photons m^{-2} s^{-1}; open triangles, E_{MAX} = 1200 μmol photons m^{-2} s^{-1}). Points represent mean values at 20-minute intervals over the day, with consecutive points joined by solid lines. Error bars represent standard error (n = 5 – 8).

net photosynthesis. In other words, although rates of electron transport via photochemistry decreased under high irradiance, rates of photosynthesis remained saturated, even for corals exposed to light levels much higher than those to which they were acclimated.

As expected, the shape of the photosynthesis/irradiance curve for colonies of *Turbinaria mesenterina* varied with photoacclimatory state. The maximum rate of photosynthesis (P_{MAX}) was significantly lower for corals acclimated to low light levels compared with the other two growth irradiances (main-effect of State for P_{MAX}, Table 2.1). P_{MAX} was also higher under exposure to more intense light for corals acclimated to all growth irradiances (main effect of Treatment, Table 2.1). This latter finding indicates that photosynthesis did not reach complete saturation under the lower diurnal irradiance cycle (also evident from the filled points in Figure 2.1D-F). The sub-saturation irradiance (E_K) appeared to increase with acclimation irradiance when corals were exposed to low light levels, but not under exposure to high light levels (Figure 2.2A c.f. B). This difference was apparent as a significant State x Treatment interaction (Table 2.1). To my knowledge, this finding comprises the first evidence for corals of a dynamic down-regulation of net oxygen evolution due to absorption of excess light. There was no evidence of any variation in E_K between morning and afternoon (all effects involving Time non-significant for E_K, Table 2.1; filled points compared to triangles, Figure 2.2A-B).

Rates of dark respiration were markedly influenced by light intensity, both in terms of acclimation irradiance (significant main effect of State, Table 1) and diurnal irradiance treatment. Under both diurnal irradiance cycles, R_{DARK} increased with acclimation irradiance (Figure 2.2C&D). Furthermore, R_{DARK} was distinctly higher in the afternoon than the morning under the high diurnal irradiance treatment (open
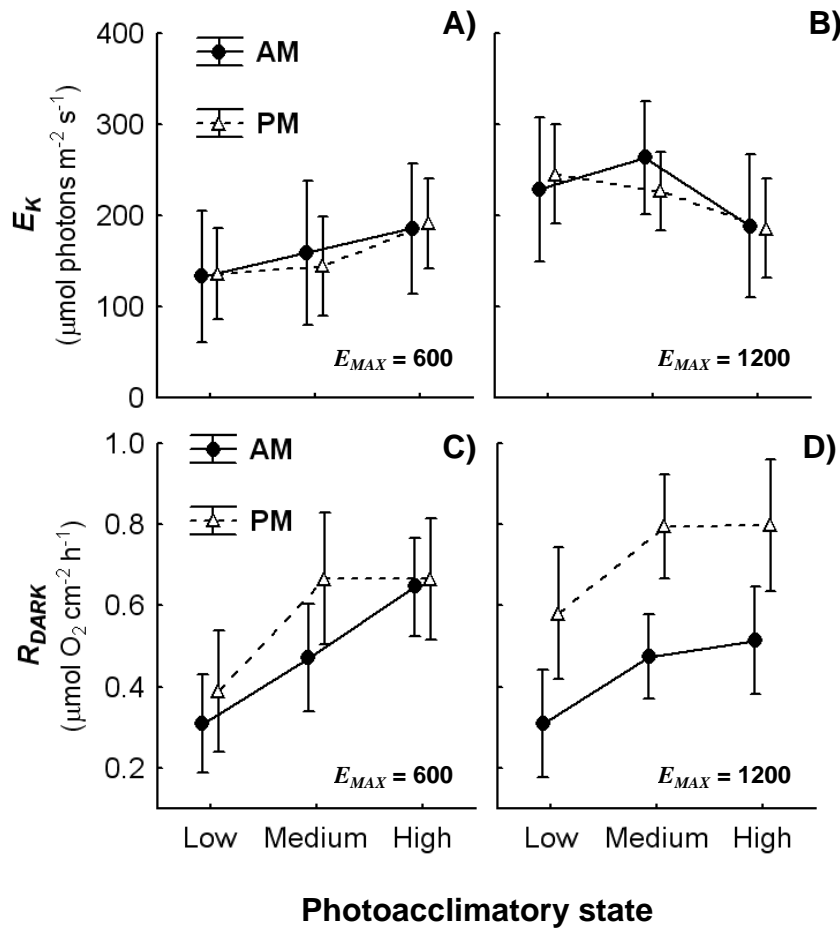
Figure 2.2: Variation in average parameter values of photosynthesis versus irradiance curves (E_K: A–B, R_{DARK}: C–D) between morning and afternoon for corals acclimated to three light regimes and exposed to two irradiance cycles (E_{MAX}, μmol photons m^{-2} s^{-1}). Error bars represent 95% confidence intervals (n = 5 – 8).

triangles compared to filled points in Figure 2.2D), but not under exposure to lower light levels (Figure 2.2C). Consequently, I found a significant Treatment x Time interaction for R_{DARK} (Table 2.1). Therefore, differences between rates of net photosynthesis in the early morning compared with the late afternoon at the same irradiance (evident in Figure 2.1E-F) are predominantly due to changes in rates of respiration. The post-illumination increase in rates of dark respiration was consistent

Table 2.1: Analysis of Variance for the effect of photoacclimatory state, diurnal irradiance cycle and time of day on photosynthesis-irradiance curve parameters (P_{MAX}, E_K and R_{DARK}). Results of post-hoc tests (Tukey's Unequal N HSD) are shown. L, M & H refer to corals acclimated to low, medium and high irradiance respectively. 600 and 1200 refer to parameters for daily irradiance cycles with E_{MAX} = 600 and 1200 μmol photons m^{-2} s^{-1}. AM refers to parameters from the morning half of the diurnal photosynthesis curve, and PM refers to afternoon.

Parameter (units)	Effect	F (df)	*P*	Post-hoc
P_{MAX} (μmol O$_2$ cm^{-2} h^{-1})	Photoacclimatory state ('State')	11 (2,29)	< 0.01	L < M = H
	Diurnal irradiance ('Treatment')	6.9 (1,29)	< 0.05	600 < 1200 for L, M & H
	State*Treatment	1.8 (2,29)	0.19	-
E_K (μmol photons m^{-2} s^{-1})	Photoacclimatory state ('State')	0.24 (2,29)	0.79	-
	Diurnal irradiance ('Treatment')	23 (1,29)	< 0.01	na
	State*Treatment	5.7 (2,29)	< 0.01	L & M, 1200 > 600
	Time of day ('Time')	0.03 (1,29)	0.86	-
	State*Time	0.33 (2,29)	0.72	-
	Treatment*Time	0.02 (1,29)	0.90	-
	State*Treatment*Time	0.03 (2,29)	0.97	-
R_{DARK} (μmol O$_2$ cm^{-2} hr^{-1})	Photoacclimatory state ('State')	22 (2,29)	< 0.01	L < M = H
	Diurnal irradiance ('Treatment')	2.6 (1,29)	0.12	-
	State*Treatment	0.71 (2,29)	0.50	-
	Time of day ('Time')	19 (1,29)	< 0.01	na
	State*Time	0.53 (2,29)	0.59	-
	Treatment*Time	4.7 (1,29)	< 0.05	AM < PM when E_{MAX} = 1200
	State*Treatment*Time	0.21 (2,29)	0.81	-

across all photoacclimation groups (i.e. none of the interaction effects involving State were significant for R_{DARK}, see Table 2.1). This suggests that increased metabolic activity following light exposure may be a general response of the coral-zooxanthellae symbiosis, and is not influenced by the degree to which exposure irradiance exceeds the irradiance to which corals are acclimated.

2.4.2 Cost of photoinhibition

Total net oxygen evolution (and equivalently, carbon fixation) was significantly lower during the afternoon than the morning for corals acclimated to all three irradiance regimes when exposed to the higher daily irradiance cycle. Specifically, integrated rates of net photosynthesis showed a 15 – 17% decline in afternoons compared with mornings under exposure to high light (Figure 2.3A; Table 2.2). Moreover, corals acclimated to the lowest light levels showed a 6% reduction in integrated net rates of photosynthesis during the afternoon when exposed to the lower daily irradiance regime. Although this reduction constitutes a considerable proportion of daily photosynthetic activity, gross photosynthetic energy acquisition (disregarding oxygen consumption through respiration) summed over the morning and the afternoon did not differ significantly for any of the comparisons (Figure 2.3B; Table 2.2). In other words, photoinhibition only represents a significant energetic cost for corals if metabolic activity associated with repair of damaged components of the photosynthetic apparatus is the major cause of post-illumination enhancement of respiration

Although daily costs of photoinhibition appear to be negligible for *Turbinaria mesenterina*, photoacclimation to high light does not maximise integrated daily photosynthesis. In fact, total daily energy acquisition per unit surface area was lower
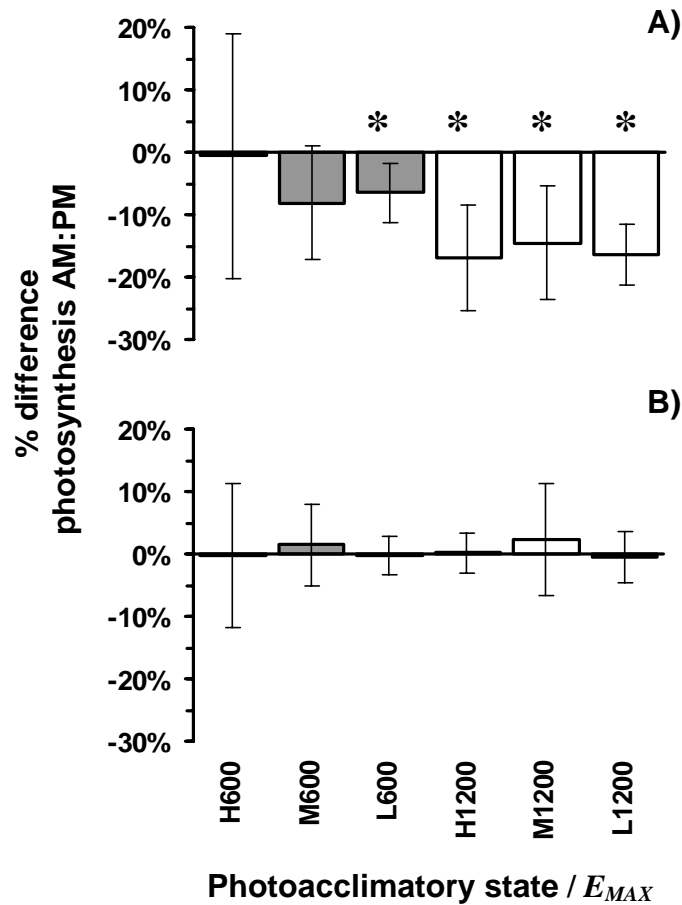
Figure 2.3: Percentage difference in net (A) and gross (B) photosynthesis over the morning compared with the afternoon for corals acclimated to three different light regimes and exposed to two diurnal irradiance cycles. Data points represent mean costs and error bars represent standard error (n = 5 – 8). Asterisks denote costs that are statistically significant (dependent samples t-tests, Table 2.2).

on average for the high-light acclimated corals than for corals acclimated to intermediate light levels when exposed to the same daily irradiance cycle (Figure 2.4). This is primarily due to a lower chlorophyll concentration, higher sub-saturation irradiance (E_K), and a higher rate of dark respiration for the high-light corals

Table 2.2: Comparison of the proportional difference between integrated net and gross photosynthesis over the course of the afternoon compared to the morning for corals acclimated to three different light regimes (State), and exposed to two diurnal irradiance cycles (E_{MAX}, µmol photons m^{-2} s^{-1}). Results of paired samples t-tests are shown (degrees of freedom in parentheses).

E_{MAX}	State	Net Photosynthesis	Gross Photosynthesis
600	High	$t(5) = -0.07$, p = 0.95	$t(5) = -0.06$, p = 0.96
	Medium	$t(4) = -1.99$, p = 0.12	$t(4) = 0.51$, p = 0.64
	Low	$t(5) = -3.37$, p < 0.05	$t(5) = -0.15$, p = 0.89
1200	High	$t(4) = 4.4$, p < 0.05	$t(4) = 0.09$, p = 0.93
	Medium	$t(7) = -4.5$, p < 0.05	$t(7) = 0.71$, p = 0.50
	Low	$t(4) = -7.6$, p < 0.05	$t(4) = -0.31$, p = 0.77

Table 2.3: Change in photosynthetic properties of corals acclimated to low light following repeated exposure to excessive irradiance (E_{MAX} = 1200 µmol photons m^{-2} s^{-1}). Values are mean and standard error of each photosynthetic property on days one and three of exposure. Results of dependent samples t-tests (3 degrees of freedom in all cases) comparing values between days are shown.

Photosynthetic property	Day 1	Day 3	Statistical test
Chlorophyll concentration (µg cm^{-2})	32 (6)	23 (8)	$t(3) = 3.3$, p < 0.05
E_K (µmol photons m^{-2} s^{-1})	229 (36)	345 (54)	$t(3) = -2.1$, p = 0.13
P_{MAX} (µmol O^2 cm^{-2} hr^{-1})	2.3 (0.06)	2.6 (0.06)	$t(3) = -7.8$, p < 0.01
R_{DARK} (µmol O^2 cm^{-2} hr^{-1})	0.29 (0.17)	0.40 (0.10)	$t(3) = 0.63$, p = 0.57
Fv/Fm (a.u.)	0.66 (0.03)	0.52 (0.06)	$t(3) = 2.4$, p = 0.10
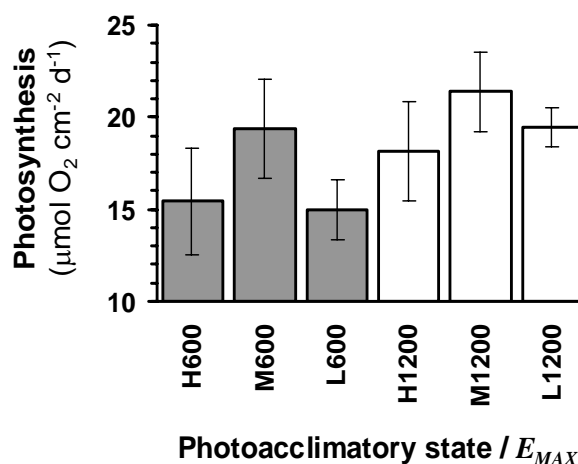
Figure 2.4: Daily integrated photosynthetic oxygen evolution for corals acclimated to three light regimes and exposed to two diurnal irradiance cycles. Bars represents means per group, error bars depict standard deviation.

compared with corals acclimated to lower light levels. When integrated photosynthesis was calculated for each photoacclimation treatment over a daily irradiance cycle with E_{MAX} equal to the growth irradiance, results indicated that higher light availability does not translate to higher daily carbon acquisition for *T. mesenterina*. In other words, photoacclimation causes carbon acquisition to remain constant across an approximately 5-fold light gradient.

To determine the medium-term consequences of photoinhibition and changes in photoacclimatory state on carbon gain I repeated measurements of photosynthesis for the low-light acclimated corals over three days of exposure to a daily irradiance cycle with E_{MAX} 1200 µmol photons m^{-2} s^{-1}. Although all of the measured photosynthetic properties varied over this timeframe (Table 2.3), changes were only statistically significant for chlorophyll concentration and the light-saturated rate of photosynthesis (P_{MAX}). The increase in (fitted) P_{MAX} was partially due to a

corresponding increase in R_{DARK}. The net effect of this was that although P_{MAX} was higher after repeated exposure to high light, integrated daily photosynthesis was actually lower, although not significantly so. In general, these changes in photosynthetic properties were consistent with photoacclimation to high light (increased P_{MAX}, E_K, and R_{DARK}, lower chlorophyll concentration and maximum photochemical efficiency). Collectively, these results indicate that while gradual loss of function of individual symbionts over the course of the day has a negligible (short-term) impact on energy budgets, repeated exposure leads to lower concentration of chlorophyll per unit surface, and consequently lower daily energy acquisition in the long term.

2.4.3 Fluorescence versus Respirometry

In contrast to the linear relationships typically assumed to hold for corals (e.g. Brown et al. 1999; Hoegh-Guldberg & Jones 1999), my results demonstrate a curvilinear relationship between fluorescence and gas exchange measures of photosynthetic activity (Figure 2.5). Furthermore, there was considerable variability in the relationship between the quantum yields of oxygen evolution and photochemistry (Figure 2.5A). At high light levels, electron transport rates may decline by more than half without having any measurable effect on the net rate of photosynthesis. Similarly, a three-fold variation in *rETR* was evident when photosynthesis had reached its maximal rate. On the other hand, *rETR* was directly proportional to rates of oxygen evolution at low light levels (at low rates of photosynthesis). The breakdown of the linear relationship between these two measures at high irradiance is driven by the substantially greater degree of hysteresis exhibited by *rETR* versus irradiance compared with photosynthesis versus irradiance
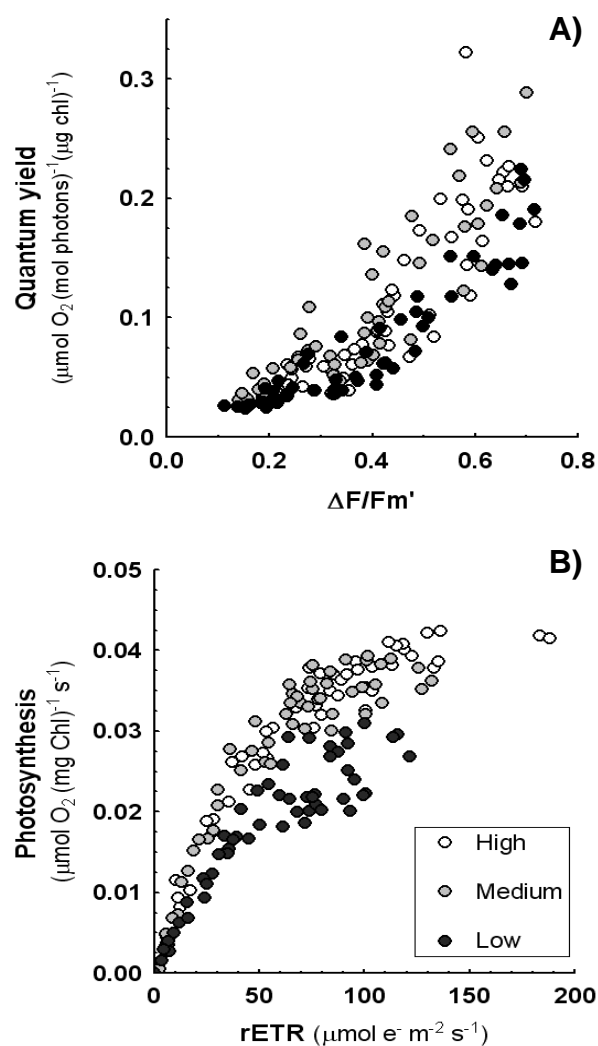
Figure 2.5: Relationships between photosynthetic activity as measured by oxygen respirometry (normalized to chlorophyll concentration) and fluorescence. A) quantum yield of oxygen evolution versus photochemical yield; and B) relative electron transport rate versus rate of photosynthesis (corrected for dark respiration). Data points represent means of 5-8 measurements. Error bars have been omitted for clarity.

when measured over a diurnal cycle. In addition to the hysteresis effect, lower

correlation at high irradiance was related to variation in the maximum rate of

photosynthesis (oxygen evolution) due to photoacclimation. For corals acclimated to low light levels, oxygen evolution per electron transported was lower (lower rate of photosynthesis at the same relative electron transport rate, Figure 2.5B). Collectively, these results demonstrate that for *Turbinaria mesenterina,* the relationship between biochemical and energetic assays of photosynthesis is influenced by the photoacclimatory state of individual colonies, even when variation in chlorophyll concentration between colonies is taken into account.

2.5 Discussion

The results of this chapter demonstrate that, for corals, exposure to high light only leads to a depression of net photosynthesis when average daily irradiances are much higher than growth (acclimation) irradiances. Moreover, reduced rates of net photosynthesis in the afternoon (compared with the morning at the same light levels) are primarily associated with increased rates of respiration in the afternoon. Previous studies of light-enhanced respiration in corals have demonstrated a 6- to 12-fold increase in oxygen consumption following light exposure (Kuhl et al. 1995; Al-Horani et al. 2003). A proportion of this increase may reflect energy expenditure for repair of damage to the photosynthetic apparatus of zooxanthellae, and/or tissue damage of the coral. However, light-enhanced respiration in corals is more likely to be attributable to enhanced metabolic activity related to, for example, increased skeletal growth (e.g. Reynaud-Vaganay et al. 2001) and increased photosynthetic activity. This is due to the fact that significant light enhancement of respiration has been measured in corals exposed to irradiances as low as $140 \mu mol$ photons m^{-2}s^{-1} (Al-Horani et al. 2003). If increased rates of respiration following exposure to high light were predominantly due to costs of repair of damaged components of the

photosynthetic apparatus, the magnitude of the change in respiration between morning and afternoon would depend upon the degree to which exposure irradiance exceeded acclimation irradiance (damage being greater for corals acclimated to lower light levels). As the same post-illumination increase in rates of respiration was observed for all acclimation treatments following exposure to the same diurnal irradiance cycle, this indicates that daily energetic costs of photoinhibition in corals are negligible.

Although dissipation of light through non-photochemical pathways is recognised as an effective photoprotective mechanism for corals (e.g. Hoegh-Guldberg & Jones 1999; Gorbunov et al. 2001), the same mechanism is present for other photosynthetic organisms for which energetic costs of photoinhibition are apparent (e.g. higher plants and phytoplankton, see Pahl-Wostl 1992; Werner et al. 2001). This raises the question as to how corals avoid these costs. Coral tissue contains amino acids that absorb, reflect or fluoresce ultraviolet light (mycosporine-like amino acids or MAAs, Jokiel & York 1982), and pigments that absorb light over photosynthetic wavelengths (Salih et al. 2000; Dove 2004). Therefore, the coral tissue layer may act as a protective screen for the zooxanthellae. Indeed, there is some evidence of host tissue reducing light levels reaching symbionts by more than 50% in other marine organisms (e.g. hydroids, Fitt & Cook 2001). Alternatively, zooxanthellae may shade each other, with symbionts in upper tissue layers shielding those in lower layers. Zooxanthellae in different parts of a coral colony experience different light environments (Jones et al. 2000), and vary in their chlorophyll fluorescence characteristics (Hill et al. 2004). Moreover, histology of bleached corals has revealed a greater loss of zooxanthellae from upper tissue layers as opposed to deeper tissues (Brown et al. 1995). Therefore, although zooxanthellae in upper tissue

layers may suffer reduced rates of photosynthesis due to photoinhibition, those in lower layers are likely to remain protected, and potentially compensate for the reduced photosynthesis of the upper layers.

If zooxanthellae do indeed shade each other, then the use of fluorometry to measure photosynthesis of corals may return biased results. For instance, in microphytobenthic assemblages, the thickness of the fluorescing layer has a pronounced impact on measured photochemical efficiency, with values overestimated by up to 60% in thick biofilms (Forster & Kromkamp 2004). An equivalent phenomenon may explain why low light-acclimated corals produce less oxygen per electron transported compared with medium- and high-light acclimated colonies. Self-shading of zooxanthellae would result in overestimation of apparent photochemical efficiency as the measured efficiency of the upper layer would be augmented by higher efficiency of symbionts exposed to lower light levels deeper in the tissue. This would in turn lead to overestimation of *rETR*, and an apparently lower rate of oxygen evolution per electron transported through PSII. Overall, the results of this chapter indicate that future studies should take account of tissue properties of corals, such as symbiont density, tissue thickness and presence of other light-absorbing pigments, when interpreting fluorescence assays of photochemistry.

Due to the insensitivity of rates of net photosynthesis to supra-saturating light levels, photochemical electron transport (of zooxanthellae) and photosynthetic oxygen evolution (or the coral-zooxanthellae symbiosis) were not correlated at high light levels. Indeed, under midday irradiances, even very low photochemical efficiencies (and high non-photochemical quenching activity) do not necessarily result in reduced rates of photosynthesis. Because the fluorescence behavior of *Turbinaria mesenterina* is consistent with that of several species investigated in other

studies (e.g. *Goniastrea aspera*, Brown et al. 1999; and *Stylophora pistillata*, Jones

& Hoegh-Guldberg 2001, Winters et al. 2003), these findings are likely to reflect

general properties of the coral-zooxanthella symbiosis. Moreover, my results

demonstrate that the influence of non-assimilatory electron flow at high irradiances

on the relationship between fluorescence and respirometry assays of photosynthesis

may represent a general trend for photosynthetic organisms. For corals, oxygen

evolution saturates prior to *rETR*, as has been shown for cyano-lichens, macroalgae,

and higher plants (Sundberg et al. 1997; Fryer et al. 1998; Figueroa et al. 2003). This

indicates that once the assimilatory reactions of photosynthesis become saturated,

electrons may still be transported through PSII. The importance of electron sinks in

addition to CO_2 reduction for avoidance of photoinhibition have been noted

previously (Krall & Edwards 1992; Hoegh-Guldberg & Jones 1999), with

photorespiration and the Mehler cycle the most obvious candidates for non-

photosynthetic electron transport (see Fryer et al. 1998; Figueroa et al. 2003). It is

clear that for a range of photosynthetic organisms, including corals, a decline in

electron transport rates at high light levels is not representative of a decline in

photosynthetic oxygen evolution.

Despite negligible costs associated with photoinhibition on a daily basis,

repeated exposure to high irradiance does have a negative impact on photosynthetic

energy acquisition in corals. Cell damage caused by prolonged exposure to

ultraviolet light represents an additional factor that may inhibit coral growth in

shallow (high-light) habitats (e.g. Jokiel & York, 1982), although there is some

evidence that higher concentrations of MAAs in shallow corals may be sufficient to

mitigate the effects of ultraviolet light on rates of photosynthesis (Shick et al. 1995).

Clearly, colonies of *T. mesenterina* acclimated to high light would have greater daily

energy acquisition if they had higher symbiont population densities, a lower sub-saturation irradiance (E_K) and a higher maximum rate of photosynthesis (P_{MAX}). Although this study demonstrates that there are negligible energetic costs associated with short-term (one-day) exposure to excessive irradiance, that the abovementioned combination of photosynthetic properties does not occur is evidence that avoiding damage to the photosynthetic apparatus is a fundamental component of acclimation to high light environments. This conclusion is supported by the observed reduction in chlorophyll concentration for low-light acclimated corals following repeated exposure to excessive irradiance. Continued reduction of chlorophyll concentration through time must eventually lead to a reduced daily energy acquisition per unit colony surface area (e.g. daily integrated photosynthesis of high-light acclimated corals compared with medium-light acclimated corals in the present study). Collectively my results indicate that costs of photoinhibition in corals are manifest over time scales of days to weeks, rather than being apparent over a diurnal irradiance cycle as observed in other taxa (e.g. Platt et al. 1980, Ogren & Sjostrom, 1990). These findings are consistent with recent observations of seasonal fluctuations in photosynthetic activity of several coral species in the Caribbean (Warner et al. 2002), and also explain why a moderate decrease in light availability within habitats either has no effect on photosynthetic energy acquisition for corals, or leads to higher photosynthesis for colonies from shaded habitats (as per Titlyanov 1991a). The trade-off between efficient utilization of light for photosynthesis and avoidance of cumulative damage to the photosynthetic apparatus due to repeated exposure to excessive irradiance suggests that higher light availability does not equate to higher energy acquisition. This phenomenon is investigated in the following Chapter.

2.6 Conclusions

This study demonstrates that changes in the photochemical activity of zooxanthellae over a diurnal irradiance cycle do not cause a reduction in photosynthetic energy acquisition for coral colonies. Indeed, for corals, photoinhibition is manifest through a different mechanism than for other photosynthetic organisms. For some species of microalgae, energetic costs of photoinhibition become apparent through decreased maximum rates of photosynthesis under exposure to light levels comparable to those used in this study (e.g. Platt et al. 1980, Pahl-Wostl et al. 1992), or through reduced photosynthetic efficiency following high light exposure that causes a reduction in rates of photosynthesis (e.g. Kana et al. 2002). In contrast, energetic costs of photoinhibition in corals become apparent as a gradual reduction in photosynthetic capacity through time (over several days) following repeated exposure to excessive irradiance. These results indicate that, for corals, long-term rather than diurnal changes in photosynthetic properties are the key to understanding ecological impacts of environmental gradients in light intensity.

3 EFFECTS OF PHOTO ACCLIMATION ON NICHE WIDTH OF CORALS: A PROCESS-BASED APPROACH

3.1 Summary

The ecology and physiology of photosynthetic organisms is highly influenced by the need to adjust the photosynthetic apparatus to suit variable light environments (i.e. photoacclimation). However, the functional relationships between growth irradiance, key properties of the photosynthetic apparatus and the width of the light niche, have not been formally quantified. In this chapter, I apply a mechanistic photosynthesis model to characterise the light niche of a reef-building coral (*Turbinaria mesenterina*), and to resolve how niche boundaries are influenced by photoacclimation. Model analyses demonstrate variation in photosystem properties that is consistent with values reported in the literature (i.e. photoacclimation to high-light decreases photosynthetic unit size, and increases the absorption cross-section of chlorophyll-*a*). When the different processes of photoacclimation were combined in a mechanistic framework, results demonstrated that habitats with the highest light availability do not lead to maximal energy acquisition. Instead, the energetically optimal environment for *T. mesenterina* falls in the mid-range of the light niche. Using a sensitivity analysis, I also showed that decreasing maximum PSU size, increasing minimum absorption cross-section and decreasing rates of respiration are the most effective mechanisms for increasing the breadth of the light niche. Further, costs associated with photo-protection in high-light habitats outweigh the energetic benefits that could be achieved through increased light-harvesting. The analyses

presented in this chapter enables identification of the specific photo-physiological

processes that define the light niche.

3.2 Introduction

The ecology and physiology of photosynthetic organisms is strongly

influenced by the requirement to adjust their photosynthetic apparatus according to

local light environments (i.e. photoacclimation). For plants in understory habitats,

rapid acclimation to increased light intensity is essential to mitigate effects of

photoinhibition caused by disturbance to the forest canopy (Houter and Pons 2005).

For phytoplankton, vertical mixing of the water column exposes cells to highly

variable irradiance regimes over diurnal cycles, requiring rapid adjustment of their

photophysiology (Flameling and Kromkamp 1997). Similarly, for benthic marine

organisms, variation in water quality and tidal cycles can drive order-of-magnitude

fluctuations in average light intensity at a given depth (Anthony et al. 2004). Past

studies have discussed the potential for photoacclimation to enhance the conditions

under which growth and survival is possible (e.g. Richardson et al. 1983; Anderson

et al. 1995), but such effects have not yet been quantified. Moreover, although there

is evidence that plants with high photoacclimation capacity occur in a broader range

of habitats compared to other species (Murchie and Horton 1997), mechanistic links

between photoacclimation and the light niche have not been established.

Exposure to different light environments during growth causes variation in

numerous properties of the photosynthetic apparatus: from light-harvesting capacity

to changes in the rate at which light is used for carbon fixation (Chang et al. 1983;

Dubinsky et al. 1986). In general, high-light acclimated organisms have enhanced

capacity for photosynthetic (oxygenic) and non-photosynthetic electron transport,

while low-light acclimated organisms harvest light more efficiently (Anderson et al. 1995; Walters 2005). However, the majority of studies measure photosynthetic responses at only two or three light-levels, (Falkowski et al. 1981; Robison and Warner 2006), or over a fraction of a species' light niche (e.g. Anthony and Hoegh-Guldberg 2003b). Where photoacclimation has been investigated over a broader range of conditions, non-monotonic relationships have been observed between photosynthetic activity and the irradiance at which organisms are grown (i.e. growth irradiance, Bailey et al. 2001; Adolf et al. 2003). Moreover, tradeoffs are evident between different elements of the photosynthetic apparatus. This suggests that quantitative analyses of the links between photoacclimation and organism performance need to consider multiple elements. For example, higher chlorophyll concentration within cells in low-light environments comes at the cost of reduced efficiency of light capture per chlorophyll molecule (see Walters 2005). At the high end of the light scale however, reductions in chlorophyll concentrations may lead to supra-optimal irradiances and potential photo-damage (Enriquez et al. 2005). The complexity of photoacclimatory responses means it is unclear how daily photosynthetic energy acquisition varies along environmental gradients of light intensity. To investigate this question, I used a mechanistic photosynthesis model that allowed me to quantify the dynamic interplay between different components of the photosynthetic apparatus, and the effects of this coupling on the size and shape of the light niche.

The primary aim of this study was to determine how variation in properties of the photosynthetic apparatus influences photosynthetic energy acquisition along a light intensity gradient, using the reef-building coral *Turbinaria mesenterina* as a model organism. I also aimed to establish which photosynthetic properties have the

greatest influence on niche width, and how the interactive effects of these properties influence energy acquisition. To achieve these objectives, I first quantified variation in oxygen quantum yield, turnover time, absorption cross-section and photosynthetic unit size over a gradient of light intensity. I then combined into a mechanistic photosynthesis model (Zonneveld 1997), the functional responses between each of these photosynthesis properties and growth irradiance. This approach provides a framework for assessing the sensitivity of energy acquisition to the overall photoacclimatory response, and to the functional responses of individual components of the photosynthetic apparatus.

3.3   Materials and methods

3.3.1   Modelling framework

To explicitly incorporate each of the major properties of the photosynthetic apparatus I used a model developed by Zonneveld (1997). This model describes the relationship between photosynthesis and instantaneous light intensity based on the activity of photosynthetic units (PSUs), rather than the empirical equations used for traditional photosynthesis versus irradiance (PE) curves (e.g. Jassby and Platt 1976). Specifically, Zonneveld (1997) models the rate of photosynthesis (P, measured as oxygen evolution) at a given light intensity are proportional to the number of transitions of activated photosynthetic units (i.e. PSUs that have absorbed light) to their resting state. In a given time interval, the probability that a PSU is in the resting state, p_r, changes as a function of the rates of activation and deactivation. Activation rate depends upon light absorption and deactivation rate depends upon the turnover time of photosynthetic electron transport, τ.

$$\frac{d}{dt} p_r = -\frac{Q\sigma E}{\gamma} p_r + \frac{(1 - p_r)}{\tau} \qquad \text{Eqn 3.1}$$

where E is irradiance (μmol quanta m^{-2} s^{-1}), Q is chlorophyll per PSU (mg chl (μmol PSU)$^{-1}$), σ is the absorption cross-section of chlorophyll (m^2 mg chl^{-1}), γ is the number of photons required to activate a PSU (equal to 1 μmol quanta (μmol PSU)$^{-1}$, Zonneveld 1997), and τ is the average time that a PSU remains in the activated state (i.e. turnover time). Setting Eqn 3.1 equal to zero and solving for p_r, gives the equilibrium probability, $\hat{p}$, that a PSU is in the resting state:

$$\hat{p} = \frac{\gamma}{\gamma + Q\sigma\tau E} \qquad\qquad \text{Eqn 3.2}$$

Multiplying this fraction by the total number of PSUs per cell or unit area (N), the transition rate per PSU ($[Q\sigma E]/\gamma$), and the total oxygen yield per transition, Φ_M, gives photosynthesis as a function of irradiance. Total chlorophyll per cell or unit area is equal to $Q\bullet N$. Therefore, the rate of photosynthesis as a function of irradiance can be normalised to chlorophyll concentration by dividing by $Q\bullet N$ (see Zonneveld 1997 for details):

$$P = \Phi_M \frac{\sigma E}{\gamma + Q\sigma\tau E} \qquad\qquad \text{Eqn 3.3}$$

Equation 3.3 expresses the relationship between photosynthesis rate and instantaneous irradiance as an explicit function of four parameters: oxygen quantum yield (Φ_M), absorption cross-section (σ), chlorophyll per PSU (Q) and turnover time (τ). Building on this mechanistic equation, I extended the model in two ways. Firstly, I expressed each parameter as a function of growth irradiance, and used experimental data to calibrate these functions (see section 3.3.4). Secondly, I calculated total daily photosynthesis, P_{day}, by integrating Eqn 3.3 over the daylight period, given irradiance as a function of time since dawn, t:

$$P_{day} = \int_{t=0}^{12} \Phi_M \frac{\sigma E(t)}{\gamma + Q\sigma\tau E(t)} dt \qquad\qquad \text{Eqn 3.4}$$

The diurnal irradiance cycle is generally modeled as a sine function (Marra 1978):

$$E(t) = E_{max}(\sin \pi t/\lambda)^3 \qquad\qquad \text{Eqn 3.5}$$

where E_{max} is maximum daily irradiance corresponding to a given growth irradiance, and λ is day length. Subsequently, the net daily energy gain (or loss) at a particular growth irradiance can be determined by subtracting daily respiration (R_{DARK}, baseline oxygen consumption) calculated over a 24-hour period, from Eqn 3.4 evaluated over the diurnal irradiance cycle.

3.3.2 Data sources for model calibration

I used the following data sources to quantify how each parameter of the mechanistic model changes with growth irradiance. To estimate Q and σ, I fitted the mechanistic model to PE curve data (normalized to chlorophyll-*a*) for colonies of the study species grown under different light conditions (see Section 3.3.3). For these same colonies, fluorescence assays of maximum quantum efficiency were measured as a proxy for oxygen quantum yield (Φ_M, see below). Finally, measurements of turnover time have been reported in the literature for a numerous photosynthetic taxa (e.g. Dubinsky et al. 1986). Therefore, to avoid high uncertainty in parameter estimates associated with fitting multiple parameters to PE curve data, literature data were used to calibrate a general relationship between PSU turnover time and growth irradiance. For each model parameter (Q, σ, Φ_M, and τ), I hypothesized the functional relationship with growth irradiance based on general trends identified in the literature (instead of fitting arbitrary regression curves). I then fit these functions to data to test whether the hypothesized relationships were supported, and to estimate the parameters that quantify the strength and shape of these relationships. All

parameter estimates were conducted using a non-linear estimation routine in Statistica (Release 7, Statsoft Inc.).

In addition to the parameters described above, estimates of dark respiration and chlorophyll concentration per unit surface area are required for calculation of daily-integrated photosynthesis. Therefore, I also measured rates of dark respiration (baseline oxygen consumption) as a function of growth irradiance (see Section 3.3.3). In addition, although the mechanistic model is expressed as the chlorophyll-specific photosynthesis rate, I expressed daily energy acquisition in units per surface area, which is ecologically the most relevant unit (for corals, biological processes such reproduction and mortality [e.g. Babcock 1991], scale with colony surface area). Therefore, I also measured (and modelled) chlorophyll concentration per unit surface area as a function of growth irradiance.

3.3.3 Data collection

I used the same methods for measuring photosynthesis/irradiance curves (PE curves) as in the previous chapter. Briefly, 40 flat colonies of *Turbinaria mesenterina* (measuring approximately 10 cm by 10 cm) were collected from between 2 and 6m depths in Nelly Bay and Cockle Bay, Magnetic Island, Australia (19°09S, 146°53E). Collecting was conducted from widely separated clones to ensure representation by a maximum number of genets. Colonies were transported to aquarium facilities at James Cook University, distributed among tanks with varying light regimes, and allowed 6 weeks for recovery and photoacclimation. To provide a source of nutrients, corals were fed newly hatched *Artemia* nauplii and/or rotifers daily. Oxygen respirometry assays were conducted using clear Perspex incubation chambers (2.7 litre volume) with calibrated Clark-type oxygen electrodes (Cheshire Systems, Australia) attached to a data logger (CR10X, Campbell Scientific

Australia). Chambers were submerged in a 1000L water jacket to ensure consistent temperature during all measurements. Light regimes for photosynthesis assays and light acclimation treatments were generated using sets of metal halide lamps (each 400W, Eye, Japan) suspended above the chambers and aquaria. Temperature was monitored across all aquaria, and was kept consistent (27ºC, similar to field conditions) using a continuous flow of temperature-controlled water. Corals were oriented parallel to the light source to ensure consistent irradiance over the entire colony surface. For the photosynthesis measurements, I increased irradiance over the course of a 9- to 11-hour period by changing the elevation of the lamps. This duration of time was required to obtain an adequate number of points on the PE curve for each colony. Light levels (photosynthetically active radiation) were measured using a cosine-corrected Licor probe (Li-192S) attached to a Li-1000 data logger (Licor, Nebraska).

Fluorescence assays were carried out using a pulse-amplitude-modulated fluorometer (Mini-PAM, Walz) fitted with a 5mm diameter optical fibre. I measured dark-adapted maximum quantum yield of photochemistry (F_v:F_m, dimensionless, see below) for colonies prior to respirometry runs. For the fluorescence assays, I collected an additional 30 small fragments (2-3cm diameter). These fragments were not used for respirometry runs because they were too small to generate a reliable oxygen flux signal during the measuring period.

For a subset of the experimental corals, colonies were sacrificed immediately after the respirometry assays, frozen at –40°C, and later used for determination of chlorophyll-*a* content. Colonies were broken into 2 replicate fragments and photographed with a ruler using a Canon-G3 digital camera. Surface areas were determined using Image Tools (UTHSCSA, version 3). Coral fragments were then

ground into a fine paste, and chlorophyll extracted in acetone. To ensure that all

chlorophyll was extracted from each fragment, the initial extraction (12hr) was

followed by two one-hour extractions. The combined volume of all extracts was

measured, the extract centrifuged and replicate absorbance readings were carried out

at 630nm and 663nm. Concentrations of chlorophyll-*a* were determined using the

equations of Jeffrey and Humphrey (1975).

3.3.4 Relationships between model parameters and growth irradiance

3.3.4.1 Oxygen quantum yield

There is little evidence as to how oxygen yield per unit light absorbed, Φ_M (µmol O$_2$

(µmol quanta)$^{-1}$), varies with growth irradiance (E_μ). However, fluorescence assays

of photochemistry indicate that the analogous fluorescence parameter (maximum

quantum efficiency, $F_v{:}F_m$) decreases with increasing growth irradiance for coral

symbionts (Warner et al. 2002). Although fluorescence assays of photochemistry

generally correlate poorly with net oxygen flux measurements measured under high

irradiance (e.g. Ulstrup et al. 2006), in the previous Chapter I showed that these two

assays are approximately linearly related when measured under near-dark conditions

(Hoogenboom et al. 2006). Therefore, I here assume that Φ_M is proportional to $F_v{:}F_m$

and use an equation presented by Suggett et al. (2003) to model this relationship. I

multiply Suggett et al's (2003) equation by the number of photons required to

activate a PSU, γ, in order to convert the equation to units appropriate to the

mechanistic model.

$$\Phi_M = \frac{\gamma}{k}\left(F_v : F_m\right) \qquad\qquad \text{Eqn 3.6}$$

where γ is as defined above, $F_v{:}F_m = (F_m{-}F_0){:}F_m$ with F_0 and F_m equal to steady-state and maximal fluorescence measured in darkness, k is the number of charge-separation events required to reduce 1 mol of O_2, and has a theoretical minimum value of 8 mol electrons mol O_2^{-1} (Suggett et al 2003). There has been considerable debate regarding the relationship between fluorescence and gas-exchange measures of photosynthesis (see Maxwell and Johnson 2000). Therefore, I used a sensitivity analysis to assess the robustness of my results to different values of k (see Results).

3.3.4.2 *Light absorption*

The PE curve measurements relate oxygen evolution per unit chlorophyll to irradiance incident to the coral tissue. On the other hand, the measure of quantum yield and the other parameters of the mechanistic model, relates oxygen evolution to light absorbed by PSUs. The absolute light absorption properties of *T. mesenterina* are unknown. However for a range of coral species the percentage of incident irradiance absorbed by tissue ranges from 42 – 100% (mean of approximately 77%), with no evidence of consistent variation in total light absorption with the position of colonies along a depth gradient (Wyman et al. 1987). Further confirmation of high light absorption by coral tissue, and a lack of variation in absorption with depth, comes from the work of Enriquez et al. (2005) on the effects of skeleton properties on light capture. Accordingly, I converted the PE curve measurements from oxygen per incident irradiance to oxygen evolution per unit irradiance absorbed by tissue assuming 77% light absorption. In addition, I conducted a sensitivity analysis to determine whether my results were sensitive to the specific value of this parameter (see Results).

3.3.4.3   Turnover time

The duration of time needed for light to be absorbed and passed through the PSU (i.e.

turnover time, τ) decreases with acclimation to high light levels for a range of

photosynthetic taxa (e.g. Dubinsky et al. 1986). In other words, high-light acclimated

plants/algae use light more quickly than those acclimated to low-light levels.

Therefore, I expected that turnover would be high at low light levels and decrease

asymptotically with acclimation to high light. This asymptote reflects the maximum

possible activity of the enzymes involved in carbon fixation. To model this

relationship, I fitted an inverse Michaelis-Menten equation (see Table 3.1) to

measurements of turnover time reported in the literature.

Table 3.1: Modelled dependence of photosynthesis parameters on growth
irradiance: summary of functional forms and parameter estimates

Model parameter	Description (units)	Equation	Parameter estimate ($\pm$ standard error)
Φ_M	Maximum quantum yield (μmol O_2 (μmol quanta)$^{-1}$)	$\Phi_M = \dfrac{\gamma}{k}(F_v : F_m),$ where: $F_v{:}F_m = \Phi\exp(-\omega E_\mu)$	$\gamma = 1$ (Zonneveld, 1997) $k = 8$ $\Phi = 0.08$ (0.0009) $\omega = 0.0006$ (0.00004)
τ	Average turnover time of PSU (ms)	$\tau = \dfrac{K_\tau + E_\mu}{\tau_{min} E_\mu}$	$K_\tau = 29$ (8) $\tau_{min} = 0.21$ (0.02)
σ	Absorption coefficient of chlorophyll (m^2 mg chl a^{-1})	$\sigma = \sigma_{min} \exp(\lambda E_\mu)$	$\sigma_{min} = 0.04$ (0.004) $\lambda = 0.002$ (0.0003)
Q	Chlorophyll per PSU (mg chl a (μmol PSU)$^{-1}$)	$Q = q/(1 + \varphi E_\mu)$	$q = 50$ (3.0) $\varphi = 0.003$ (0.0007)
C	Chlorophyll a concentration (mg chl cm^{-2})	$C = c_{max}/(1 + \varepsilon E_\mu)$	$c_{max} = 35$ (3) $\varepsilon = 0.005$ (0.002)
R_D	Rate of dark respiration (μmol O_2 mg chl a^{-1} s^{-1})	$R_D = r \exp(\rho E_\mu)$	$r = 0.05$ (0.006) $\rho = 0.002$ (0.0002)

3.3.4.4   Chlorophyll concentration

Based on evidence in the literature for corals and phytoplankton (Wyman et al. 1987;

Behrenfeld et al. 2002), I expected chlorophyll concentration to decline

asymptotically with acclimation to high irradiance (see Table 3.1).

3.3.4.5   Absorption cross-section and PSU size

The absorption cross-section of chlorophyll, σ, is generally lower for photosynthetic organisms from low-light habitats (reviewed in MacIntyre et al. 2002). Conversely, PSU size (Q) is often lower for high-light acclimated organisms (e.g. Falkowski and Owens 1980; Iglesias-Prieto and Trench 1994). As mentioned above, the mechanistic model (Eqn 3.3) was fitted to PE-curve measurements in order to measure these parameters for the experimental colonies. Because Q is measured as chlorophyll per PSU, as a first approximation I expected that this parameter would be proportional to chlorophyll per unit area. Therefore, I fitted the same asymptotically declining equation to Q data as that used for chlorophyll data (see Table 3.1). Finally, I expected an inverse relationship between PSU size and absorption cross-section (i.e. that small PSUs capture more light per unit PSU size). Therefore, an exponential equation was used to capture variation in the latter as a function of growth irradiance (Table 3.1).

3.3.4.6   Dark respiration

Baseline rates of respiration, R_{DARK} (μmol O_2 mg chl-a^{-1} s^{-1}), represent maintenance metabolism along with energy expenditure for growth and reproduction (Raven 1976). For corals, high-light acclimated colonies generally have higher respiration rates than those grown under shaded conditions (Dustan 1982, Chapter 2). I hypothesized that acclimation to high light levels would have an increasingly strong effect on respiration rate. Therefore, an exponential function was fitted to to measurements of respiration rate (R_{DARK}) as a function of growth irradiance.

3.3.5   Daily energy acquisition

Energy acquisition was calculated as the ratio of daily-integrated photosynthesis to total costs of respiration (P:R ratio). I calculated integrated

photosynthesis across a range of growth irradiances between 50 - 1000 μmol quanta

m^{-2} s^{-1} (daily maximum irradiance between 120 and 2000 μmol quanta m^{-2} s^{-1}). This

light gradient approximates the depth range of the study species at collection sites. A

numerical discretization written in Matlab (Release 13, MathWorks) was used to

evaluate Eqn 3.4, with time-steps of 72s (beyond which the numeric evaluation

converged to a constant value). In this study, the light niche for *Turbinaria*

mesenterina is defined as the range of conditions where the P:R ratio is greater than 1

(i.e. photosynthesis is greater than respiration, see Chapter 1).

I used a Monte Carlo simulation technique to analyse the influence of

uncertainty in parameter estimates on the calculations of niche width, and on the

relationships between the different photosynthesis parameters. To do this, I iterated

calculations of daily energy acquisition as a function of growth irradiance 1000

times, each time using different parameter values for each photoacclimation sub-

model that were randomly selected from 2-dimensional Gaussian uncertainty

distributions (each photoacclimation sub-model has 2 fitted parameters). These

distributions were generated using the best-fit parameters and covariance matrix for

each sub-model. Finally, I analysed the sensitivity of the upper and lower niche

boundaries for *T. mesenterina* to a fixed change (10%) in each parameter. This

analysis indicates what changes to the photoacclimation strategy would be required

for this species to expand its light niche. This latter technique was also used to

measure the sensitivity of both the niche boundaries and the fitted model parameters

to variation in the value of k (Eqn 3.6) and the % of irradiance absorbed by tissue.

3.4 Results

All four components of the photosynthetic apparatus varied substantially

across the experimental light gradient, although each responded to growth irradiance

in a different way (Figure 3.1A-D). In all cases, plots of residuals versus predicted

values indicated that the hypothesized functional forms adequately captured the

response for each photosynthesis parameter. Moreover, all of the parameter estimates

of the photoacclimation models were significantly different from zero (Table 3.1).
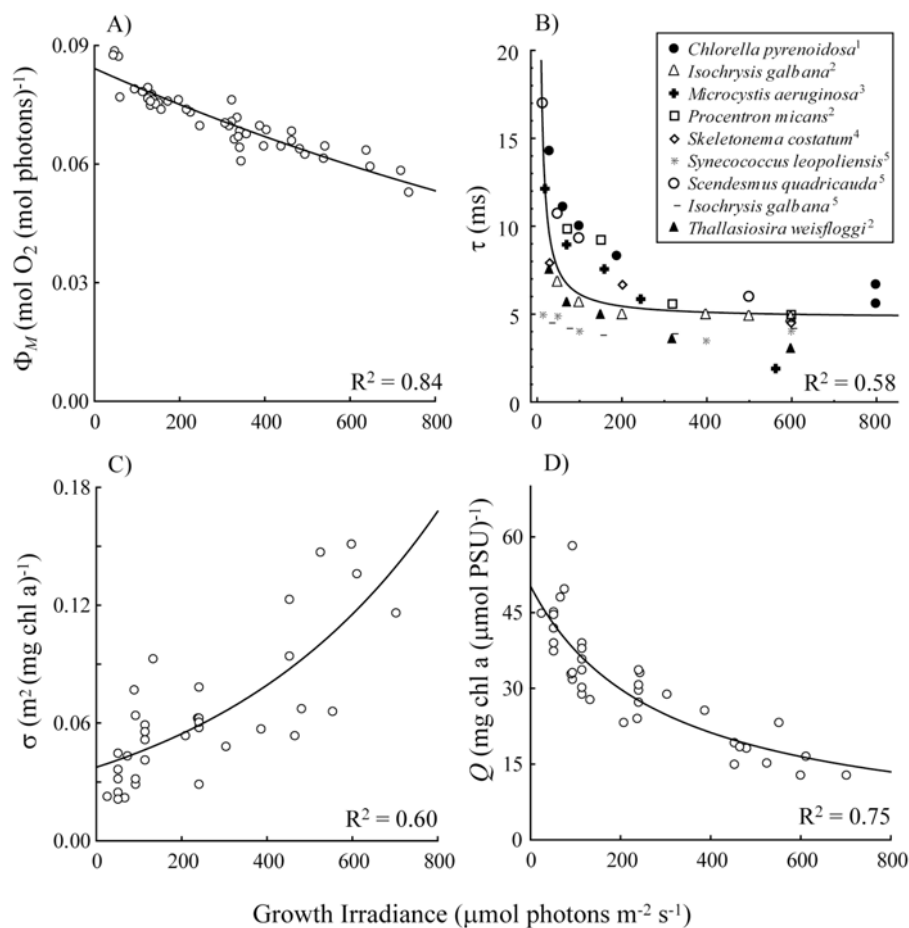
Figure 3.1: Effects of growth irradiance on photosynthesis properties of *Turbinaria mesenterina*. A) oxygen quantum yield, B) photosynthetic turnover time for 8 phytoplankton species (1. Myers and Graham 1971, 2. Dubinsky et al. 1986, 3. Raps et al 1983, 4. Falkowski et al. 1981, 5. Herzig and Dubinsky 1992). C) and D) absorption cross-section and PSU size respectively, as estimated from photosynthesis/irradiance curves. See Table 3.1 for parameter estimates.

An approximately 2-fold exponential decline in maximum quantum yield of oxygen evolution (Φ_M) was observed over the experimental light-intensity gradient ranging from 50 – 75 μmol quanta m^{-2} s^{-1} (Figure 3.1A). This decline was driven mainly by an increase (approximately 1.5-fold) in F_0 across the light intensity gradient (Product moment correlation, r = 0.54, p < 0.05). In addition, F_m declined with increasing growth irradiance, albeit to a lesser extent (13% decline, r = -0.20, p < 0.05). The observed relationship between quantum yield and growth irradiance was consistent for both 10cm colonies and small (2-3cm diameter) fragments.

Based on data from the literature for 8 different phytoplankton species, PSU turnover time decreased with acclimation to high light (Figure 3.1B). However, most of the variation in this parameter occurred over the low-light region of the growth irradiance gradient for each species – that is, turnover time for most species was approximately the same for cells acclimated to all light levels above approximately 300 μmol quanta m^{-2} s^{-1}. When fitted individually to the data for each species, parameter estimates of the inverse Michaelis-Menten function varied between 4 and 80 for K_τ, and between 0.15 and 0.29 for τ_{min}. However, the curve based on average parameter values (across species) of $K_\tau = 29 \pm 8$ (standard error), and $\tau_{min} = 0.21 \pm 0.02$ (standard error), explained 58% of the total variance in the combined dataset, despite inclusion of several different phytoplankton groups (green algae, cyanobacteria, dinoflagellates and diatoms).

Analysis of experimental data for *Turbinaria mesenterina* revealed a 3-fold increase in the absorption cross-section of chlorophyll (σ) (Figure 3.1C), and a 4-fold decrease in PSU size (Q, Figure 3.1D) over a growth irradiance gradient ranging from 20 and 700 μmol quanta m^{-2} s^{-1}. In other words, high-light acclimated colonies

of the study species have smaller PSUs (fewer chlorophyll molecules associated with

each reaction center), with a corresponding increase in the probability that a given

molecule of chlorophyll will absorb light. In both cases, the model provided adequate

fit to the data (see Table 3.1 for parameter estimates).

Chlorophyll concentration per unit surface area showed the expected

relationship with growth irradiance, declining markedly with acclimation to high

light for the study species (Figure 3.2A). Based upon comparison of the relative rates

of decline of chlorophyll per unit area and chlorophyll per PSU, these results suggest

an approximately 25% decline in the number of PSUs per unit surface area ($N =$

C/Q) across the experimental light-intensity gradient. This occurred in addition to the

decline in PSU size (although differences in the rates of decline of C and Q with

increasing growth irradiance were marginally non-significant, t = 1.5, df = 70, p

=0.06). Finally, rates of dark respiration increased strongly with acclimation to high

light levels, and the hypothesized relationship provided a good fit to the measured

data (Figure 3.2B).
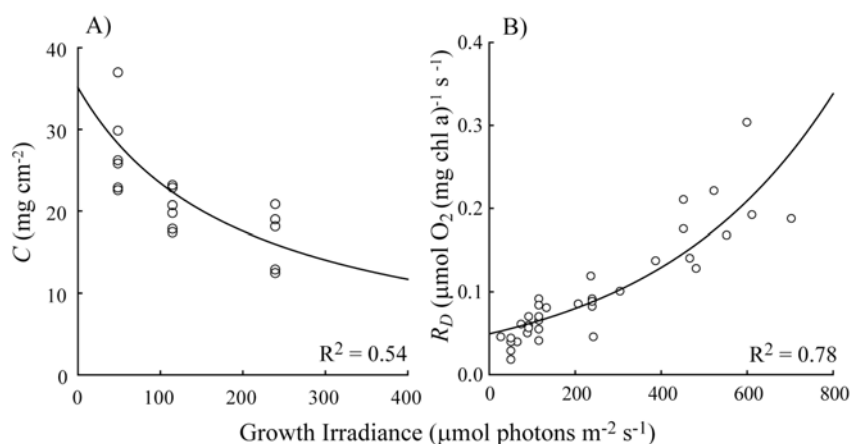
Figure 3.2: Effects of growth irradiance on chlorophyll concentration per unit tissue surface area (A) and rate of dark respiration (B) for *Turbinaria mesenterina*. See Table 3.1 for parameter values of fitted functions.

Consistent with expectations, the parameters estimated from fitting the mechanistic model to PE curve data indicate trade-offs between properties of the photosynthetic apparatus (Figure 3.3). Absorption-cross section was inversely related to PSU size, indicating the presence of a 'package effect' (Figure 3.3A). However, these analyses also revealed that for low-light acclimated colonies (high values of Q) increasing PSU size has a diminishing influence on light absorption. Conversely, for high-light acclimated colonies, a small increase in PSU size yielded a large decrease in absorption cross-section. The opposite pattern was apparent for the relationship between turnover time and PSU size (Figure 3.3B). For low-light acclimated colonies, small changes in PSU size were accompanied by large changes in turnover time whereas the reverse was true for high-light acclimated colonies.
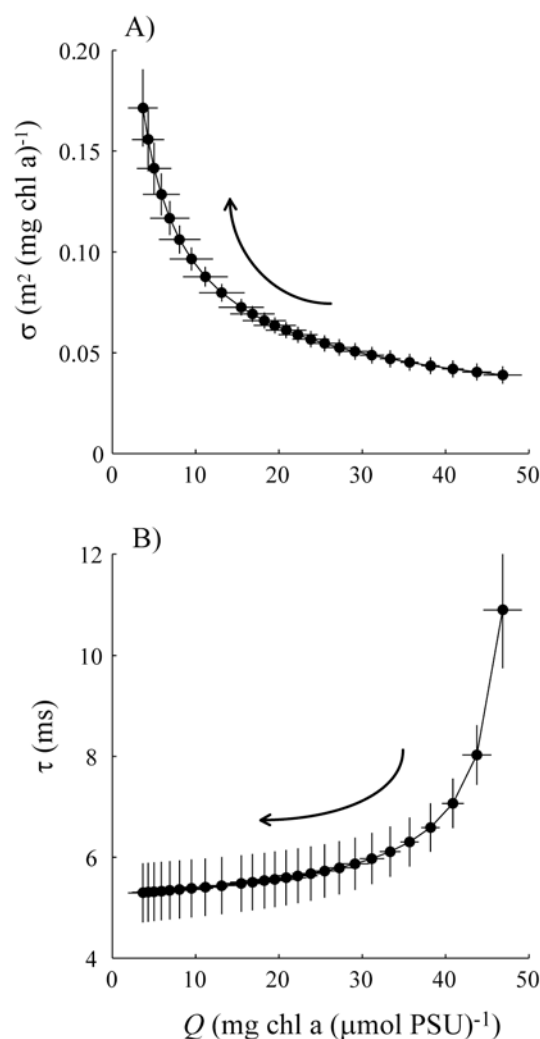
Figure 3.3: Tradeoffs between different properties of photosynthesis showing the relationships between A) absorption cross-section (σ) and B) turnover time (τ) with photosynthetic unit size (Q). Error bars represent standard deviation of average parameter values generated by 1000 Monte Carlo iterations. Arrows indicate direction of increasing growth irradiance.

3.4.1 Daily energy acquisition and the light niche

Daily-integrated net photosynthesis showed a hump-shaped relationship with growth irradiance (Figure 3.4). These analyses showed that *Turbinaria mesenterina* has a positive energy balance (P:R ratio > 1) at growth irradiances between 91 and 696 μmol quanta m^{-2} s^{-1} (thick horizontal bar in Figure 3.4). The upper (high-light) boundary of the niche was more sensitive to uncertainty in the parameter estimates of the photoacclimation sub-models than the lower boundary (whiskers on horizontal bar in Figure 3.4). However, there were no combinations of parameter values for which the highest growth irradiance allowed a positive energy balance. In addition, the optimal growth irradiance of approximately 300 μmol quanta m^{-2} s^{-1} was relatively low (peak of the solid curve in Figure 3.4) and when uncertainty in parameter estimates was taken into account, varied only between 236 and 326 μmol quanta m^{-2} s^{-1}.
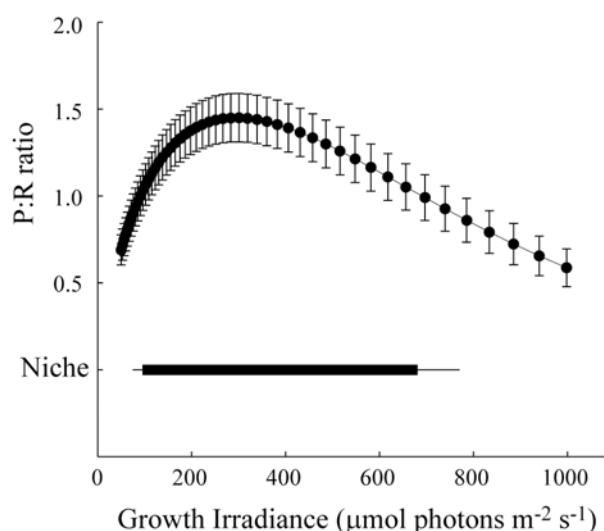
Figure 3.4: Dimensions of the light niche for *Turbinaria mesenterina* based on photosynthesis to respiration ratios along a growth irradiance gradient. Error bars are standard deviations due to uncertainty in parameter estimates, generated by 1000 Monte Carlo iterations. Horizontal bar indicates the mean niche width, with whiskers depicting standard deviation.

The position of the light-niche boundaries for *Turbinaria mesenterina* were insensitive to variation in both the proportion of incident irradiance absorbed by colonies, and the value of the constant (*k*) used to derive maximum quantum yield from the fluorescence assay of maximum quantum efficiency (Figure 3.5). This lack of sensitivity is related to the fact that the shape of the niche in my analyses is ultimately determined by the underlying photosynthesis versus irradiance curves. In effect, varying the values of *k* and % light absorption adjusts the height (*k*, influences oxygen production per light) and width (lower % absorption reduces the span of the light axis) of the PE curve. These parameters therefore influence the magnitude of the other fitted model parameters (*Q* and *σ*, Table 3.2). However, because *k* and % light absorption do not influence the curvature of the PE curve, variation in the magnitude of these parameters does not influence the light niche.
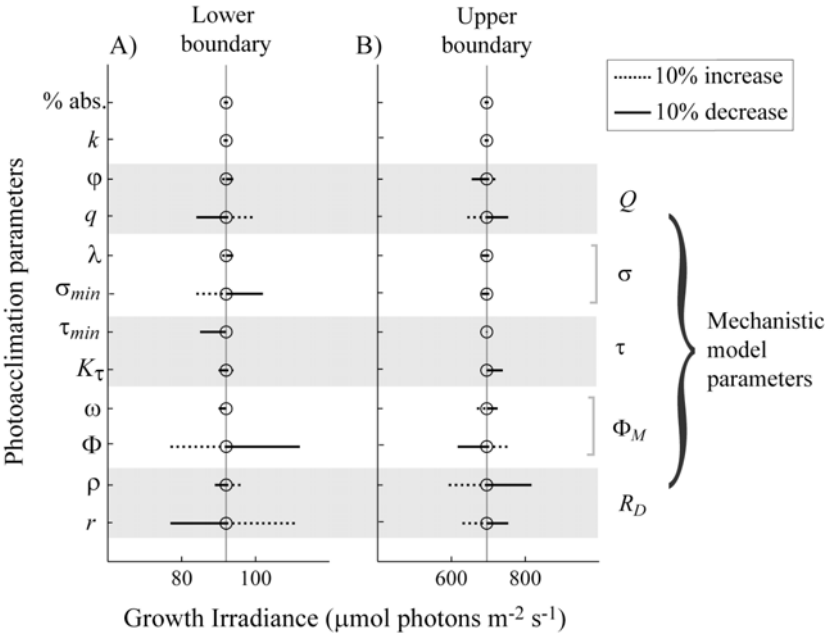
Figure 3.5: Sensitivity of lower (A) and upper (B) niche boundaries to each parameter that describes photoacclimation to growth irradiance for *Turbinaria mesenterina*. Circles mark the position of the mean niche boundary, and lines indicate the shift in the niche boundary due to a 10% increase or decrease in each parameter.

Table 3.2: Sensitivity of the relationships between PSU size (Q) and absorption cross-section (σ) with growth irradiance due to variation in the values of k (number of charge separation events required to reduce O_2) and % light absorption. Q and σ are related to growth irradiance (E_μ) by the following functions: $Q = q/(1 + \varphi E_\mu)$ and $\sigma = \sigma_{min}\exp(\lambda E_\mu)$. Standard errors of parameter estimates are shown in parentheses.

Parameter	Original value $k = 8$ light abs. = 77%	Sensitivity to k		Sensitivity to light absorption	
		$k = 8.8$	$k = 7.2$	85%	69%
q	50 (3)	46 (3)	56 (3)	50 (3)	50 (3)
φ	0.003 (0.0007)	0.003 (0.007)	0.003 (0.007)	0.003 (0.007)	0.003 (0.007)
σ_{min}	0.04 (0.004)	0.041 (0.005)	0.034 (0.004)	0.042 (0.005)	0.034 (0.004)
λ	0.002 (0.0003)	0.002 (0.0003)	0.002 (0.0003)	0.002 (0.0003)	0.002 (0.0003)

For *T. mesenterina*, the boundaries of the light niche were most sensitive to variation in respiration rates, quantum yield, absorption cross-section and PSU size (Figure 3.5A & B). In general, the rates at which properties of photosynthesis changed with growth irradiance (slopes of curves in Figure 3.1 & 3.2) had less influence on niche width than the maximal or minimal values (y-intercepts or asymptotes in Figure 3.1 & 3.2). For example, in the equation describing changes in PSU size (Q) with growth irradiance (E_μ) as $Q = q \exp(-\varphi E_\mu)$, the y-intercept of this equation, q (maximum PSU size), has a greater influence on niche width than the slope, φ (Figure 3.5A & B). One exception to this pattern was the sensitivity of the upper niche boundary to the rate at which respiration rate increases with increasing growth irradiance (ρ, Figure 3.5B): decreasing this parameter widened both the upper

and lower niche boundaries. Similarly, decreasing the lower asymptote of the relationship between turnover time and growth irradiance also widened the niche. Counter-intuitively, decreasing maximum PSU size (q) increased niche width. This appears to be related to an increase in the number of PSUs caused by decreasing PSU size without decreasing total chlorophyll (see above). Finally, increasing the minimum value of absorption cross-section also influenced niche width, but only affected the lower bound (Figure 3.5A).

3.5 Discussion

Using a mechanistic framework for linking photoacclimation parameters to photosynthetic performance, this study demonstrates that the light conditions that allow maximal photosynthesis per unit chlorophyll are not the conditions that allow maximal photosynthesis per unit surface area. That is, as corals photoacclimate to high-light levels, increased photosynthesis per unit chlorophyll does not compensate for decreased chlorophyll per unit surface area. Instead, the optimal growth irradiance for *Turbinaria mesenterina* falls in the lower half of the light gradient within which these corals are abundant. Although a similar phenomenon of optimal growth irradiances occurring in the middle of the light-niche has been observed for phytoplankton (Richardson et al. 1983; Babin et al. 1996), this has not previously been shown for corals.

This study is the first to combine multiple processes of photoacclimation into a model that predicts daily-integrated photosynthesis. On balance, the weight of evidence indicates that decreased daily-integrated photosynthesis in high-light habitats is likely to be a general phenomenon for photosynthetic organisms. The generality of my conclusions is supported by evidence of reduced (area or cell

specific) rates of maximum photosynthesis for high-light acclimated corals (Wyman et al. 1987), symbiotic dinoflagellates (Chang et al. 1983) and phytoplankton (Gordillo et al. 2001). From a conceptual standpoint, if tradeoffs between different photosynthesis properties were not apparent, and no factors other than light intensity limited photosynthesis, maximal energy acquisition would be generated by having many rapidly-functioning PSUs, each of which have high chlorophyll content, high light absorption per chlorophyll and generate high oxygen yield per unit light absorbed. However, my results show that for *Turbinaria mesenterina*, photoacclimation to high light results in reduced oxygen quantum yield, less chlorophyll per PSU and fewer PSUs per unit tissue surface area. These findings are consistent with observations of photoacclimation in a range of other taxa (e.g. Dustan 1982; Richardson et al. 1983). Therefore, reduced energy acquisition in high-light habitats may be ubiquitous for photosynthetic organisms.

Based on PE curve data, the calibrated models generated estimates of photochemical parameters generally consistent with experimental data. For corals, measured values of absorption cross-section generally lie within the range of 0.01 to 0.09 (Wyman et al. 1987; Rodriguez-Roman et al. 2006). For *T. mesenterina*, estimates for this parameter range from 0.02 to 0.15 m^2 (mg chl-*a*)$^{-1}$. That these estimates are slightly higher than observed can be explained by the fact that fitting the mechanistic model to PE curve data attributes all light absorption to chlorophyll-a specifically (therefore overestimating absorption cross-section), whereas many other accessory pigments contribute to light absorption by coral colonies (e.g. Chang et al. 1983; Dove et al. 2006). Model estimates of PSU size were approximately an order of magnitude lower than empirical measurements. Converted to units of mol chlorophll-*a* (mol PSU)$^{-1}$ model fits yielded values between 17 – 67 mol^{-1} whereas

measures of PSU size are in the range 200 - 600 mol^{-1} for symbiotic dinoflagellates (Iglesias-Prieto and Trench 1994). Empirical methods generally measure PSU size as the ratio of chlorophyll concentration and oxygen evolved under single-turnover saturating light flashes (e.g. Falkowski et al. 1981; Iglesias-Prieto and Trench 1994). In this study, estimates are derived from net oxygen evolution of symbionts within coral tissue, and are therefore influenced by oxygen consumption (respiration) by the coral tissue. Although the oxygen consumption of coral tissue cannot be separated from that of symbionts, based on relative differences in biomass this is the most likely explanation for the lower than observed estimates of PSU size. This suggests a potential limitation of this approach for estimating photochemical properties of symbionts *in hospite*. For these analyses, Q is best interpreted as the functional size of PSUs generating oxygen that is not consumed by the coral host, rather than a precise estimate of the actual PSU size of symbionts. My analyses are based on measurements of net oxygen evolution at the colony scale and these results are therefore robust to the differences between fitted parameter values and values reported in the literature. In addition, I note that despite potential limitations of estimating symbiont photochemistry from measurements of colony photosynthesis, the alternative approach using empirical measurements of PSU size as model inputs would bias calculations significantly unless differences in oxygen consumption of host and symbionts could be quantified.

Results of this study indicate that photoacclimation of oxygen quantum yield decreases potential energy acquisition. That is, if *T. mesenterina* could maintain high quantum yield across the light gradient, colonies in high-light habitats would have greater energy acquisition and the width of the light niche would increase. Quantum yield may decrease through damage to PSUs, reduced light capture efficiency, and/or

increased dissipation of excitation energy through other pathways (see Maxwell &

Johnson 2000). Increased capacity for dissipation has frequently been observed in

high-light acclimated photosynthetic organisms, generally through increases in

photoprotective pigments (e.g. xanthophyll pigments and carotenoids, Demmig-

Adams and Adams 1992), or in the ratio of these pigments to chlorophylls

(MacIntyre et al. 2002). Similarly, there is evidence for corals that high-light

exposure induces an increase in dark-adapted steady-state fluorescence (F_0) and a

corresponding decline in quantum yield due to damage to PSUs (Gorbunov et al.

2001). For *T. mesenterina*, the variation in quantum yield with acclimation to high-

light was largely driven by an increase in F_0, indicative of damage to PSUs (Krause

1988). However, I cannot entirely distinguish whether this was attributable to

photoinhibition (impairment of function) or photoprotection (enhanced dissipation),

because both processes are increased in high-light acclimated colonies. Importantly,

if costs of damage repair and/or avoidance were less than the reduction in energy

acquisition due to lower quantum yield for high-light colonies, then quantum yield

would not vary with growth irradiance, and damage would most likely be repaired as

it occurred. The fact that the maximum potential value of quantum yield cannot be

maintained in high-light habitats suggests that there are substantial costs associated

with repair of damage to the photosynthetic apparatus.

The analysis of literature data presented in this study indicates that the scope

for photoacclimation of turnover time is limited, with variation in these rates

apparent principally over growth irradiances between 20 and 300 µmol quanta m^{-2} s^{-1}. Turnover time is generally related to concentration of carbon fixation enzymes

(RuBisCo, Sukenik et al. 1987). Interestingly, the functional relationship between

RuBisCo content and growth irradiance also reaches an asymptote at a growth

irradiance of approximately 200 μmol quanta m^{-2} s^{-1} (Bailey et al. 2001). Faster

processing of light through PSUs (i.e. shorter turnover times, τ) represents an

alternative mechanism for avoiding damage under high-light conditions, because

rapid processing of light reduces the probability that an activated PSU will absorb

additional light and becoming damaged (Behrenfeld et al. 1998). However, over the

majority of the light niche, changes in PSU size and quantum yield are not

accompanied by changes in turnover time. In summary, my analyses indicate that the

energetic benefit of increased turnover rate may be outweighed by the costs

associated with building and maintaining additional enzymes needed to achieve this

increase. Overall, it appears that increased dissipation of light through non-

photosynthetic pathways is the major mechanism by which photodamage is avoided.

The analyses presented in this chapter quantify the tradeoff between PSU size

and absorption cross-section, and show how coupling between these two processes

influences the width of the light niche. As observed for other photosynthetic

organisms (e.g. Wyman et al. 1987; Mercado et al. 1996), chlorophyll absorption

cross-section clearly decreases as PSU size increases in symbionts of *Turbinaria*

mesenterina. Therefore, my results support the hypothesis that the principal

mechanism of acclimation to low light (i.e. increased chlorophyll) is self-limiting

because shading between densely packed pigments reduces light absorption per unit

chlorophyll (Anderson et al. 1995; Walters 2005). However, *T. mesenterina* appears

to adopt a sub-optimal strategy with respect to these parameters. Sensitivity analysis

of the model revealed that increasing light absorption and decreasing PSU size both

widened the niche at the low-light boundary. In other words, my data indicate that

low-light acclimated colonies have larger PSUs than is energetically optimal. The

benefit of such redundancy in chlorophyll content is unclear and supports the

hypothesis that maximization of carbon acquisition is not the only mechanism

governing photoacclimation (MacIntyre et al. 2002).

The optimal growth irradiance for *Turbinaria mesenterina* is low compared

to the breadth of light conditions under which this species is found. Under natural

conditions, *T. mesenterina* is morphologically plastic and develops a flat morphology

in deep water, and a vertically oriented, convoluted morphology in shallow waters

(Willis 1985). Previous research indicates that varying colony morphology with

depth adjusts the light environment within colonies to a modal value of

approximately 100-250 μmol quanta m^{-2} s^{-1} (Anthony et al. 2005). This value is close

to the energetically optimal growth irradiance identified in this study (236 to 326

μmol quanta m^{-2} s^{-1}), and suggests that morphological plasticity in this species

optimizes photosynthetic energy acquisition. This phenomenon is investigated in the

following chapter of my thesis.

In the absence of morphological strategies to moderate light capture, the

decline in energy acquisition in high-light habitats raises the question as to why

corals growing under these conditions do not increase their chlorophyll content.

Using turnover time as a proxy for the concentration of carbon-fixation enzymes, the

inverse relationship between turnover time and PSU size describes a trade-off

between the light-harvesting and light-utilisation apparatus. This indicates that

symbionts in coral tissue are nutrient-limited (e.g. Dubinsky and Jokiel 1994)

because if nutrients were in adequate supply an inverse relationship between these

two properties of the photosynthetic apparatus would not be expected. A similar

phenomenon has been observed for leaves within plant canopies, with redistribution

of nitrogen into light-harvesting components of the photosynthetic apparatus

following shade acclimation (Eichelmann et al. 2005), and a greater proportion of

nitrogen allocated to light-use enzymes in high-light acclimated leaves (Terashima & Evans 1988; Hikosaka and Terashima 1996).

3.6 Conclusions

By adopting a mechanistic approach to model changes in the photosynthetic apparatus along a light intensity gradient, this study identifies the processes that respond to growth irradiance and quantifies how they interact to determine the light niche. This chapter shows that, although photoacclimation to high irradiance results in greater capacity for oxygen evolution per unit chlorophyll, habitats with the highest light availability do not provide maximum energy acquisition for *Turbinaria mesenterina*. Instead, my analyses suggest that there are considerable energetic costs associated with living in high-light habitats, including increased baseline metabolic rates and lower oxygen quantum yield related to damage to the photosynthetic apparatus. In addition, this study suggests that nutrient limitation for symbionts within tissue reduces energy acquisition in high-light habitats. High-light acclimated corals have less chlorophyll and therefore acquire less carbon per unit surface area. Rather than allocating limited nutrients to increased light harvesting, these nutrients are instead allocated toward maximizing light utilization. This apparently sub-optimal photoacclimation strategy also indicates that costs associated with building, maintaining and protecting chlorophyll under high irradiance conditions must be substantial.

4 ENERGETIC IMPLICATIONS OF PHENOTYPIC PLASTICITY IN FOLIOSE CORALS

4.1 Summary

Morphological plasticity in response to environmental heterogeneity may be performance enhancing, or may simply result from an intrinsic instability in morphology during development. Although patterns of morphological change are well documented for numerous taxa, it is often unclear whether this plasticity enhances the performance of organisms in the habitat to which they have acclimatized. Reef-building corals are an ideal model system in which to investigate this question. I here develop a three-dimensional geometric model, and present a comprehensive photosynthesis dataset with experimentally calibrated photosynthesis models, that predicts energy acquisition by foliose corals as a function of colony shape. This allowed me to assess the extent to which changes in colony morphology along an environmental gradient track the predicted optimal colony morphologies. My results provide strong evidence that phenotypic plasticity in foliose corals optimizes photosynthetic energy acquisition and is not simply a mechanism to increase light capture. I show that the optimal morphology is constrained at the boundaries of the environmental gradient, with non-optimal morphologies in these habitats having greatly reduced energy acquisition. However, at the center of the environmental gradient, flexibility in photophysiology allows energy acquisition to be very similar for multiple morphologies. These results highlight the importance of phenotypic plasticity at multiple scales. Variation in overall morphology is important at niche boundaries where conditions are consistently more stressful, whereas

physiological flexibility is important in intermediate and less predictable habitats where a rapid and reversible response to environmental fluctuations is required.

4.2 Introduction

The adaptive significance of phenotypic plasticity (i.e. variation in the expression of a genotype in relation to an environmental influence, *sensu* Bradshaw 1965) has captured the interest of researchers for decades. It is generally understood that the potential benefits of plasticity are linked to environmental heterogeneity (Stearns 1989; Via et al. 1995). Specifically, plasticity can be advantageous when dispersal occurs between local populations that occupy varying habitats (Kingsolver et al. 2002; Sultan & Spencer 2002), and when the range of phenotypes produced through plasticity is at least equal to that achievable through genetic differentiation (De Witt et al. 1998). In other words, plasticity is advantageous because it allows organisms to assume the morphology most suited to their immediate habitat (e.g. De Witt et al. 1998; Alpert & Simms 2002). Although phenotypic plasticity is well documented for a range of taxa (e.g. butterflies, Kingsolver 1995; frogs, van Buskirk 2002; plants, Dong 1995, Dudley 1996; and reef-building corals, Willis 1985; Bruno & Edmunds 1997), the observed change in phenotype is not always advantageous. Although some changes in morphology appear to be performance enhancing, others are inconsequential and may simply result from flexibility in the way organisms grow during development (e.g. Schlichting 1986; Stearns 1989; Meyers & Bull 2002).

For photosynthetic organisms, the benefits of plasticity have primarily been related to resource acquisition (e.g. Dustan 1975; Hutchings and de Kroon 1994; Grime and Mackey 2002). For plants in shaded habitats, plasticity can enhance

resource acquisition by increasing the area of photosynthetic tissue, or by promoting leaves into higher light environments to reduce inter- and intra-specific competition (Dong 1995; Dudley and Schmitt 1996; van Kleunen & Fischer 2001; Steinger et al. 2003). In addition, plasticity in the distance between aggregations of leaves and roots can increase the proportion of biomass within favorable habitat patches (e.g. de Kroon and Hutchings 1995). Nonetheless, the optimal morphology in a given habitat is not always obvious. For example, shade plants may decrease their canopy height and adopt a more horizontal growth direction to enhance light capture (O'Connell & Kelty 1994), or they may increase stem length in an effort to move leaves away from shading competitors (Dudley & Schmitt 1996; van Kleunen & Fischer 2001). These examples demonstrate that very different morphological strategies may be adopted in response to similar environmental gradients. For all organisms, a range of interacting biotic and abiotic factors determine which morphological strategy most benefits performance. In this study I use a combination of laboratory experiments, field observations and mathematical modeling to investigate the extent to which photosynthetic energy acquisition drives morphological variation in a species of reef-building coral.

Reef-building corals are an ideal model system in which to investigate the performance consequences of morphological variation. Corals inhabit a range of environments (e.g. Vermeij and Bak 2002), disperse larvae over large distances (Ayre and Hughes 2004) and display pronounced morphological variability (see Table 4.1). Although corals vary greatly in colony architecture, many species exhibit a trend of increasing 'openness' as light availability decreases, for example in deep water. Analogous to resource acquisition being the principal explanation for plasticity in plants, growth-form variation in corals has been proposed as a

Table 4.1: Phenotypically plastic corals: extent of morphological variation and environmental cue. L, S and H refer to light, sedimentation and hydrodynamics. Numbered references are 1) Potts 1978, 2) Oliver et al. 1983, 3) Roos 1967, 4) Helmuth et al. 1997b, 5) Todd et al. 2004, 6) Bruno & Edmunds 1997, 7) Foster 1979, 8) Graus & McIntyre 1982, 9) Foster 1983, 10) Maragos 1972, 11) Danaher 1998, 12) Lesser et al. 1994, 13) Kaandorp & Sloot 2001, 14) Brakel 1983, 15) Gleason 1992, 16) Rex et al. 1995, 17) Muko et al. 2000, 18) Jaubert 1981, 19) Willis 1985. ⇔ denotes that reciprocal transplant experiments were carried out.

Species	Morphology	Plastic Trait	Cue (Reference)
Acropora cuneata	Columnar - encrusting	Columnar growth	L, S, H (1)
Acropora formosa	Branching	Secondary branching	L, H (2 ⇔)
Acropora palifera	Columnar - encrusting	Column dimensions	L, S, H (1)
Agaricia agaricites	Foliose	Plate dimensions/spacing	L (3)
Agaricia tenuifolia	Foliose	Plate/branch spacing	L, H (4)
Colpophyllia natans	Massive	Angle of growth	L (3)
Dichocoenia stokesii	Massive	Angle of growth	L (3)
Diploastrea heliopora	Massive	Corallite structure	L (5 ⇔)
Favia speciosa	Massive	Corallite structure	L (5 ⇔)
Madracis mirabilis	Digitate	Branch spacing	H (6 ⇔)
Meandrina meandrites	Massive	Angle of growth	L (3)
Montastrea annularis	Massive	Corallite structure	L, S, H (7 ⇔)
Montastrea annularis	Massive	Angle of growth	L (8 ⇔)
Montastrea cavernosa	Massive	Corallite structure	L, S, H (9 ⇔)
Montipora verrucosa	Submassive	Angle of growth	L, S, H (10)
Mycetophyllia spp.	Plating	Skeletal ridge formation	L, H (11)
Pocillopora damicornis	Branching	Branch diameter & spacing	H (12, 13)
Pocillopora meandrina	Branching	Branch diameter & spacing	L, S, H (10)
Porites astreoides	Massive	Angle of growth (3,	L (3, 14, 15 ⇔)
Porites compressa	Branching	Branch length & spacing	L, S, H (10)
Porites cylindrica	Branching	Branch diameter	H (16)
Porites sillimaniani	Branching – massive	Presence of branches	L (17 ⇔)
Siderastrea siderea	Massive	Corallite structure	L, S, H (7 ⇔)
Synaraea convexa	Branching	Branch dimensions	L (18)
Turbinaria mesenterina	Foliose	Angle of growth	L (19 ⇔)

mechanism to maintain energy acquisition across a gradient of decreasing energy availability (i.e. colonies adopt a flat/open morphology in deep water in order to increase light interception, Dustan 1975; Jaubert 1981; Gleason 1992). However, this hypothesis does not explain why flat morphologies do not persist in high light environments, nor does it predict where along the depth gradient the shift in morphology would occur, or how rapid the transition between alternative morphologies would be. There is now some indication that detrimental effects of exposure to excessive light may cause colonies to adopt self-shading morphologies in shallow habitats (e.g. Kuhl et al. 1995; Winters et al. 2003). Indeed, in the previous Chapter I showed that energy balance in substantially reduced for high-light acclimated colonies. However, it remains unclear whether these energetic factors adequately explain observed patterns of morphological variation. An alternative explanation is that vertically oriented growth is beneficial for reasons unrelated to light acquisition (e.g. competition for space, nutrient acquisition), and that maximising light acquisition is only important in low-light habitats.

The principal aim of this study was to evaluate whether the observed plasticity in colony morphology for a species of foliose coral (*Turbinaria mesenterina*) represents a strategy to maximize energy acquisition, thereby benefiting colonies through increased energy availability for growth, reproduction and survival. Because light intensity is the principal environmental correlate of colony morphology for foliose corals including my study species (Willis 1985; Helmuth et al. 1997a), I focus on variation in energy acquisition across a light-intensity gradient. To analyse the effects of morphological variation on colony energetics, I developed a three-dimensional light acquisition model coupled with a photosynthesis model to calculate daily net energy acquisition. To calibrate the latter model, I used the

photosynthesis dataset analysed in Chapter 3 to account for within-colony flexibility in the shape of the photosynthesis-irradiance relationship due to photoacclimation. This approach allowed me to calculate the potential energy acquisition of a range of colony morphologies for conditions under which those morphologies do not occur naturally. Therefore, using this framework, it is possible to assess the energetic implications of phenotypic plasticity by predicting the energetically optimal morphology across a depth gradient, and comparing the extent to which observed morphological variation conforms to the predicted optima.

4.3 Model formulation

4.3.1 Study species

Turbinaria mesenterina (Dendrophyllidae) has a wide distribution across reef types in the Indo-Pacific but occurs most abundantly in turbid coastal waters (Veron 2000). Across light habitats (e.g. with depth), colonies occur with varying degrees of openness. Specifically, the angle of the uppermost tier of the colony, and the spacing between tiers, change with depth (Anthony et al. 2005). Reciprocal transplant experiments between shallow and deep sites have demonstrated that this morphological variation is due to phenotypic plasticity (Willis 1985).

4.3.2 Colony Geometry

In the geometric model developed in this chapter, the morphology of colonies of *Turbinaria mesenterina* is represented by a series of cones nested within each other (Figure 4.1). Type morphologies of *T. mesenterina* that are characteristic of different depths (Figure 4.1A-C) were defined using an existing dataset (see Anthony et al. 2005 for details). Light intensity over the colony surface was calculated using the position of points on the colony surface relative to the path of the sun across the sky.

These points were defined by their location on cardinal axes defined by angle ϕ, (°, measured from south) and distance from the edge of the cone (see Figure 4.2). I used a fixed radius of 30cm for all model colonies, approximating the average radius of colonies in the dataset.
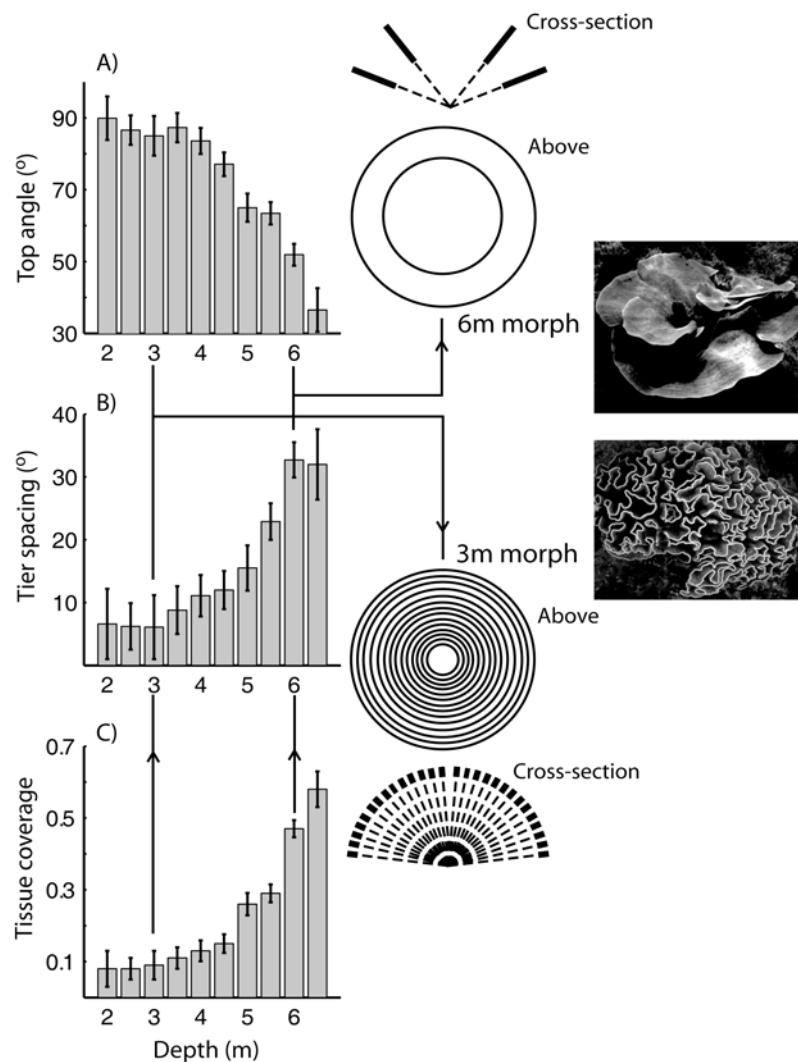
Figure 4.1: Variation in colony morphology with depth for *Turbinaria mesenterina.* (A) Angle of the top tier of the colony, B) Spacing between tiers and C) Proportion of each tier that supports live tissue. Two-dimensional representations of morphologies characteristic of 3m and 6m depths are shown in cross-section and from above, photos are colonies from corresponding depths in the field. Thick bars in cross-section view depict live tissue coverage. Data is modified from Anthony et al. (2005). Errors bars represent standard error of colony morphology for each depth category respectively.
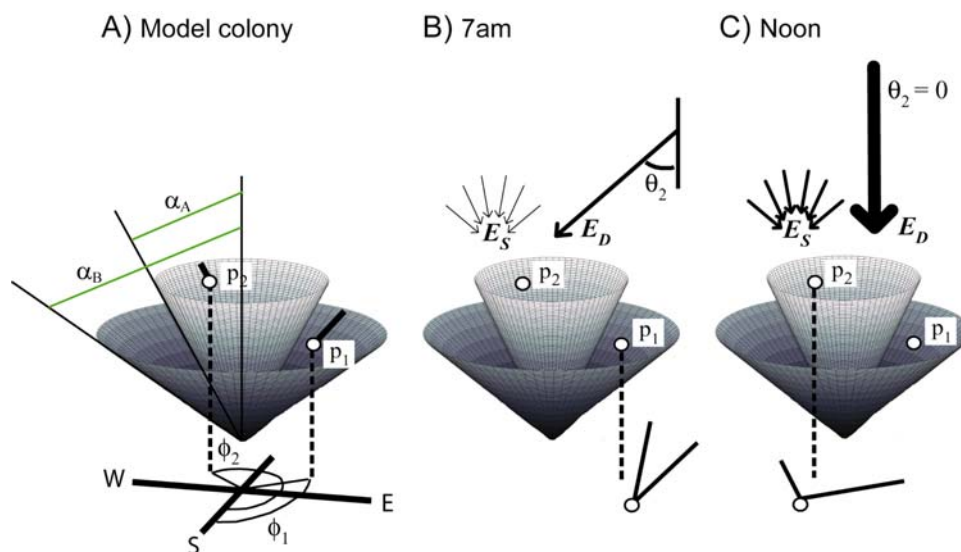
Figure 4.2: Geometric rendition of model colonies. A) Points (p_1 and p_2) on the colony surface are identified by their distance from the edge of tiers of known angle of inclination (α_A and α_B), and their location on cardinal axes (ϕ_1 and ϕ_2). In the morning (B) direct light approaches the surface at an angle and the intensity of scattered light is low. At midday (C) the sun is directly overhead, and direct and scattered radiance are high. The range of angles from which light may approach p_1 is smaller than for p_2 due to its position on the lower tier.

4.3.3   Photosynthesis model

I used the hyperbolic tangent model (Jassby and Platt 1976) to calculate photosynthesis, *P*, as a function of incident irradiance at time, *t*, over the course of the day, *E(t)*, as calculated by the light model. This empirical model was used in place of the mechanistic model analysed in the previous Chapter in order to reduce the number of estimated parameters. To take photoacclimation into account, the model allows for variation in the three parameters of this model, P_{MAX} (the maximum rate of photosynthesis at light saturation), E_K (the irradiance at which photosynthesis is 75% of P_{MAX}) and R_{DARK} (the rate of respiration in darkness) to depending upon growth irradiance (E_μ, the average irradiance experienced by the colony or region within the colony, e.g. Falkowski & Raven 1997).

$$P(E(t),t) = P_{MAX}(E_\mu) \tanh\left(\frac{E(t)}{E_K(E_\mu)}\right) - R_{DARK}(E_\mu)$$
Eqn 4.1

To determine the functional relationship between the photosynthesis parameters and growth irradiance, I re-analysed the photosynthesis-irradiance (PE) dataset for *T. mesenterina* presented in Chapter 3. This dataset measures PE curves for colonies grown under irradiances between 20 and approximately 700 µmol photons m^{-2} s^{-1} (see Methods). I first estimated the parameters P_{MAX}, E_K and R_{DARK} by fitting Eqn 4.1 to the PE curve data for each colony using a Levenberg-Marquardt non-linear estimation routine in Statistica (StatSoft). I then used the set of fitted parameters to calibrate the relationship between PE curve parameters and growth (acclimation) irradiance (see Table 4.2 for details). Linear regression was used to describe variation in R_{DARK} per unit surface area with growth irradiance. To model P_{MAX} as a function of growth irradiance I adapted a general function developed by Platt et al. (1980) that allows for a potential decline in P_{MAX} under high growth irradiances due to photoinhibition. Note that in this case, 'photoinhibition' represents long-term photoacclimatory changes in PE curves rather than a decline in rates of photosynthesis over a diurnal cycle (based on the results of Chapters 2 and 3). Finally, in absence of formal theory relating photoacclimatory state to growth irradiance, I fitted a polynomial equation (Table 4.2) to E_K estimates as a function of growth irradiance.

4.3.4 Light model

In the model, the intensity of incident light at a point on a colony surface (irradiance, µmol quanta m^{-2} s^{-1}) varies according to the depth below the water surface at which the colony is located, the orientation of the point relative to the path of the sun, and the position of the point within the colony as a whole. I used the Beer-Lambert law

(Mobley 1994) to model the exponential decline in light intensity with depth below the water surface:

$$E_{MAX}(z) = E^0 \exp\left(-\kappa\, z\right)$$
<div align="right">Eqn 4.2</div>

where E_{MAX} *(z)* is maximum total (downwelling) irradiance at depth, *z*, E^0 is maximum daily irradiance immediately below the water surface and κ describes light attenuation with depth. Variation in irradiance over the day was modeled as a sine function of time (after Marra 1978):

$$E_D(z,t) = E_{MAX}(z)\sin\left(\frac{\pi t}{\lambda}\right)^3$$
<div align="right">Eqn 4.3</div>

where *t* is time of day (hours since dawn), and ℓ is day-length (12 h in these calculations). Because the photosynthesis model is parameterized from the empirical relationship between irradiance incident to coral tissue and photosynthetic oxygen evolution it implicitly accounts for potential light-scattering effects of the coral skeleton (e.g. Enriquez et al. 2005), and variation in optical properties of the coral tissues over the colony surface.

Following the approach of other models of irradiance within complex structures (Pearcy & Yang 1995; Muko et al. 2000), the light model developed here divided total irradiance into direct (E_D) and scattered (E_S) components and assumed that the scattered component of the light field was diffuse (i.e. equal intensity from all angles). To quantify E_D and E_S, I hypothesized that as total irradiance increased (e.g. moving shallower in the water column), the overall light regime would become increasingly dominated by direct light. Therefore, I modelled the intensity of scattered light as a non-linear function of total irradiance (using data from Hoogenboom 2003, see Methods), as:

Table 4.2: Summary of parameters and equations together with best-fit parameter estimates for light and photosynthesis models.

EQUATION	PARAMETER	DESCRIPTION AND UNITS	ESTIMATE (± STANDARD ERROR)
LIGHT MODEL			
General parameters	E_μ	Growth (acclimation) irradiance calculated from light model as average daily irradiance incident to points on a colony surface, μmol photons m^{-2} s^{-1}	Variable
	t	Time since dawn, s	Variable
	z	Depth below the water surface, m	Variable
	$E_T(z,t)$	Total instantaneous downwelling irradiance, a function of time and depth, μmol photons m^{-2} s^{-1}	Variable
	E_D, I_D	Direct irradiance (E_D) and radiance (I_D), units are μmol photons m^{-2} s^{-1} and μmol photons sr^{-1} s^{-1}	Variable
	E_S, I_S	Scattered irradiance (E_S) and radiance (I_S), units are μmol photons m^{-2} s^{-1} and μmol photons sr^{-1} s^{-1}	Variable
	θ_1	Angle of incidence of light to the water surface, rad	Variable
	θ_2	Refracted angle of incidence of direct light	Variable
	θ_D	Angle of incidence of direct radiance to a surface, rad, measured from perpendicular to the surface	Variable
	θ_S	Angle of incidence of scattered radiance to a surface, rad, measured from perpendicular to the surface	Variable
	ϕ	Location of position on a colony surface on cardinal axes	Variable
	ϕ_S	Horizontal angle of incidence of scattered radiance to the surface of a model colony, rad	Variable
	α	Angle of inclination of tiers (cones) within model colonies, rad, measured from vertical	Variable
	z'	Distance between a point of a colony surface and the rim of the tier/cone that the points lies on, cm	Variable
Light attenuation with depth (Eqn 4.2) $E_{MAX}(z) = E_{MAX}\, e^{(-\kappa z)}$	$E_{MAX}(z)$	Maximum total daily irradiance at depth, z, μmol photons m^{-2} s^{-1}	Variable
	E^0	Maximum total daily irradiance immediately below the water surface, μmol photons m^{-2} s^{-1}	*2118 (46)
	κ	Light attenuation coefficient, m^{-1} (* Hoogenboom, Unpubl. data.)	*0.28m^{-1}
Diurnal irradiance cycle (Eqn. 4.3) $E_T(z,t) = E_{MAX}(z)\, \sin^3\left(\dfrac{\pi t}{\lambda}\right)$	λ	Daylength	12 hours
Scattered irradiance versus total irradiance (Eqn 4.4) $E_S = S_x\left[\dfrac{\chi E_T}{\sqrt{S_x^{\,2} + \chi E_T^{\,2}}}\right]$	S_x	Maximum intensity of scattered irradiance, μmol photons m^{-2} s^{-1}	**292 (3.4)
	χ	Rate at which scattered irradiance approaches maxima with increasing total irradiance, (μmol photons m^{-2} s^{-1})$^{-1}$ (**estimates based on data from Hoogenboom 2003)	**0.47 (0.01)

EQUATION	PARAMETER	DESCRIPTION AND UNITS	PARAMETER ESTIMATE (± STANDARD ERROR)
PHOTOSYNTHESIS MODEL			
Rate of photosynthesis versus irradiance, hyperbolic tangent model (Eqn 1) $$P = P_{MAX}(E_\mu)\tanh\left(\frac{E(t,z)}{E_K(E_\mu)}\right) - R_{DARK}(E_\mu)$$	P P_{MAX} E_K R_{DARK}	Rate of photosynthesis, μmol O_2 cm^{-2} h^{-1} Maximum rate of photosynthesis, μmol O_2 cm^{-2} h^{-1} Sub-saturation irradiance, μmol photons m^{-2} s^{-1} Rate of respiration in darkness, μmol O_2 cm^{-2} h^{-1}	Variable Variable Variable Variable
Maximum rate of photosynthesis as a function of growth irradiance $$P_{max}(E_\mu) = P_x(1 - e^{-aE_\mu})e^{-bE_\mu}$$	P_x a b E_μ	Maximum value of P_{MAX}, μmol O_2 cm^{-2} h^{-1} Rate at which P_{MAX} approaches P_x Photoinhibition of P_{MAX} Growth (acclimation) irradiance calculated from light model as average daily irradiance (see above)	2.4 (0.26) 0.03 (0.01) 0.001 (0.0003)
Sub-saturation irradiance as a function of growth irradiance $$E_K(E_\mu) = E_{K(MIN)} + \rho E_\mu + \gamma E_\mu^2$$	$E_{K(MIN)}$ ρ γ	Minimum value of E_K (at $E_\mu = 0$), μmol photons m^{-2} s^{-1} Coefficient, (μmol photons m^{-2} s^{-1})$^{-1}$ Coefficient, (μmol photons m^{-2} s^{-1})$^{-1}$	186 (18) 0.49 (0.16) -0.0008 (0.0003)
Dark respiration as a function of growth irradiance $$R_{DARK}(E_\mu) = rE_\mu + c$$	r c	Increase of R_{DARK} with increasing irradiance (μmol O_2 cm^{-2} h^{-1} (μmol photons m^{-2} s^{-1})$^{-1}$) Baseline dark respiration, μmol O_2 cm^{-2} h^{-1}	0.0006 (0.0001) 0.3 (0.03)

$$E_S(z,t) = S_x \left[\frac{\chi E_D(z,t)}{\sqrt{S_x^2 + \chi E_D(z,t)^2}} \right]$$ Eqn 4.4

where S_x defines the asymptotic intensity of scattered irradiance and χ is the rate at

which scattered irradiance approaches this maximum as total irradiance increases.

The intensity of scattered light per angle of incidence (scattered radiance) at a given

depth and time of day, $I_S(z,t)$, is found by dividing $E_S(z,t)$ by π (Appendix B.1, B.2).

During the day, direct irradiance varies with the progression of the sun across

the sky, and is proportional to the cosine of the angle (θ) between the normal

(perpendicular) to the colony surface and the beam of incident direct light (Mobley

1994; Falkowski & Raven 1997). The direction of the surface normal is a function of

both colony steepness (the angle of each tier of the colony, α_T) and cardinal

orientation (the direction that the surface faces relative to the direction of incident

light, ϕ, Figure 4.2). Steeper sloped colonies have a surface normal that is more

horizontal, so when the sun is directly overhead and direct radiance (light passing

through a volume of water) is at its most intense, direct irradiance (intensity of light

illuminating a surface) approaches zero (*cos* 90° = 0, see Appendix B.1 for detailed

explanation). Steeper sloped colonies are also self-shaded from direct radiance over a

greater proportion of the day. The model calculates the intensity of direct light at

points on the colony surface by determining the cosine of the angle between the

surface normal and the direction of incident direct light, and calculating the range of

angles along the path of the sun from which direct light is not shaded by other parts

of the colony (see Appendix B.3).

Scattered irradiance is calculated from the integral of scattered radiance over

the range of angles from which scattered rays may approach the colony surface

(Smith & Wilson 1977). At the upper edge of the colony, scattered light may

approach from within a hemisphere of angles. Moving deeper into the colony, this range of angles becomes restricted due to self-shading. Total scattered irradiance, $E_S(z,t,p)$, at a point, p, on a colony surface at depth, z, and time, t, is defined as:

$$E_S(z,t,p) = I_S(z,t) \int\limits_{\theta_S} \int\limits_{\phi_S} \cos\theta_S \sin\theta_S \, d\phi_S \, d\theta_S \qquad \text{Eqn 4.5}$$

where $I_S(z,t)$ is the intensity of photons approaching from each angle (Appendix B.2), θ_S is the angle between the surface normal and the direction of incident scattered light, and the integral over $sin\theta_S \, d\phi_S \, d\theta_S$ is effectively the surface area of the proportion of hemisphere encompassed by the range of angles (Appendix B.4).

4.3.5   Model Analysis:

The complicated mathematics defining the range of angles from which light approaches colony surfaces mean that analytically integrating photosynthesis over the colony surface is not possible. Therefore, a numerical discretisation was used to calculate total colony photosynthesis.

Firstly, due to colony symmetry, it is only necessary to calculate irradiance and photosynthesis for one quarter of the colony surface. The light model equations therefore apply only to regions of the colony between cardinal angles of 0 - 90°. To determine the appropriate increments of the discretization I analysed the dependence of model outputs upon the size of the segments of the colony over which photosynthesis was calculated. The model converged at increments of 0.625° of cardinal angle (ϕ), 0.125 cm increments of distance from tier edges and time increments of 72s. This discretisation resulted in model colonies with between 69 thousand and 519 thousand segments. All calculations were performed using the High Performance Computing facilities at James Cook University.

Subsequently, irradiance at each point of the colony surface, at each time of day, was used to calculate rates of photosynthesis (μmol O_2 cm^{-2} h^{-1}). These rates were then multiplied by surface area (cm^2 –Appendix B.5) and time (h), and summed over the colony surface to obtain gross rates of daily photosynthesis (μmol O_2 d^{-1}). Daily respiratory costs were likewise calculated, and the ratio of daily photosynthesis to respiration (P:R ratio) subsequently used as a measure of net photosynthetic energy acquisition of the whole colony. Because my focus was on the relative performance of different morphologies rather than absolute carbon fixation, rates of photosynthetic oxygen evolution were not converted into units of carbon fixation (see Muscatine et al. 1981). Calculations of P:R ratio were performed for each of 11 type morphologies that were generated based on the average top tier angle, number of tiers and proportional tissue coverage of tiers, that were observed in the colony morphology dataset (Figure 4.1), plus an additional single-tiered colony consistent with the flattest observed morphology. A gradient of light conditions, corresponding to depths between 1 and 7m depth at the study site, was then simulated for each type-morphology. Model outputs were analysed to determine which morphology maximized photosynthetic energy acquisition at each depth.

I used Monte Carlo simulation to account for uncertainty in parameter estimates for the photosynthesis sub-models. To do this, I iterated calculations of total daily energy acquisition for each morphology at each depth 200 times, each time using randomly selected parameter values from gaussian uncertainty distributions for each photoacclimation sub-model. These distributions were generated using the best-fit parameters and variance-covariance matrix for each sub-model. Finally, I compared the fit of the model prediction of optimal colony morphologies to data with that of a Generalised Additive Model (GAM) fitted to raw

(not depth categorized) colony morphology data using Statistica's GAM module. The correspondence between the GAM and the optimal morphology model indicates how well the model captures the central tendency of the observed variation in morphology with depth.

4.4   Materials and methods

Fieldwork was conducted at Nelly Bay and Cockle Bay, Magnetic Island (19°09S, 146°53E) between February 2003 and March 2005. Data from Hoogenboom (2003) were used to determine the relative contributions of direct and scattered irradiance to the total light regime at the study site. Briefly, in earlier work, I deployed pairs of light loggers ('Odyssey', DataFlow Systems, NZ) at depths of 2m and 6m (corresponding to approximately 0 and 4m below lowest astronomical tide). Light loggers were positioned so that one sensor from each pair was horizontal (measuring total downwelling irradiance), and the other was vertical and facing due south to measure scattered irradiance only.

Photosynthesis/irradiance (PE) curves were assayed using methods described in Chapters 2 and 3. Briefly, flat fragments of colonies were collected from between 2m and 6m depth, transported to aquarium facilities at James Cook University, divided between tanks with varying light regimes and allowed 6 weeks for recovery and photoacclimation (ample for this species, Anthony & Hoegh-Guldberg 2003b). Colonies were fed newly-hatched *Artemia* nauplii and/or rotifers daily. The water temperature and salinity within aquaria were maintained between 26.5 and 28°C, and between 34 and 36ppt respectively, corresponding to field conditions at the time of collecting. Oxygen respirometry assays were conducted using an array of six closed, clear-perspex incubation chambers (2.7 litre volume) coupled with calibrated Clark-type oxygen electrodes (Cheshire Systems, Australia). Oxygen concentrations were

recorded every 20 seconds using a data logger (CR10X, Campbell Scientific

Australia). Light regimes for photosynthesis assays and light treatments were

generated using sets of metal halide lamps (each 400W, Iwasaki Electronics, Japan)

suspended above the incubation chambers and the aquaria.

4.5 Results

Scattered irradiance demonstrated a curvilinear relationship with total

irradiance (Figure 4.3, Table 4.2). The fitted model explained 94% of the variance in

the data, and all parameters were significantly different from zero (t-test, df = 1390, p

< 0.05 for S_x and χ). No difference in the composition of the light field was apparent

between 2 and 6m depths at the study site (dashes versus circles in Figure 4.3). This

indicates that, over the depth range considered here, the proportion of scattered light

in the irradiance field depends on total light intensity rather than depth. I therefore

use the fitted relationship shown in Fig. 4.3 to model the composition of the light

field across all depths.
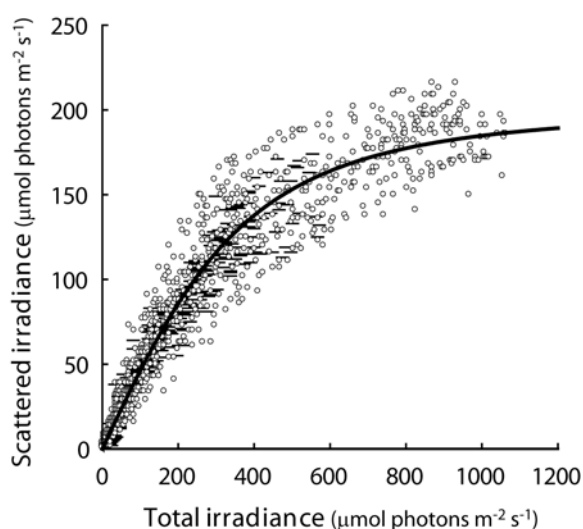
Figure 4.3: Relationship between scattered and total irradiance. Curve represents fit
of Eqn. 4.4 to data, parameters values of S_x and χ are shown in Table 4.2. The
composition of the irradiance field was the same at both 2m (circles) and 6m
(dashes) depths. Data are reanalyzed from Hoogenboom (2003).

Photosynthesis parameters varied significantly with growth (acclimation) irradiance (Figure 4.4). Although P_{MAX} initially increased with growth irradiance there was a strong decline in this parameter for colonies acclimated to the highest light levels (Figure 4.4A). The photoinhibition model adequately explained this variation ($R^2 = 0.58$), with all parameters significantly different from zero (t-test, df = 36, p < 0.05 for each of P_x, a and b, Table 4.2). The linear model predicting rates of respiration (R_{DARK}, Figure 4.4B, Table 4.2) explained 47% of the variance in the data with both parameters significantly different from zero (t-test, df = 36, p < 0.05 for both r and c). Contrary to my expectations, sub-saturation irradiance, E_K, showed a hump-shaped relationship with growth irradiance (Figure 4.4C).

The plasticity model captured the observed trends of increasing colony flatness, and increased angular spacing between tiers, with depth (Figure 4.5). In general agreement with the observed pattern of variation in colony morphology, there was greater uncertainty around the predicted optimal angle and spacing at intermediate depths (increased width of the 95% confidence envelope between 5 and 7m depths). In other words, although upright and flat morphologies were clearly optimal at shallow and deep depths respectively, at intermediate depths a wide range of morphologies had similar energy acquisition and this translated into greater uncertainty about which morphology was optimal. Therefore, at intermediate depths individual variation in photophysiology allows morphologies ranging from the most convoluted to the most open forms to be nearly energetically equivalent. Although the model appeared to under-predict the extent of colony flatness and tier spacing at intermediate depths (colonies in the field were flatter and more widely spaced than predicted: see Discussion), the GAM prediction fell within the 95% confidence interval of the model predictions (dashed lines versus shaded regions in Figure 4.5).
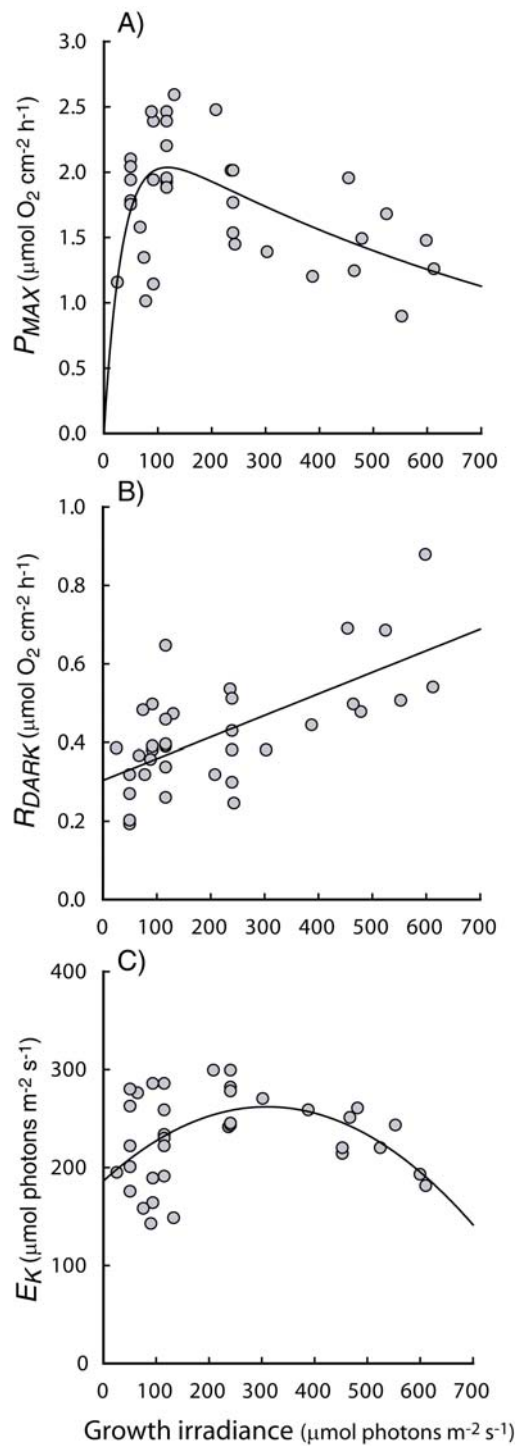
Figure 4.4: Variation in parameters of photosynthesis versus irradiance relationship for colonies of *Turbinaria mesenterina* acclimated to different light regimes (n = 36); (A) maximum rate of photosynthesis, P_{MAX} (μmol O_2 cm^{-2} h^{-1}), (B) rate of dark respiration, R_{DARK} (μmol O_2 cm^{-2} h^{-1}), and (C) sub-saturation irradiance (E_K, μmol photons m^{-2} s^{-1}).
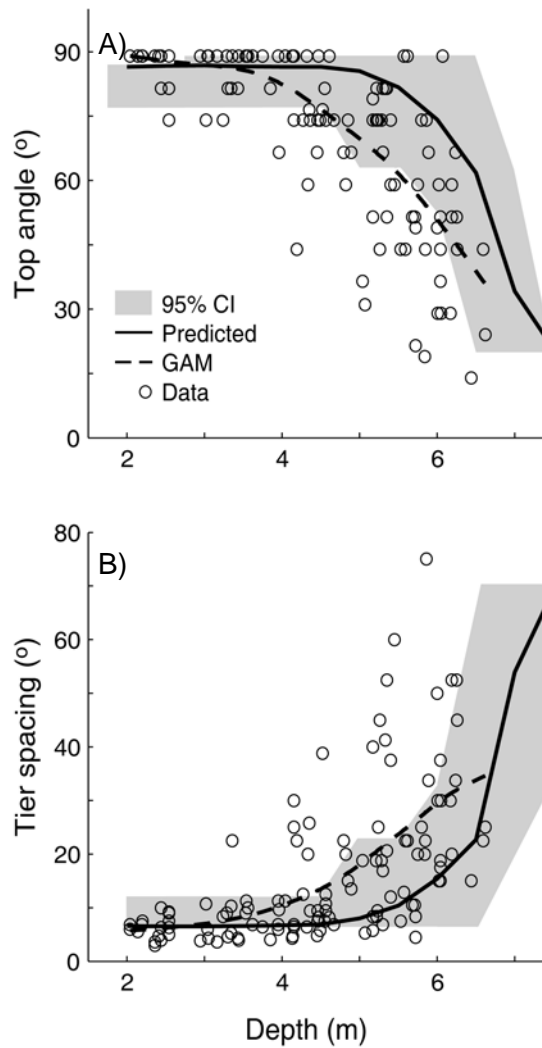
Figure 4.5: Comparison of observed variation in colony morphology along a depth gradient with optimal colony morphologies predicted by the plasticity model. A) observed and predicted top tier angle and B) angular spacing between tiers. The solid line is the average predicted optimal morphology, and the shaded region shows the 95% confidence interval around the mean prediction from 200 Monte Carlo iterations. Dashed line shows GAM fit to the data (circles represent measurements for individual colonies).

4.6 Discussion

The three-dimensional light-interception model and calibrated photoacclimation models developed in this study provide strong evidence that phenotypic plasticity in foliose corals optimizes photosynthetic energy acquisition. Moreover, these results demonstrate that maximal energy acquisition is not achieved through maximal light interception. Although flat morphologies have the highest light capture over the entire depth range, the decline in maximum rates of photosynthesis per unit area due to photoacclimation to high light means that these morphologies perform worse in shallow water than vertically oriented forms. Previous studies of morphological variation in corals have mentioned the potential importance of light-stress as a driver of colony morphology (Oliver et al. 1983; Muko et al. 2000; Anthony et al. 2005). The modelling framework developed in this chapter quantifies the action of this mechanism, and indicates that the trade-off between light capture and avoidance is an important driver of morphology. These findings are consistent with previous investigations of plant canopy structure, wherein changes in foliage orientation and increased self-shading during periods of high light intensity can significantly reduce light stress (Valladares & Pugnaire 1999; Falster & Westoby 2003).

Overall, results of this chapter show that the colony morphologies of *T. mesenterina* characteristic of different depths in the field are energetically optimal morphologies. However, over the middle half of the depth-distribution, there is no single morphology that has markedly greater energy acquisition than others. Instead, at depths where light intensity is neither so high as to cause damage to the photosynthetic apparatus (i.e. photoinhibition), nor so low as to be energetically limiting, small variations in the shape of the relationship between photosynthesis and

irradiance allow colonies of very different shapes to have very similar energy acquisition. At these intermediate depths, the light environment fluctuates over time due to natural variation in tidal cycles and water turbidity, whereas light levels are always high at the shallow end of the depth gradient and always low in deep water (e.g. Anthony et al. 2004). The consensus view in the literature is that a stable environmental gradient, that serves as a reliable cue for development of the appropriate phenotype, is required in order for plasticity to be advantageous (Stearns 1989; Via et al 1995; Meyers & Bull 2002). In variable and/or unpredicatable environments (such as at intermediate depths at my study sites) a capacity for rapid and reversible changes will be beneficial (Piersma & Drent 2003). My analyses indicate that at intermediate depths, physiological flexibility (i.e. photoacclimation) equalizes differences in energy acquisition caused by variation in colony shape and may be the more important mechanism for adjusting to local conditions. Conversely, at the boundaries of the depth range, photoacclimation cannot compensate for changes in morphology and adjustment of colony shape appears to be the dominant phenotypic response.

4.6.1 Alternative explanations for morphological variation

An alternative to the hypothesis that energetic constraints are the primary driver of phenotypic plasticity in corals, is that colony morphology maximizes the surface area of living tissue within the limited area of reef occupied by a colony, even where the morphology assumed reduces energy acquisition per unit surface area (e.g. Helmuth et al. 1997c, Sebens 1997). In their study of the adaptive significance of plasticity in a species of irregularly branching coral, Muko et al. (2000) found support for this hypothesis, demonstrating that colony morphology in *Porites sillimaniani* optimised living tissue area. In contrast, the model developed here

shows that maximisation of energy acquisition alone adequately captures phenotypic plasticity in *T. mesenterina*. To explain this difference, I suggest that the maximal surface area hypothesis is unlikely to apply in turbid, inshore reef habitats where coral cover is typically low and space is unlikely to be limiting. However, this inconsistency might also be due to differences in the way that colonies with different architecture respond to variation in environmental cues: morphology in branching corals correlates with gradients of water flow velocity (e.g. Lesser et al. 1994; Bruno and Edmunds 1997)*,* whereas morphology in foliose and massive corals appears to be more strongly correlated with light intensity (see Table 4.1).

A third explanation for morphological variation in corals is that colony morphology represents a passive response to the environment rather than an active choice to position resource acquiring surfaces in areas of optimal resource availability. This hypothesis is supported by radiate accretive growth models that simulate colony morphology based on the density of nutrients arriving at different points over the colony surface (e.g. Kaandorp et al. 1996; Merks et al. 2003). These models generate realistic morphologies over hydrodynamic gradients with thick-branched colonies arising in high-flow habitats because convective delivery of nutrients over the entire colony surface causes generalized rapid growth. Conversely, tall and lightly calcified morphologies arise in low-flow habitats because growth is localised at branch tips due to the formation of stagnant zones in colony interiors (e.g. Kaandorp et al. 1996). Nevertheless, water flow and the corresponding variation in nutrient and gas exchange is unlikely to explain patterns of colony morphology at my study sites where swells are only very rarely above 1m in height, and water turbulence is correspondingly minimal. That is, gradients in water flow velocity at

sites where *T. mesenterina* is abundant are likely to be much too small to account for the magnitude of differences in colony shape.

4.6.2 Accuracy of model predictions

Although the central tendency of observed colony morphology fell within the 95% confidence band of model predictions, it was close to the lower bound of this region at intermediate depths. Therefore, the data provide some evidence that the optimality model tends to predict colony morphologies that are, on average, more upright and closely spaced than those observed in the field. There are three possible explanations for the divergence between the observed and predicted colony morphologies. Firstly, the geometric model represents colonies as regular, equally spaced sets of nested cones with equal tier length. This geometry captures trends in morphological change with depth for *T. mesenterina* but inevitably oversimplifies some of the variation in real colony shape. For example, tiers of colonies in deep water are rarely the same length, with upper tiers generally being shorter than lower tiers (Hoogenboom, pers. obs.). Moreover, shallow water morphologies in the field are highly convoluted and can form vertically oriented cylinders that prevent the formation of the more horizontal lower tiers that are generated in model colonies. Both of these factors would cause flatter morphologies generated in nature to acquire comparatively more carbon than in the model, and this could explain why some colonies in the field are flatter than the model predicts. The second possibility is that colony morphology may respond to the most energetically limiting light conditions, rather than the average conditions observed at my study site. That is, the optimal morphology predicted under average irradiance conditions at each depth may not survive during prolonged periods of low light availability (e.g. during high-turbidity events caused by run-off and/or high winds, Anthony et al. 2004). This would also

cause colonies to adopt flatter morphologies than predicted by a model based on average irradiance.

A final possibility is that variation in the magnitudes of energetic costs not incorporated into the model may influence colony morphology in the field. There are several potential energy sinks for corals in addition to the allocation of photosynthate between colony growth and/or reproduction; including ultraviolet light (UV), sedimentation and temperature . Of these, only temperature can explain the tendency of the model to underestimate colony flatness for the following reasons. Firstly, if costs related to UV exposure were a significant driver of morphology, colonies should be more vertically oriented than predicted by the model in order to reduce UV intensity, whereas this study shows that colonies are flatter than predicted. Secondly, while sediment loads represent a considerable energetic burden for corals in turbid habitats (Anthony & Connolly 2004), there is no evidence to suggest that sediment effects vary between shallow and deep water. Moreover, avoidance of sedimentation would again cause colonies to be more upright than predicted in order to assist in shedding sediment (see Riegl et al. 1996). Finally, the energy acquisition model is calibrated from measurements of photosynthesis made at approximately average sea surface temperature at the study site, whereas temperatures in the field generally decrease with depth. The bell-shaped relationship between temperature and productivity is well established (Falkowski & Raven, 1997), and there is evidence that low temperatures can reduce photosynthesis by limiting the rate at which light is supplied to the photosynthetic apparatus (see Staehr & Birkeland 2006). Therefore, although any temperature differential across the 6 m depth gradient at the study site is likely to be small, there is some potential for temperature effects to result in flatter colonies in the field than predicted by my optimality model.

4.7 Conclusions

These results demonstrate that morphological plasticity for foliose corals is a mechanism to facilitate resource acquisition, as has previously been shown for other photosynthetic organisms (e.g. de Kroon & Hutchings 1995; Dong 1995). This chapter shows that a model based on energy acquisition adequately captures the observed variation in colony morphology for the study species. In addition, my results indicate a significant reduction in energy acquisition for flat colonies in high-light habitats, suggesting that the trade-off between light capture and avoidance previously observed in plants is also an important driver of morphology for corals. Moreover, this work demonstrates that developing the morphology appropriate for local conditions carries a greater advantage at the boundaries of the light niche. For *T. mesenterina*, developing a self-shading, vertical colony morphology in shallow water is an important mechanism to avoid photoinhibition, whereas flat colonies have optimal energy acquisition in deep habitats where light is limiting. Conversely, at intermediate positions along the resource axis, flexibility in photophysiology allows multiple morphologies to have comparable energy acquisition. These findings highlight the importance of phenotypic plasticity on multiple scales. Morphological variation is important at niche boundaries where conditions are consistently more stressful, whereas physiological flexibility is important in intermediate and less predictable habitats where a rapid and reversible response to environmental fluctuations carries additional benefits.

5 DEFINING FUNDAMENTAL NICHE DIMENSIONS OF CORALS: SYNERGISTIC EFFECTS OF COLONY SIZE, LIGHT AND FLOW

5.1 Summary

The 'fundamental niche' is the range of conditions under which an organism can survive and reproduce in the absence of biotic interactions. Niche measurements are often based on statistical relationships between species presence and environmental variables, or inferred from measured responses of species along hypothesized niche axes. In this chapter, I use novel, process-based models of how irradiance and gas diffusion influence photosynthesis and respiration, to predict niche dimensions for three coral species (*Acropora nasuta*, *Montipora foliosa* and *Leptoria phrygia*). Using a combination of mathematical modeling, laboratory experiments and field observations, this study establishes a link between energy acquisition and the dominant environmental gradients on reefs – light intensity and water flow velocity. This approach allowed me to quantify how the shape of the niche varies in response to light and flow conditions. The model predicts that, due to its higher photosynthetic capacity, the branching coral *A. nasuta* has a positive energy balance over a wider range of conditions than both a massive (*L. phrygia*) and a foliose species (*M. foliosa*). Moreover, colony size influences niche width, with larger colonies of all three species achieving a positive energy balance over a broader range of conditions than small colonies. Comparison of model predictions with field data demonstrates that observed tissue biomass and reproductive output are strongly correlated with model predictions of energy acquisition. These results show how interactions between light and flow determine organism performance along

environmental gradients on coral reefs. In addition, this study demonstrates the utility of process-based models for quantifying how physiology influences ecology, and for predicting the ecological consequences of varying environmental conditions.

5.2 Introduction

The niche is a core concept in ecology. Although this term carries many different meanings (e.g. Whittaker et al. 1973; Pulliam 2000), the 'fundamental niche' is conventionally defined as the range of conditions under which an organism can survive and reproduce in the absence of biotic interactions (e.g. Hutchinson 1957). Over time, methods for measuring the niche have evolved from a conceptual niche axis or 'hypervolume' (Hutchinson 1957), to the use of statistical methods to identify environmental variables that are strong correlates of species occurrence (e.g. Austin et al. 1990; Wright et al. 2006). Another approach is to experimentally quantify organism performance (e.g. growth rate) along hypothesised niche axes (e.g. Greulich et al. 2000; Antoine & McCune 2004). Although these techniques identify correlates of species occurrence, they do not characterize the physiological processes that underlie such relationships. An alternative is to describe the niche based on the underlying mechanisms that determine how specific environmental conditions influence organism performance. Although there are few examples of this approach, in one such effort, Kearney & Porter (2004) combined physiological measurements, biophysical models and climate data to describe the fundamental niche of a lizard. Mechanistic approaches to niche studies are beneficial because they explicitly identify drivers of species' distributions, and allow greater confidence when extrapolating niche properties to conditions not included in multivariate datasets (Pulliam 2000; Kearney 2006).

An additional complication for niche measurement is that over the course of an organism's life, changes in body size can alter how the environment influences individuals. These ontogentic changes are most commonly observed in 'trophic niches': for example, as predators grow larger their prey selection changes (e.g. Scharf et al. 2000). However, such effects are also likely to be evident in the niche of sessile organisms, particularly because they are committed to their site of settlement irrespective of any unfavorable conditions that may prevail as they grow larger. Although investigations of this kind are rare, rainforest plants occur under a broader range of conditions as juveniles than adults (Webb & Peart 2000). Similarly, correlative approaches to niche measurement indicate that, for some taxa, the presence of juveniles may be predicted by a different set of environmental variables than that identified for adults (e.g. tree ferns, Jones et al. 2007).

Physiology and energy balance are fundamental to organism performance (Kooijman 2000; Kearney 2006). Therefore, the axes delimiting the fundamental niche should include those variables that influence energy and mass balance (Kearney & Porter 2004). For photosynthetic organisms, generating energy for growth and reproduction requires light to activate the photosynthetic machinery, together with exchange of CO_2 and O_2 gases during carbon fixation and metabolism (e.g. Falkowski & Raven 1997). Despite the existence of general principles that describe diffusion of gases from smooth surfaces, such models do not include light intensity as a factor influencing photosynthesis under natural conditions (e.g. Patterson et al. 1991). Therefore, although it is clear that the niche of photosynhthetic organisms is strongly influenced by both light intensity and gas exchange, the interactive effects of these processes on the size and location of the fundamental niche are unknown. The primary aim of this study was to develop a model of energy

acquisition as a function of light, gas exchange and organism size, and to use this framework to describe the fundamental niche of three coral species.

Reef-building corals inhabit heterogeneous environments in which light intensity and water flow (i.e. potential gas exchange) decrease with depth (Helmuth et al. 1997a). Therefore, corals are appropriate model organisms for developing mechanistic hypotheses about the relationships between environmental gradients and the niche. In this study, I use a combination of mathematical modeling, laboratory experiments and field observations to model the niche. I focus on the fundamental niche, which is generally defined as the conditions under which a species' birth rate exceeds death rate in the absence of crowding effects (e.g. Pulliam 2000). In some cases, birth or death rates cannot be readily quantified. For example, the fraction of offspring produced by an individual, that survive to establish as juveniles, cannot be reliably determined in organisms which produce offspring that disperse over large distances (such as corals). In these cases, physiological or energetic proxies of the capacity for population growth are often used (e.g. Anthony & Connolly 2004; Kearney & Porter 2004). In this chapter, I define the niche as the conditions under which individuals have a positive energy balance. In other words, I delineate the conditions under which individuals are able to survive, and have a surplus of energy that may be allocated to reproduction. As outline in Chapter 1, this definition of the niche is based on a central concept of ecophysiology and life-history theory: that all organisms require a net gain in energy for growth, reproduction and survival to be possible (Kooijman 2000). Specifically, I aimed to: 1) measure niche width along gradients of light and flow for different coral species; and 2) explicitly account for colony size as a potential factor influencing niche size. To assess the predictive accuracy of this model I compared predicted energy acquisition with measures of

tissue quality and reproduction for colonies of known size, sampled from field sites where light and flow were also quantified.

5.3 Materials and methods

5.3.1 Modelling framework

Corals are symbiotic organisms that obtain the majority of their energy (carbon) from photosynthesis (e.g. Muscatine et al. 1981). In all environments, photosynthetic gas exchange occurs across a diffusive boundary layer (DBL, i.e. a layer of stagnant fluid adjacent to the photosynthesizing surface, Nobel 1983). The rate at which molecules diffuse across DBLs depends upon the concentration of molecules on either side of the layer, and the overall thickness of the layer (Fick's laws, Nobel 1983). In turn, DBL thickness depends upon fluid velocity and turbulence (Nobel 1983; Denny 1988). Based on this principle, general models of gas exchange have been developed. These models relate photosynthesis to water flow using non-dimensional parameters (Reynolds number, *Re*, and Sherwood number, *Sh*) to quantify the extent to which mass flux is enhanced by fluid motion relative to that possible through diffusion (e.g. Helmuth et al. 1997a; Falter et al. 2007). *Re* summarises the ratio of inertial to viscous forces of the fluid, and characterises flow over a surface (Denny 1988):

$$Re = \frac{uW}{v} \qquad\qquad \text{Eqn 5.1}$$

where u is flow velocity, W is organism size (e.g. length in the direction of flow) and v is the kinematic viscosity of the fluid. *Sh* indicates how much mass flux is assisted by direct transfer (advection) relative to the potential flux if diffusion was the only mechanism operating (Denny 1988; Patterson 1992), and is given by:

$$Sh = \frac{h_m W}{D}$$ Eqn 5.2

where h_m is the mass transfer coefficient, and D is the diffusion coefficient (i.e. the time taken for the gas to diffuse a set distance, Denny 1988). An additional dimensionless parameter, the Schmidt number (Sc), defines the relative thickness of diffusion and momentum boundary layers ($Sc = v/D$), and is a constant for a given molecule and fluid medium. The relationship between Sh and Re has been well characterized experimentally, as:

$$Sh = aRe^b$$ Eqn 5.3

where a and b are empirically determined coefficients that depend upon organism shape and surface roughness. Because Reynolds number is a function of flow velocity and organism size, analysis of the relationship between Sh and Re allows these effects to be incorporated into the general gas exchange model:

$$P = h_m A \left(P_{vs} - P_{vf} \right)$$ Eqn 5.4

where P is the rate of gas exchange (in this case, photosynthetic oxygen flux), h_m is the mass transfer coefficient, P_{vf} and P_{vs} are the concentrations of gas in the fluid and at the photosynthesizing surface respectively and A is the surface area.

Accurate quantification of the parameters of the $Sh{:}Re$ relationship (Eqn 5.3) is critical for analyses of the effects of flow on photosynthesis. Engineering theory provides estimates of a and b for regularly-shaped, smooth structures such as cylinders and spheres (see Helmuth et al. 1997c). However, for rugose, irregular structures like corals, these parameters must be determined empirically. While several studies have explored the relationship between Sh and Re for corals, estimates of a and b based on live tissue measurements are only available for two species, *Montastrea annularis* (Patterson et al. 1991) and *Pocillopora damicornis*

(Lesser et al. 1994). Other studies have instead explored mass-flux dynamics by measuring water evaporation from coral skeletons in a wind tunnel (e.g. Helmuth et al. 1997a,c), or the flux of calcium carbonate from plaster-covered skeletons (Falter et al. 2007). In addition, previous studies generally assume that gas diffusion is the only factor limiting metabolic rates; however, in reality, oxygen fluxes become limited by rates of photosynthetic processes above a threshold flow velocity (see Hurd 2000).

An important consequence of previous methods for parameterising mass-flux models, is that different values for the coefficients *a* and *b* were obtained for photosynthesising compared with respiring colonies. For example, Patterson et al. (1991) estimated *b* equal to 1.3 during respiration and 0.6 during photosynthesis of *Montastrea annularis*, and Lesser et al. (1994) found $b = 0.16 - 2.45$ for *Pocillopora damicornis*. Using different values for these coefficients changes the relationship between h_m, organism size and fluid motion. By definition, h_m summarises the interaction of organism morphology with fluid motion (Patterson 1992). Rearranging equations 5.2 and 5.4, h_m becomes:

$$h_m = \frac{a \, \text{Re}^b \, D}{W} \qquad\qquad \text{Eqn 5.5}$$

where *a*, *b*, *D* and *W* are as defined above (see Table 5.1). From this expression, h_m is independent of rates of gas exchange (*P*), and concentrations of gases within tissue or the water column (P_{vs}, P_{vf}). Allowing *a* and *b* to vary between photosynthesising and respiring colonies is tantamount to assuming that the physical properties of diffusive boundary layers differ between metabolic processes. Although diffusion certainly influences gas flux, differences between the magnitudes of photosynthetic versus respiratory gas fluxes should depend upon the concentration gradient between the tissue surface and the water column, rather than on the direction the solute is

Table 5.1: Definitions of mass-transport and photosynthesis model parameters.

Parameter	Definition (units)	Estimate and Source
v	Kinematic viscosity of seawater ($cm^2\,s^{-1}$)	10^{-2} (Patterson et al. 1991)
D	Molecular diffusivity of O_2 in seawater ($cm^2\,s^{-1}$)	2×10^{-5} (Patterson et al. 1991)
u	Flow velocity ($cm\,s^{-1}$)	Variable
h_m	Mass-transfer coefficient ($cm\,s^{-1}$)	Variable (light & flow dependent)
a & b	Coefficients of relationship between Sh:Re (dimensionless)	This study (Figure 5.1)
P_{vs}	Oxygen concentration at tissue surface during maximum photosynthesis ($O_2\,cm^{-3}$)	Variable (light and flow dependent)
R_{vs}	Oxygen concentration at tissue surface during respiration in darkness ($O_2\,cm^{-3}$)	Variable (light and flow dependent)
P_{vf}	O_2 concentration within seawater ($O_2\,cm^{-3}$)	This study (280)
P	O_2 flux from tissue ($O_2\,cm^{-2}\,s^{-1}$)	Variable
P_{day}	Daily integrated energy acquisition ($O_2\,cm^{-2}\,d^{-1}$)	Variable
x_P and x_R	Deviation of asymptotic oxygen tissue concentration from 100% during photosynthesis (x_P) and respiration (x_R, $O_2\,cm^{-3}$)	This study (Table 5.2)
α_P and α_R	Rate at which P_{vs} approaches saturation with increasing Re during photosynthesis (α_P) or respiration (α_R) ($O_2\,cm^{-3}\,Re^{-1}$)	This study (Table 5.2)
β_P and β_R	Maximum (β_P) or minimum (β_R) tissue oxygen concentration as Re approaches zero ($O_2\,cm^{-3}$)	This study (Table 5.2)
E	Light intensity (μM photons $m^{-2}\,s^{-1}$)	Variable
E_K	Sub-saturation irradiance (μM photons $m^{-2}\,s^{-1}$)	100
E_{max}	Maximum daily irradiance (μM photons $m^{-2}\,s^{-1}$)	Variable

moving (toward tissue during respiration, away from tissue during photosynthesis).

Based on these properties, the *a-priori* expectation should be that experimentally-measured DBL's have the same thickness for photosynthesising and respiring colonies (see Larkum et al. 2003 for experimental confirmation). Indeed, the engineering literature (from which this approach is derived), estimates the allometric coefficients (*a, b*) independently of what is diffusing (e.g. heat/gas, summarised in Patterson et al. 1991). For this reason I used a fixed relationship between h_m, colony

size and water flow to model both of these processes, and calibrated this relationship from replicated measurements of P_{vs}, P_{vf} and P during photosynthesis at different flow rates, for colonies of different sizes.

In this study, I extended the general model outlined above in two ways. Firstly, I improved on existing methods for calculating the mass transfer coefficient (h_m). Suitable equipment for measuring tissue-surface oxygen concentrations (P_{vs}) was only developed recently. For this reason, previous studies evaluated h_m by setting $P_{vs} = 0$ in darkness, and assuming P_{vs} is 'at saturation' when colonies are photosynthesising (Patterson & Sebens 1989; Patterson et al. 1991). However, recent studies have found tissue oxygen concentrations between 10-91% of saturation in darkness, and between 107-400% of saturation during photosynthesis (Shashar et al. 1993; Gardella & Edmunds 1999; Larkum et al. 2003). To allow for such variation in tissue oxygen concentrations, I calibrated the relationship between h_m, flow and colony size using simultaneous direct measurements of total oxygen flux from colonies of known surface area, oxygen concentration in the water column, and oxygen concentration at the tissue surface (P, P_{vf} and P_{vs} in Eqn 5.4 respectively, see 'Photosynthesis experiments').

Secondly, I extended the general model (Eqn 5.4) to calculate daily energy acquisition (P_{day}) from rates of photosynthesis integrated over the diurnal cycle, explicitly incorporating light intensity. Expressed in this way, Eqn 5.4 becomes:

$$P_{day} = \int_{t=0}^{24} h_m(u,W)\left[P_{vs}(E(t),u) - P_{vf}\right] dt \qquad \text{Eqn 5.6}$$

where the mass transfer coefficient $h_m(u,W)$ is calibrated experimentally as outlined above. To incorporate the dependence of photosynthesis on light intensity, I allow $P_{vs}(E(t),u)$ to follow the hyperbolic tangent equation: as light intensity increases, P_{vs}

rises from its minimum value in darkness (R_d) up to its saturated value at P_{max}. Both R_d and P_{max} are dependent upon flow velocity, u.

$$P_{vs}(E(t),u) = \left[P_{\max}(u) - R_d(u)\right]\tanh\frac{E(t)}{E_k} + R_d(u) \qquad \text{Eqn 5.7}$$

For these analyses, I set P_{vf} as a constant, equal to the average value measured during the experiments. Finally, I allowed light intensity to vary over the day as a sine function defined by maximum daily irradiance (E_{MAX}), time of day (t) and day length (λ, 12 hours).

$$E(t) = E_{MAX}\sin^2\left(\frac{\pi t}{\lambda}\right) \qquad \text{Eqn 5.8}$$

Due to time constraints during data collection, I was unable to obtain estimates of E_K (light intensity at which photosynthesis is 75% of its maximum value). For many corals, estimates of E_K lie between 50 and 400 μM photons m^{-2} s^{-1} (Chalker et al. 1983; Anthony & Hoegh-Guldberg 2003a). In this study, I used a fixed value of 100 μmol photons m^{-2} s^{-1} as a baseline value. However, to confirm that my results were robust to this assumption, I explored the sensitivity of the model predictions to the value of E_K.

To predict the niche for each species, I evaluated Eqn 5.6 at maximum daily irradiance values between 50 and 1800 μM photons m^{-2} s^{-1} and at average water flow velocities between 2 and 40 cm s^{-1}. Subsequently, for each species, at all combinations of light and flow conditions, I calculated daily photosynthetic oxygen evolution (P_{day}) and daily respiratory costs (R_{day}) and measured the niche as the conditions where the ratio of daily photosynthesis to respiration (P:R ratio) is greater than 1. Oxygen fluxes were converted to carbon equivalents based on molar weights, as P_{day} = mol O$_2$ produced•12/PQ and R_{day} = mol O$_2$ consumed•12•RQ (Anthony &

Fabricius 2000) where PQ and RQ are photosynthetic and respiratory quotients (1.1 and 0.8 respectively, Muscatine et al. 1981).

5.3.2   Study species and aquarium set-up

Fieldwork for this study was conducted in May-June 2006 at One Tree Island (Great Barrier Reef [GBR], Australia, 23°28S, 152°04E). Data collection and model calibration was implemented for three species with contrasting morphologies: *Acropora nasuta* (branching), *Leptoria phrygia* (mound-shaped) and *Montipora foliosa* (plating). These species are common on the GBR and occur across a range of light and flow conditions (Veron 2000).

For each species, 15 – 18 colonies measuring 15 - 20cm diameter, were collected from 4 and 9m depths and maintained in a large aquarium (200 L) with continuous water supply from One Tree lagoon. This aquarium was divided into high- and low-light treatments using shade-cloth (HL and LL respectively), and 7-9 colonies per species were allocated to each treatment. Light and temperature within each area of the tank was continuously monitored using Odyssey loggers (Odyphoto and Odytemp, Dataflow systems, New Zealand). During the experiments, average maximum daily irradiance in treatments was 460μM photons m^{-2} s^{-1} (HL) and 140μM photons m^{-2} s^{-1} (LL). Thermostat controlled aquarium heaters maintained water temperature between 18°C and 20°C, approximating water temperature in the field at the time of collecting (19.4°C). Colony surface area was determined by foil-wrapping (Marsh 1970). For the mass flux measurements, I defined the characteristic dimension of colonies (*W*, cm) as length in the direction of flow (after Patterson 1991), and calculated this length by photographing colonies using a fixed grid as a scale bar, and analyzing photos using Image Tools Software (UTHSCSA, v2).

5.3.3 Water flow and photosynthesis experiments

For each colony, rates of photosynthesis per unit surface area were measured at 3-6 flow speeds, using a set of 4 custom-built respirometry chambers (Appendix C). These chambers had a volume of 19.5L, and were built from a 15cm diameter perspex working section (3mm wall thickness), made into a closed loop using 10cm diameter pipe. Propellers driven by variable speed 12V DC motors generated unidirectional, re-circulating flow within the chambers. Different flow speeds were produced by varying the power input to the motors, and ranged between 6 and 38 cm s^{-1} (estimated by visual particle tracking: Appendix D). These values capture the range of flow velocities commonly experienced in reef environments (e.g. Sebens & Johnson 1991; Helmuth et al. 1997a). For the respirometry assays, motors were enclosed in a water-proof housing, and the entire chamber assembly was submerged in a 200L water jacket to ensure consistent temperature during measurements.

Each day of data-collection (18 days in total), 4 colonies were selected at random and maximum rates of photosynthesis (P_{MAX}) and dark-respiration (R_D) were measured in a darkened room, where the only light source was a set of 400W metal halide lamps (Iwasaki Electronics, Japan). Together, these two parameters allow good estimates of daily-integrated photosynthesis (Anthony & Hoegh-Guldberg 2003a). Rates of oxygen evolution and consumption were determined by continuously measuring oxygen concentration within chambers over a 45 minute period using Clark-type oxygen electrodes connected to a signal-linearising device (Cheshire Systems, Australia), and recorded using a data-logger (CR10X, Campbell-Scientific, Australia). Following each measuring period, motors were turned off and chambers were flushed with fresh seawater. Oxygen electrodes were calibrated immediately prior to and after respirometry runs, using seawater at 100% O_2

saturation, and nitrogen gas as a 0% O_2 baseline. Water temperature and salinity

were monitored twice daily to account for potential variation in oxygen solubility

during data-collection. Measurements of P_{MAX} were carried out between 11am and

4pm, with colonies exposed to a constant irradiance of 720μM photons m^{-2} s^{-1} during

this period. Following this, colonies were rested in darkness for 1.5 hours with

chambers continuously flushed with seawater. Dark respiration was subsequently

measured at 3-6 flow speeds between 5:30pm and 10:30pm. To control for possible

photosynthesis and respiration of water-borne microorganisms, I conducted control

(empty-chamber) runs at each flow speed, and subtracted the oxygen

evolution/consumption by the water column from colony photosynthesis and

respiration data.

To calibrate the relationship between Reynolds and Sherwood number (Eqn

5.3), simultaneous measurements of a) whole colony rates of photosynthesis, b)

oxygen concentrations at the tissue surface c) free-stream oxygen concentrations,

were carried out in a separate (10L) chamber. This chamber had the same overall

design as the respirometry chambers (and the same turbulence regime: Appendix D).

Photosynthesis assays were conducted at 2–3 flow speeds, for 3-4 colonies of each

species from each light-acclimation treatment. A truncated range of flow conditions,

between 2 and 10 cm s^{-1}, was used for this set of measurements to encompass only

those flow velocities over which mass flux is limited by gas diffusion (i.e. below 10

cm s^{-1}, Hurd 2000). Whole colony photosynthesis was measured using the same

oxygen-electrode system and measuring protocol as above. Tissue-surface (P_{vs}) and

free-stream (P_{vf}) oxygen concentrations were measured using oxygen micro-optodes

(PreSens, Germany, 140μm thick), that were positioned using a micro-manipulator

either in the water column well above the colony (measuring P_{vf}) or directly at the

tissue surface (measuring P_{vs}). Optodes were connected to a single-channel fibre-optic oxygen meter (Microx TX, PreSens, Germany), with the signal logged and monitored in real-time (every 3 seconds) using a laptop computer. For each colony, P_{vs} and P_{vf} were measured at 6-8 points on the colony surface, with the measurement for each point calculated as the average of 6 replicate measurements over a 20s time period. Optodes were calibrated twice daily.

5.3.4   Parameter estimation and statistical analyses

Using the simultaneous measurements of rates of photosynthesis and tissue-surface oxygen concentrations, I evaluated the mass transfer coefficient (h_m) as the ratio of average mass flux over the colony surface, P, to the (average) oxygen concentration gradient ($P_{vs} - P_{vf}$). *Sh* and *Re* were then determined from Eqn 5.1 and Eqn 5.2 (see Table 5.1). The coefficients *a* and *b* of the *Sh*:*Re* relationship (see Figure 5.1) were estimated from linear-regression of $\log_{10}$ values for these parameters using the software package Statistica (StafSoft, v7). I estimated these coefficients separately for high- and low-light acclimated colonies, and then used t-tests to determine whether the slopes of these relationships differed across light treatments.

Oxygen concentrations within coral tissue may potentially become limited by photosynthetic activity (i.e. enzyme processing) rather than by diffusion of gases from tissue. To account for this, I used the species-specific calibrations of the dependence of h_m on u and W to calculate tissue oxygen concentration from independent measurements of P_{max} and R_d over a range of flow conditions between 6 – 38cm s^{-1} (Appendix D). I expressed tissue oxygen concentration as a percentage relative to the water column, and made separate calculations for P_{vs} (tissue O$_2$ based

on measurements of P_{max}) and R_{vs} (tissue O_2 based on measurements of dark respiration). I then fitted an equation of the form:

$$\%O_2 = (100 + x) + \beta\exp^{-\alpha\,\mathrm{Re}} \qquad\qquad \text{Eqn 5.9}$$

to P_{vs} and R_{vs} data for each species, where β is the percentage by which O_2 at the tissue surface deviates from saturation at $Re = 0$, α is the rate at which O_2 saturation changes with increasing Re and x allows for an asymptote at values different from 100%.

5.3.5 Tissue quality and reproductive output

As an independent validation of model performance, I tested the agreement between calculations of energy acquisition with measures of tissue quality and reproductive output in the field. To do this, I established 10 sites in and around One Tree Island lagoon (Figure 5.1). These sites were stratified to encompass a range of light and flow conditions, and were spread between the windward and leeward sides of the reef exterior, as well as within the lagoon itself. At each site, light and temperature profiles were measured during November 2005 and 2006 using Odyssey loggers and sensors (see above). Water flow was measured using the plaster-dissolution technique of Fulton & Bellwood (2005). This technique relates the dissolution of spherical gypsum balls to average flow velocity within a flume with a similar design to the flow chambers used in this study, allowing me to reliably equate chamber and field flow velocities. Flow measurements were taken at all sites over a period of 10 days during November 2006, and additionally during May/June 2006 at sites within the lagoon. During each of 5 deployments of 24 – 48 hour duration, 3 replicate gypsum balls were affixed to individual stakes 15 cm above the substratum at each monitoring site. Gypsum balls were dried to constant weight prior to and after deployment.
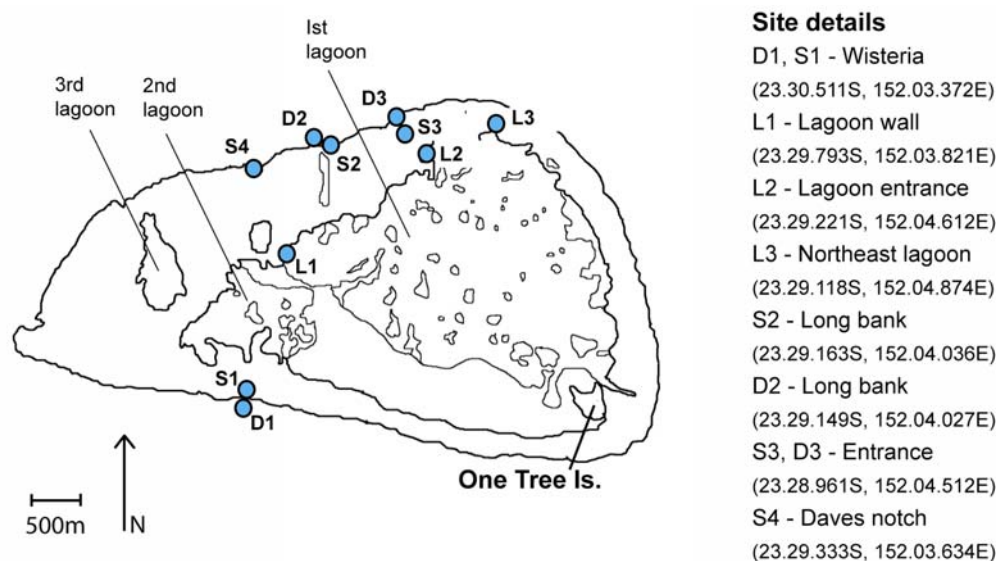
Figure 5.1: One Tree Island is a coral cay within the Capricorn Bunker group of Islands in the southern section of the Great Barrier Reef (Queensland, Australia). Study sites were stratified to encompass a broad range of light and flow conditions, and depths ranged between 11m (D1), 9m (D2, D3), 5m (S2), 4m (S3, S4) to <1m (L1, L2, L3).

During November 2005, I collected 4 fragments measuring 3-4cm diameter from 6 colonies of *Acropora nasuta* and *Leptoria phrygia* at 9 sites (these species were absent from one site), and 4 fragments from 2-6 colonies of *Montipora foliosa* from 8 sites (this species was absent from 2 sites and less abundant at all sites). In order to measure colony diameter, sampled colonies were photographed in the field with a ruler as a scale bar. Two fragments were immediately frozen for subsequent analysis of total protein concentration as a proxy for tissue biomass. Total protein was measured using Bio-Rad's total protein kit and protocol (Bio-Rad laboratories). Standards of known protein concentration between $0 - 2$ mg ml^{-1} were prepared using bovine-serum-albumen (BSA, Sigma Chemicals Australia). Tissue from each fragment (2 replicates per colony) was solubilised using 2 successive 1h digestions in

1M NaOH held at 90°C. I then combined 100µl of protein solution with 5ml of protein dye reagent and determined absorbance at 595nm spectophotometrically. Finally, total protein of samples was determined by comparison with the absorbance of the calibration standards. For the estimates of reproductive output, the remaining fragments from each colony were fixed in 10% formalin in seawater and later decalcified in 10% formic acid. Reproductive output was then determined by counting the number of eggs in each of 12-15 polyps per fragment for *Acropora nasuta* and *Montipora foliosa*. Corallites in *Leptoria phrygia* form valleys in place of discrete polyp units. Therefore, for this species I counted eggs contained in each of 12-15 mesenteries (i.e. tissue containing reproductive organs). As for the protein analyses, egg counts were conducted for 2 replicate fragments per colony.

To explore the association between measured tissue properties and energetics calculated by the model, energy acquisition was calculated for each of the sampled colonies based on their diameter, average light and flow conditions at collection sites, and the calibrated mass-transfer model for each species. Uncertainty in parameter estimates for mass fluxes was incorporated using a Monte Carlo simulation technique. To do this, 1000 replicate calculations of energy acquisition were made for each colony, using parameters drawn randomly from multivariate Gaussian distributions based on the variance-covariance matrices of the fitted models. I then correlated predicted P:R ratio (averaged over the 1000 iterations) with both protein content and reproductive output. Spearman's rank correlation was used because the reproduction data contained tied values.

5.4 Results

5.4.1 Mass flux relationships

The expected power law relationship between Sherwood and Reynolds numbers was observed for all species (Figure 5.2). That is, with increasing *Re* the degree to which mass flux was enhanced by advection, relative to that possible through diffusion, also increased. The rate of increase in *Sh* with *Re* was highest for *Montipora foliosa* (*b* = 1.3), followed by *Acropora nasuta* and *Leptoria phrygia* (*b* = 0.85 and 0.74 respectively, see Figure 5.2). Enhancement of mass flux due to flow/colony size was consistent across light-acclimation treatments for all three species. Best-fit values of *b* (Figure 5.2) for high-light and low-light acclimated colonies of each species were not significantly different (t-test; *A. nasuta*, $t_{2,0.05}(df=11) = 0.9$, p = 0.4; *L. phrygia*, $t_{2,0.05}(df=13) = 1.8$, p = 0.1; *M. foliosa*, $t_{2,0.05}(df=9) = 1.4$, p = 0.2). In other words, I found no evidence that photoacclimatory state influenced mass flux dynamics for the study species.

5.4.2 Diffusion limitation of photosynthesis and respiration

For all three species, tissue surface oxygen concentrations were not affected by increasing colony size or water flow velocity (Reynolds number) over at least the upper half of the range of conditions tested (Figure 5.3). The average standing stock of O_2 at the tissue surface was always higher than ambient when colonies were photosynthesizing, and always less than ambient when colonies were respiring. That is, the fitted parameter *x* (Eqn 5.9) was significantly different from zero in all cases (Table 5.2), with the magnitude of these differences highest for *L. phrygia* followed by *A. nasuta* and then *M. foliosa*. The value of *Re* at which oxygen concentration at the tissue surface reached 95% of its saturated value (dashed lines in Figure 5.3)

varied between species, and between photosynthesizing compared with respiring
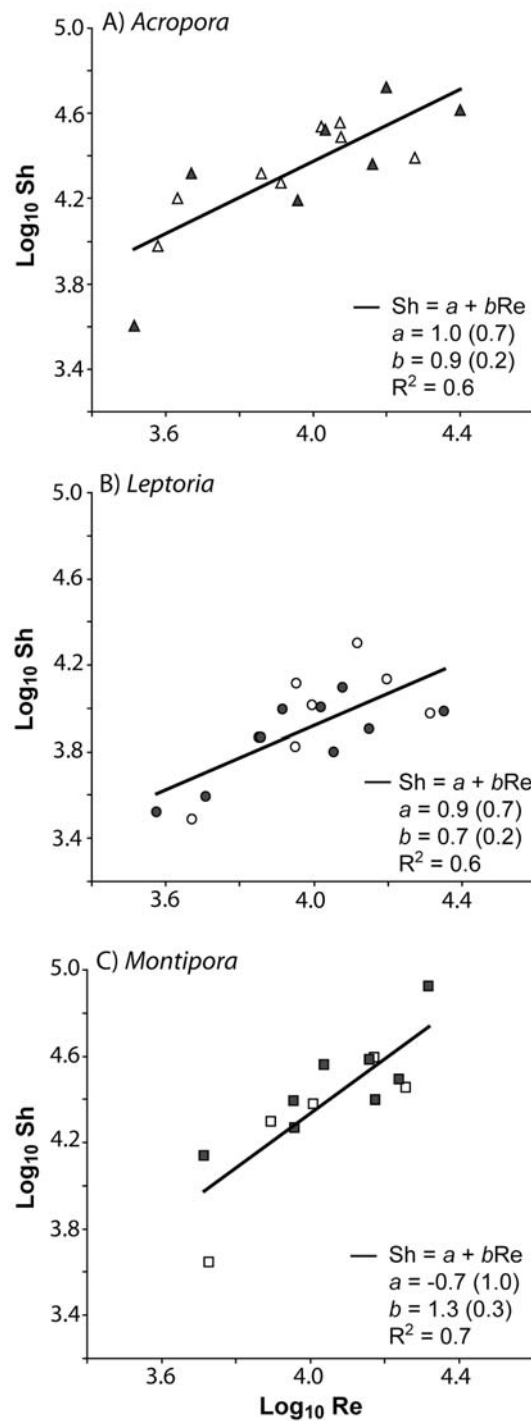
colonies.

Figure 5.2: Sherwood (Sh) versus Reynolds (Re) relationship for colonies of
Acropora nasuta (A), *Leptoria phrygia* (B) and *Montipora foliosa* (C) acclimated to
high (open symbols) and low light levels (filled symbols). Data are $\log_{10}$ values
calculated for individual colonies at different flow speeds. Regressions parameters
are presented within figure panels.
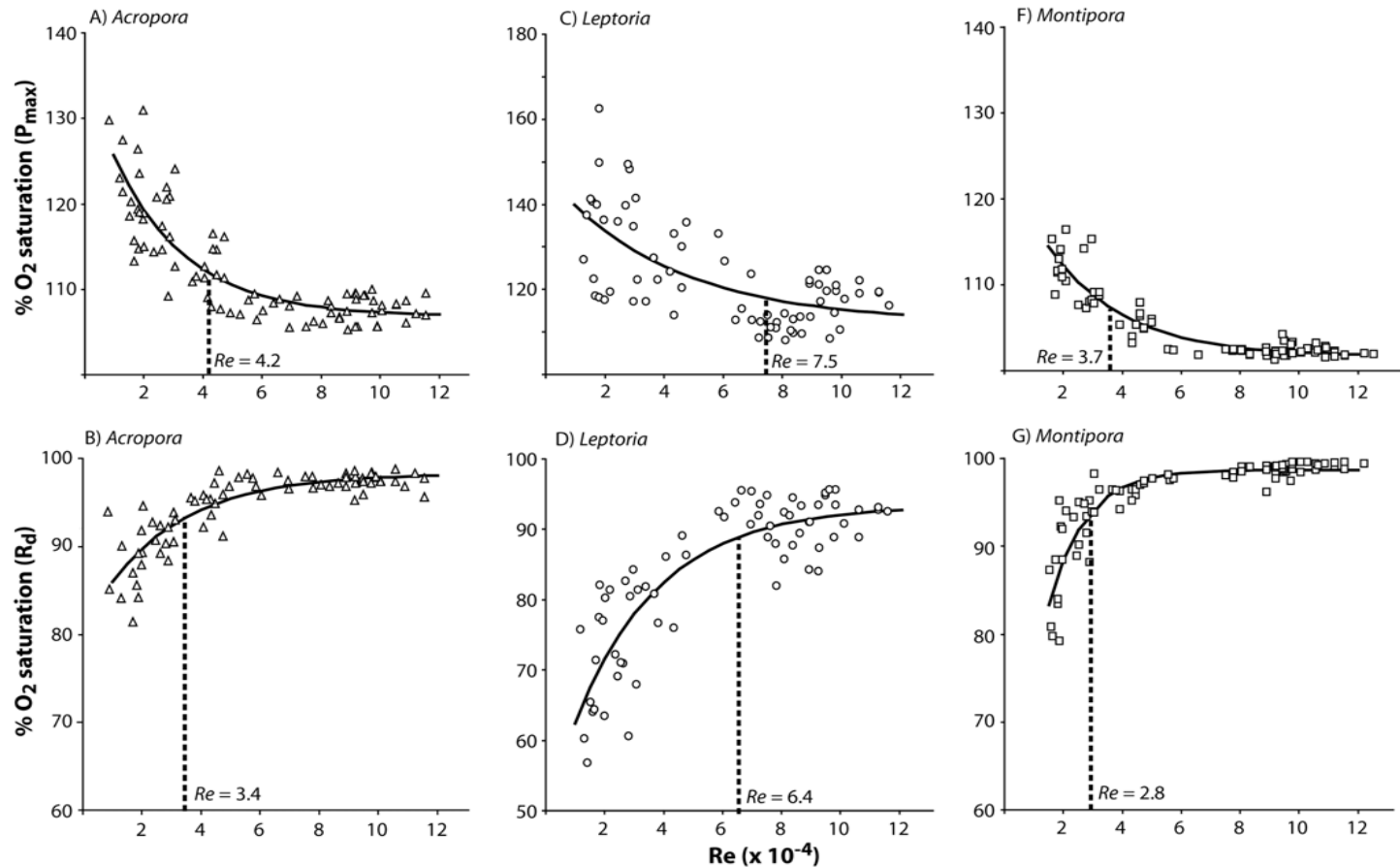
Figure 5.3: Tissue surface oxygen concentration, expressed as a percentage of dissolved oxygen concentration in seawater, for *Acropora nasuta* (△), *Leptoria phrygia* (◯) and *Montipora foliosa* (▢) during photosynthesis (A, C, E) and respiration (B, D, F). Data points are from measurements of maximum rates of photosynthesis (P_{max}) and dark respiration (R_d) for colonies at different flow speeds, taking into account the relationship between flow and mass-transfer. Parameter estimates for fitted curves are given in Table 5.2.

Table 5.2: Best-fit parameter estimates of equation describing variation in tissue oxygen concentration with increasing Reynolds number (Re) during photosynthesis (P_{max}) and respiration (R_d) for colonies of *Acropora nasuta*, *Montipora foliosa* and *Leptoria phrygia*. Parameter estimates were obtained by fitting Eqn 5.9 to the data shown in Figure 5.3 using a Levenberg-Marquardt non-linear estimation routine. [*] denotes parameters significantly different from zero .

Species	R^2	Parameter estimate ($\pm$ s.e)
A. nasuta (P_{max})	0.75	$x_P = 6.8\ (0.8)$[*] $\alpha_P = 0.41\ (0.07)$[*] $\beta_P = 28\ (3.2)$[*]
A. nasuta (R_d)	0.73	$x_R = -1.7\ (0.64)$[*] $\alpha_R = 0.36\ (0.07)$[*] $\beta_R = -18\ (1.9)$[*]
M. foliosa (P_{max})	0.56	$x_P = 1.7\ (0.39)$[*] $\alpha_P = 0.39\ (0.06)$[*] $\beta_P = 23\ (2.5)$[*]
M. foliosa (R_d)	0.79	$x_R = -1.4\ (0.35)$[*] $\alpha_R = 0.81\ (0.11)$[*] $\beta_R = -52\ (11)$[*]
L. phrygia (P_{max})	0.42	$x_P = 12\ (6)$[*] $\alpha_P = 0.25\ (0.15)$ $\beta_P = 35\ (6)$[*]
L. phrygia (R_d)	0.74	$x_R = -6.7\ (1.9)$[*] $\alpha_R = 0.35\ (0.1)$[*] $\beta_R = -44\ (6)$[*]

For all 3 species, tissue oxygen concentrations were less sensitive to flow and colony size (i.e. reached saturation at lower Reynolds numbers) during respiration compared with photosynthesis.

5.4.3   Tissue quality and reproductive output

Model predictions of daily energy acquisition were positively correlated with tissue biomass (total protein) and reproductive output (eggs per polyp/mesentery) for both *A. nasuta* and *L. phrygia* (Figure 5.4). Conversely, for *M. foliosa,* the model did
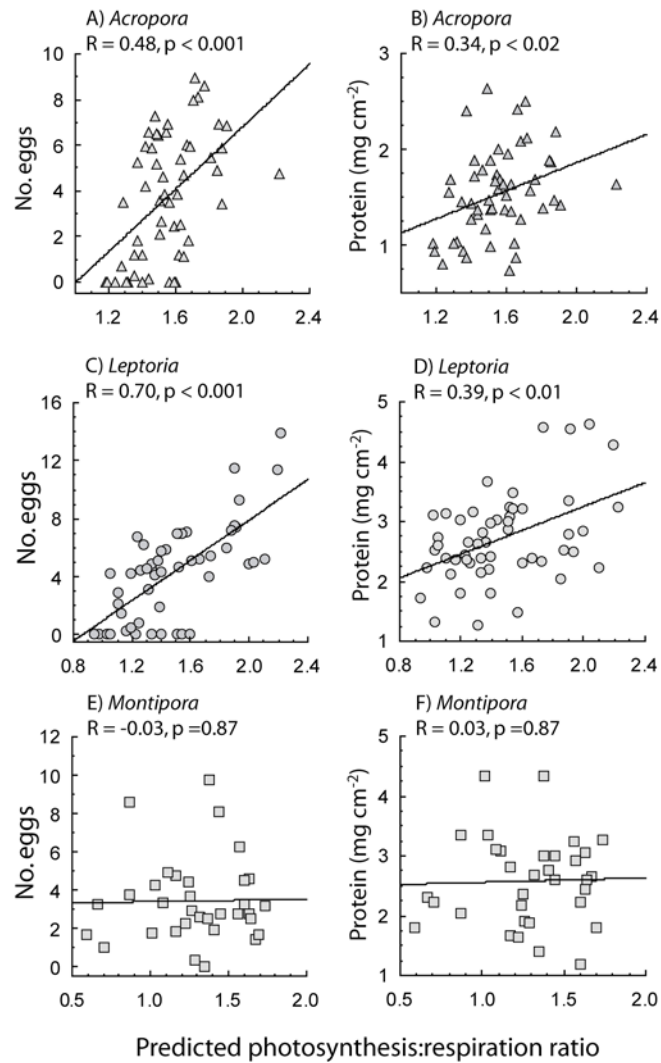
Figure 5.4: Correlations between predicted energy acquisition with reproductive output (no. eggs) and tissue biomass (total protein) for colonies of *Acropora nasuta* (△), *Leptoria phrygia* (○) and *Montipora foliosa* (□). Spearman's rank correlations (R) are shown together with significance level. Linear regression lines are presented to indicate trends. Points represent photosynthesis:respiration ratios averaged over 1000 Monte Carlo simulations.

not capture variation in tissue properties observed in the field. For this species, tissue quality varied between colonies, but this variation was uncorrelated with energy acquisition predicted by the model. Nevertheless, the mechanistic model based on the combined effects of light and flow on photosynthesis and respiration was a better

overall predictor of tissue properties than multiple regression models incorporating these two variables (Appendix E). Indeed, regression analyses indicated a negative correlation between tissue biomass and water flow. This trend is opposite what one would expect given that flow enhances flux of photosynthetic gases by reducing diffusive boundary layers. Overall, these results indicate that the process-based model captures nonlinear interactions between light and flow that are unlikely to be captured with regression-based approaches.

5.4.4 Niche width: Energy Acquisition

The influence of light intensity and water flow velocity on daily energy acquisition differed among the study species, and was variably influenced by colony size (Figure 5.5). In general, small colonies of each species had a positive energy balance across a narrower range of conditions than larger colonies (Figure 5.5). Of the species considered here, the niche of *A. nasuta* was the least sensitive to flow and colony size. For this species, niche size increased only slightly with colony size, due to an increase in the range of light conditions tolerable under high flow conditions for large colonies (Figure 5.5 A&B). For *L. phrygia,* the size of the niche increased with colony size to a much greater extent (Figure 5.5 C&D). The model predicted that small colonies of *L. phrygia* should be restricted to habitats of high-light and high-flow, but large colonies had a positive energy balance unless light and/or flow were low. The niche for *M. foliosa* responded differently to increasing colony size than the other species. Small colonies of this species had a positive energy balance at most light levels only if flow rates were high (Figure 5.5E). As colony size increased, the niche generally expanded with more flow levels becoming viable.
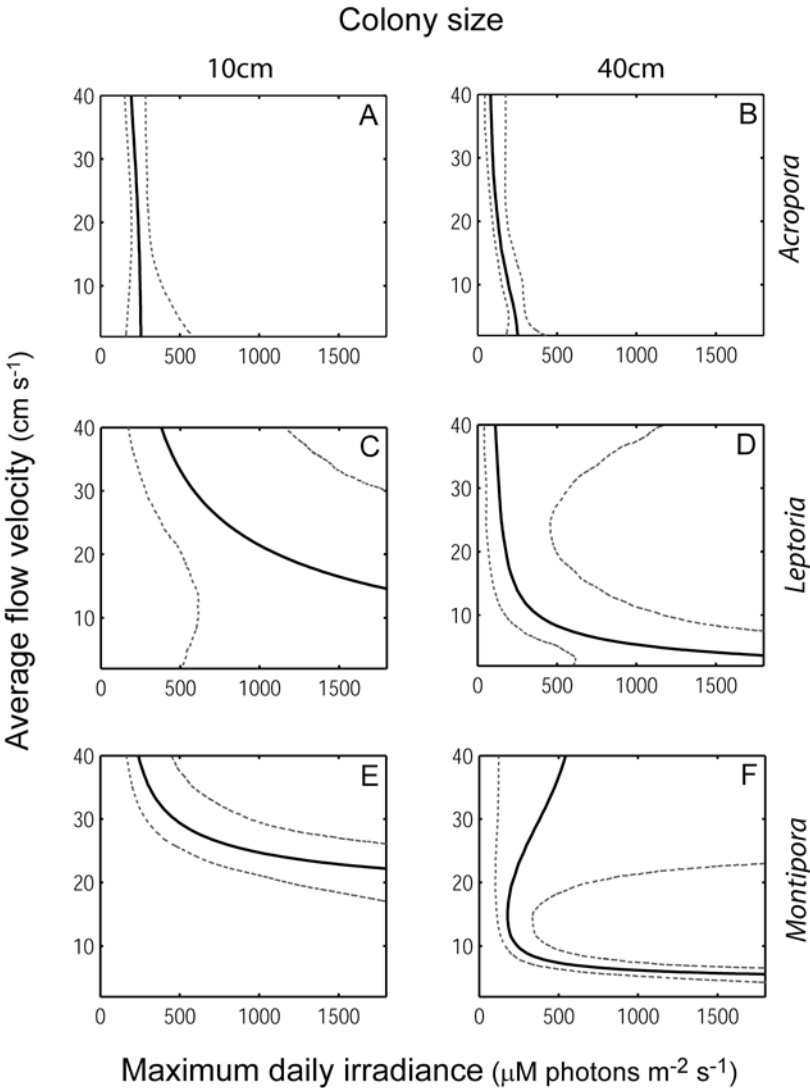
Figure 5.5: Energetic niche dimensions for 10 and 40cm diameter colonies of *Acropora nasuta* (top row), *Montipora foliosa* (middle row) and *Leptoria phrygia* (bottom row) along gradients of light intensity (x-axis of panels) and flow velocity (y-axis of panels). Lines represent mean contours (solid lines) of positive energy acquisition (daily photosynthesis > respiration) and 95% confidence intervals (dashed lines) generated from 1000 Monte Carlo simulations.

Mechanistically, the differences between species were driven by the magnitudes of the differences in tissue oxygen between photosynthesizing and respiring colonies. For *A. nasuta* photosynthetic oxygen fluxes were greater than

respiratory fluxes at low Reynolds numbers (*Re*) but the opposite was true for *L. phrygia* and *M. foliosa* (see best-fit values of β in Table 5.2). This meant that colonies of *A. nasuta* that were small and/or exposed to low flow conditions (low *Re*) had a positive energy balance, whereas energy acquisition for small colonies of *L. phrygia* and *M. foliosa* was sensitive to the relationship between tissue oxygen and *Re*. Results also indicated that, for large colonies of *M. foliosa* and *L. phrygia*, high flow conditions were only tolerable if irradiance levels were also high (Figure 5.5 D&F). For these two species, rates of photosynthesis at high *Re* were only slightly greater than rates of respiration. This meant that, unless light levels were high over most of the day, at high flow there were some combinations of parameter values for which energy acquisition by large colonies of *M. foliosa* and *L. phrygia* was less than maintenance costs.

Despite a robust characterization of the physiological mechanisms underlying photosynthetic energy acquisition for the three study species, the combination of uncertainties in parameter estimates meant that the 95% confidence interval of energy balance contours was in some cases quite large. Niche boundary predictions (area between the dashed lines in Figure 5.5) were most precise for *A. nasuta*, and most variable for small colonies of *L. phrygia* and large colonies of *M. foliosa*. Greater uncertainty in niche contours for the latter 2 species was due to higher between-colony variance in oxygen production and consumption (e.g. Figure 5.3 C&D) and corresponding uncertainty in the parameters of the relationships between tissue oxygen concentrations and *Re* (Table 5.2). Despite uncertainty about the exact position of the niche boundary, the model identifies some important general trends. Niche size increases with colony size; decreasing light availability leads to a narrowing of the flow conditions that allow a positive energy balance for large

colonies of *L. phyrgia* and *M. foliosa*; and *A. nasuta* has a positive energy balance over a broader range of environmental conditions compared to the other species.

As mentioned (see "Mass flux relationships" above), there was no evidence that photoacclimatory state influenced gas diffusion dynamics for any of the study species. However, the light-acclimation irradiances used in this study did not include irradiances as high as those that might be observed in shallow, clear waters on sunny days. Therefore, to test how acclimation to high-light influenced niche boundaries, I re-calculated energy acquisition, varying tissue oxygen concentrations (P_{vs}, R_{vs}) to capture the essential components of photoacclimation. Photoacclimation to high light typically increases maximum rates of photosynthesis (P_{max}) and dark respiration (R_d) per unit surface area, and also increases the light level at which P_{max} is reached (summarized by the sub-saturation irradiance parameter, E_K). To test the sensitivity of niche boundaries to variation in photoacclimatory state, I re-calculated energy acquisition allowing for variation in the relationship between tissue surface oxygen concentration and Reynolds number (Eqn 5.9 and Figure 5.3). These calculations were made for 3 photoacclimatory states in addition to the low-light acclimated colonies for which the model was parameterised. Variation in photophysiology for these additional photoacclimatory states was designed to capture changes in oxygen production and consumption with acclimation to high light, as follows:

1) Rates of oxygen production at maximum photosynthesis increase with acclimation to intermediate irradiance but decline at the highest light levels (e.g. Green et al 1998, Chapters 3 and 4). I modelled these dynamics by allowing an increase in tissue oxygen concentrations in stagnant water (parameter β_P) and a decrease in the rate at which tissue oxygen concentrations decline with increasing flow (parameter α_P, Table 5.3). The effect of these

parameter changes is to increase oxygen flux during photosynthesis at all flow

speeds by increasing the concentration gradient across the DBL.

2)   Rates of respiration typically increase with acclimation to high light. To

simulate high-light acclimation of respiration I decreased tissue oxygen

concentrations in stagnant water (parameter β_R) and decreased the rate at which

tissue oxygen concentrations increase with flow (parameter α_R, Table 5.3).

Again, these changes increase oxygen flux during respiration by increasing the

concentration gradient across the DBL.

3)   The subsaturation irradiance parameter (E_K) generally shows a saturating

increase with acclimation to high light (Anthony and Hoegh-Guldberg 2003b).

I modified the values of this parameter accordingly (Table 5.3).

Table 5.3: Parameter values describing the relationship between Reynolds number
and tissue oxygen concentrations for simulated photoacclimatory states.

Species	Parameter	Photoacclimatory state			
		Low	Low – Intermediate	High – Intermediate	High
A. nasuta	α_P	0.41	0.35	0.35	0.41
	β_P	28	36	36	28
	α_R	0.36	0.32	0.28	0.24
	β_R	-18	-20	-22	-24
	E_K	100	160	190	200
M. foliosa	α_P	0.39	0.32	0.32	0.39
	β_P	23	31	31	23
	α_R	0.81	0.78	0.75	0.72
	β_R	-52	-56	-60	-64
	E_K	100	160	190	200
L. phrygia	α_P	0.25	0.19	0.19	0.25
	β_P	35	44	44	35
	α_R	0.35	0.32	0.29	0.26
	β_R	-44	-46	-48	-50
	E_K	100	160	190	200

These simulations revealed that the niche was insensitive to light-acclimation over a broad range of parameter combinations. However, the niche of high-light acclimated colonies of each species was reduced, and shifted toward the high-light/high-flow area of the environmental gradient for *A. nasuta* and *L. phrygia* and toward the high-light/intermediate-flow region for *M. foliosa* (Figure 5.6). Overall, this indicates that the niche boundaries calculated by the model are robust over much of the realistic range of light conditions, but may overestimate energy acquisition in very high-light habitats, particularly for *M. foliosa*.
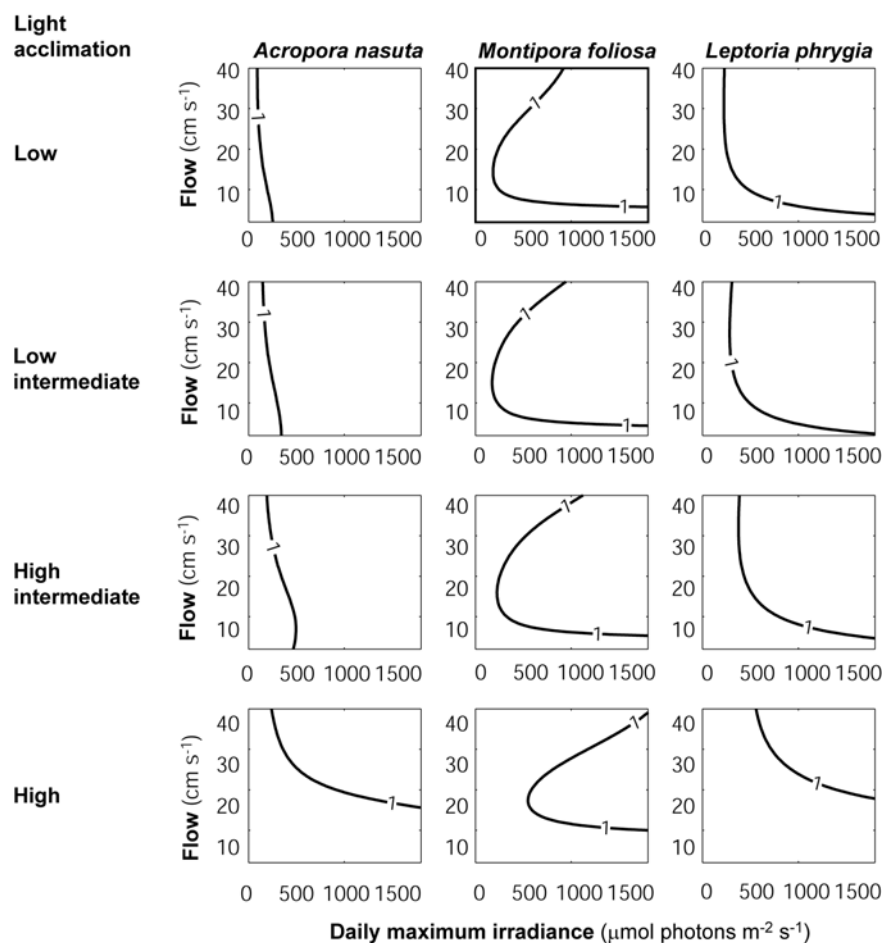
Figure 5.6: Niche dimensions for colonies of three species acclimated to different light levels. Panels show positive energy acquisition contours along gradients of light intensity (daily maximum irradiance, x-axis of panels) and flow (y-axis of panels), for corals acclimated to low, intermediate low, intermediate high and high light levels respectively (see Table 5.3 for details).

5.5 Discussion

This study establishes a quantitative link between metabolic rates and the dominant environmental gradients on coral reefs (light intensity and water flow), enabling prediction of the conditions under which a positive energy balance is possible. These analyses demonstrate that tissue biomass and reproductive output are strongly influenced by environmental gradients of light and flow, through their effects on photosynthetic energy acquisition. In addition, the mechanistic framework developed in this study identifies important ecological implications of variation in physiology. Firstly, due to its higher photosynthetic capacity, the branching coral *A. nasuta* has a positive energy balance over a wider range of conditions than *L. phrygia* and *M. foliosa*. Secondly, niche size increases with colony size: larger colonies of all three species had a positive energy balance over a greater range of conditions because photosynthesis was more strongly enhanced by changes in colony size and flow (Reynolds number, *Re*) than respiration. Finally, the influence of flow on energetics was variable across the light gradient. Surprisingly, for *M. foliosa* and *L. phrygia*, model predictions suggested that low light habitats were only tolerable under low to intermediate flow conditions. This is because rates of photosynthesis and respiration of these species are similar at high *Re*. The net effect of this is that for large colonies at high flow (high *Re*), unless light levels are high, respiration over a 24 h period is greater than photosynthesis during daylight hours. In addition, the synergistic effects of light and flow influence performance in a way that is not monotonically related to the effects of either of these variables individually, or together. This highlights the importance of accounting for the interaction of these variables in a mechanistic framework.

5.5.1   Mass flux model

My results indicate that respiration becomes limited by oxygen consumption within tissue at lower *Re* than does oxygen evolution during photosynthesis. In other words, flow stops affecting respiration before it stops affecting photosynthesis. Although the magnitude of the difference in the values of *Re* at which this occurs is small, the consistency of this pattern across three species suggests that greater flow-sensitivity of photosynthesis compared with respiration is a general phenomenon. The energetic model developed here stems from a general model that can be used to calculate the uptake and/or release of other solutes if the solubility of these molecules is known (e.g. NO_3 and PO_4: Sanford & Crawford 2000). However, variation in diffusion potential for different solutes highlights an underlying assumption of the model: that efflux of oxygen during photosynthesis is linearly related to influx of carbon dioxide. This assumption is supported by experimental evidence that flow has the same affect on photosynthesis when measured by changes in dissolved organic carbon compared with dissolved oxygen (Carpenter & Williams 2007), and that boundary layer resistance to different molecules decreases in parallel with increasing flow (Koch 1994). Therefore, boundary layer properties are not likely to be responsible for the differences in flow effects on respiration compared with photosynthesis. A more likely explanation is that this phenomenon is driven by spatial segregation in the sites of oxygen production and respiration within tissue. During respiration, oxygen is consumed by both coral tissue and symbionts, whereas during photosynthesis oxygen produced by symbionts must pass through tissue before it reaches the diffusive boundary layer (and CO_2 must diffuse likewise in reverse). The net effect of this is an additional impediment to oxygen efflux during photosynthesis compared with oxygen influx during respiration. This would increase

the resistance to gas exchange, and increase the conditions over which flow enhances mass flux.

5.5.2 Predictive accuracy of the niche model

Energy acquisition calculated by the model proved to be a strong predictor of both tissue biomass and reproductive output for two of the three study species (*A. nasuta* and *L. phrygia*). However, the model did not capture variation in these properties for *M. foliosa*. There are three main reasons why this may have occurred. Firstly, *M. foliosa* has a laminar growth form, and all sampled colonies grew approximately flat along the substrate. However, my field measurements of flow velocity were taken 15cm above the substrate, a typical height for colonies of *A. nasuta* and *L. phyrgia*. Due to small-scale topographical differences, water flow at the substrate is highly variable within sites (Eagle et al. in press), and flow over substrate-attached *M. foliosa* colonies may therefore differ substantially from the measured values. Secondly, due to its horizontal growth form, *M. foliosa* may be more strongly influenced by inter-specific competition (i.e. by overtopping, e.g. Stimson 1985), or by other substrate-associated processes such as instability and bioerosion. These factors would influence tissue quality for this species (e.g. due to damage, Ward 1995b), but are not accounted for in the physiological model.

The third possibility is that heterotrophic feeding may make a larger contribution to the energy budget of *M. foliosa* than for the other study species. Under normal conditions (such as those investigated here), heterotrophic feeding provides only a small fraction of total energy acquisition (Anthony & Fabricius 2000; Grottoli et al. 2006). Moreover, a high capacity for heterotrophy is particularly unexpected for *M. foliosa* because enhanced particle feeding is generally associated with large polyp size (Porter 1976 but see Sebens et al. 1996), whereas *Montipora*

have very small polyps (Veron 2000). Nevertheless, recent experimental work indicates that heterotrophy plays a greater role in coral energetics than previously believed. Studies have shown that calcification rates may be 50-75% higher in corals fed with zooplankton (Houlbreque et al. 2004), and that overall growth rates may double with feeding (Miller 1995). For *Montipora*, a surprisingly high capacity for heterotrophy has been demonstrated. For instance, Grottoli et al. (2006) showed that, following a bleaching event which strongly reduced photosynthesis, a *Montipora* species was able to up-regulate heterotrophic feeding to a level that provided sufficient carbon to meet daily maintenance costs. A greater reliance on heterotrophic feeding would explain the lack of agreement between model predictions of energy acquisition and performance of *Montipora foliosa* in the field.

5.5.3 Effect of colony size on predicted niche dimensions

For all three species considered here, the niche model predicts that large colonies have a positive energy balance over a broader range of light and flow conditions than small colonies. In other words, niche size increases with colony size, mainly through an expansion of the tolerable flow conditions at a given light intensity. From a physiological basis, this result is surprising, particularly in light of the well-known negative allometric scaling of metabolism with body size in many organisms (West et al. 1997). Moreover, there is evidence for corals of a reduction in rates of photosynthesis and particle capture per unit surface area with increasing colony size (Jokiel & Morrisey 1986; Kim & Lasker 1998). Both of these factors indicate that the conditions allowing a positive energy balance should decrease as coral colonies grew larger. On the other hand, in agreement with my findings of positive effects of size on energy balance for the study species, long-term monitoring of small colonies from several coral genera has shown positive effects of colony size

on growth rates (Edmunds 2006). Similarly, energy surplus has been shown to increase with size for solitary corals (Edmunds & Elahi 2007a). For the species considered here, colony size positively influences energy balance because photosynthesis is enhanced by flow over a greater range of Reynolds numbers than respiration is. These results demonstrate that different metabolic processes cannot be assumed to respond to environmental conditions in the same way.

5.6 Conclusions

Based on a mechanistic understanding of species-specific relationships between dominant environmental gradients and metabolic processes, this study quantifies the conditions that allow different coral species to survive and reproduce. Given the current threats to coral reefs worldwide, this framework may be particularly useful for predicting environmental tolerances of different species. These results highlight the importance of incorporating organism size into physiological models and investigations of niche size: for corals, colony size directly influences the conditions under which a positive energy balance is possible. In addition, this study demonstrates the utility of process-based models for quantifying how physiology influences ecology, and for predicting the ecological consequences of varying environmental conditions.

6   GENERAL DISCUSSION

6.1   Summary of results

This thesis provides a deeper understanding of the processes that influence the habitat distributions of reef-building corals, achieved by quantifying environmental effects on coral physiology and integrating these effects into a framework for coral energetics. Firstly, I investigated how energy available for growth and reproduction varied in response to light intensity for a species of foliose coral (*Turbinaria mesenterina*). It was previously unclear whether exposure to high light levels, like those generally experienced in shallow-water reef habitats, had consequences for the energetics of coral symbioses. For several other photosynthetic taxa, including higher plants and phytoplankton, photoinhibition results in a 6 – 25% decline in daily carbon gain (Ogren & Sjostrom 1990; Pahl-Wostl 1992; Werner et al. 2001), leading to reduced growth rates (Laing et al. 1995). Analogously, fluorescence assays of the photosynthetic activity of symbionts within coral tissue demonstrate that light use efficiency is reduced under high irradiance (e.g. Brown et al. 1999; Jones & Hoegh-Guldberg 2001; Winters et al. 2003). It is likely that changes in fluorescence in corals have been interpreted as indicating a decline in rates of photosynthesis (e.g. Brown et al. 1999) based on the premise that photoinhibition is energetically costly in other taxa. Instead, a direct comparison of these assays in this thesis (Chapter 2) revealed a strongly non-linear relationship between fluorescence and rates of photosynthesis. Indeed, large changes in fluorescence can occur without any measurable change in gas exchange (Chapter 2, see also Ulstrup et al. 2006). My work demonstrates that over a diurnal cycle, changes in photochemical efficiency of symbionts do not cause a decline in energy acquisition of coral symbioses although rates of respiration are light-enhanced. This

conclusion is based on the observation that, following exposure to high-light over a diurnal cycle, respiration was equally enhanced for corals acclimated to low, intermediate and high-light levels. If light-enhancement of respiration was due to increased metabolic costs of repairing photo-damage (chronic photoinhibition), respiration would be more strongly enhanced in corals acclimated to low light, because their capacity to use other biochemical pathways to dissipate excitation energy is reduced. Overall, these results indicate that for coral colonies exposed to ecologically relevant light intensities, costs of photoinhibition are negligible under short-term exposure to high irradiance (Chapter 2). However, these analyses did suggest that changes in the properties of the photosynthetic apparatus following several days of exposure to high-light can have a negative impact on energy balance.

Building on these findings, I subsequently investigated whether costs of photoinhibition are manifest via changes to the photosynthetic apparatus during photoacclimation to high light intensities (Chapter 3). Using a process-based model of photosynthesis (Zonneveld 1997) I quantified how changes in the major components of the photosynthetic apparatus influenced coral energy balance. Analyses revealed that, as corals photoacclimate to high light intensities, changes in several components of the photosynthetic machinery mean that high-light habitats do not provide maximal energy acquisition. In fact, for the foliose coral *Turbinaria mesenterina*, I found evidence of a strong reduction in the amount of energy available for growth and reproduction for corals growing under high light. Importantly, these costs appear to be sufficiently large to prevent survival of colonies in the long-term. Negative effects of high-light have previously been observed for the energetics of plants and phytoplankton (e.g. Richardson et al. 1983; Murchie & Horton 1997; Green et al. 1998) but not for corals. A common view in the literature

has been that detrimental effects of high irradiance are primarily observed for corals when temperatures are elevated (Yentsch et al. 2002; Lesser 2004; Levy et al. 2004). This thesis shows that, on the contrary, light can have negative effects on coral performance, and that energy balance is optimal in intermediate habitats.

Altering colony shape is one potential strategy for avoiding costs of excessive light exposure (e.g. Muko et al. 2000; Anthony et al. 2005). In the field of coral biology, the dominant hypothesis that purports to explain patterns of variation in coral colony shape is that morphological plasticity maximizes light capture and energy acquisition as light levels decrease in deep water (e.g. Dustan 1975; Graus & MacIntyre 1982; Gleason 1992). However, prior to this thesis, no framework was available that allowed comparison of energy acquisition for a range of complex morphologies in response to varying light conditions, while also taking into account flexibility in photophysiology. Using a model of light capture in combination with experimental data on photosynthesis, I demonstrate in this thesis that morphological plasticity optimises the amount of energy corals have available for growth and reproduction. My analyses show that the optimal morphology is clearly defined at the boundaries of the environmental gradient, with non-optimal morphologies in these habitats having greatly reduced energy acquisition. However, at the center of the environmental gradient, flexibility in photophysiology means that energy acquisition is very similar for multiple morphologies. Therefore, variation in morphology is most important at niche boundaries and physiological flexibility is important in intermediate and less predictable habitats where a rapid and reversible response to environmental fluctuations may be beneficial.

In addition to light intensity, water flow velocity varies markedly between reef habitats and has a strong influence on coral metabolism (e.g. Jokiel 1978, Lesser

et al. 1994). Previously, researchers have considered the effects of these environmental gradients independently (Chalker et al. 1983 c.f. Sebens et al. 2003). In this thesis, I built on existing models of gas exchange (e.g. Patterson 1992) to integrate the effects of light intensity, flow velocity and colony size into a single model. Analysis of this model showed that, due to its higher photosynthetic capacity, the branching coral *A. nasuta* has a positive energy balance over a wider range of conditions than both a massive (*L. phrygia*) and a foliose species (*M. foliosa*). In addition, colony size was revealed as having a strong influence on niche width. Although recent studies have indicated that ageing of coral tissue (i.e. polyp senescence) leads to a reduction in calcification rates (Elahi & Edmunds 2007b) and branch initiation rates (Permata & Hidaka 2005), the results of Chapter 5 showed that large colonies of all three species had a positive energy balance over a broader range of conditions than small colonies.

The overarching aim of my thesis was to evaluate the performance of corals in response to environmental gradients. Using process-based models, my research quantified the mechanisms through which light intensity and water flow velocity influence coral performance. Model predictions of energy balance were strongly correlated with observed tissue biomass and reproductive output for *Acropora nasuta* and *Leptoria phrygia*. In addition, an optimality model based on morphology-specific energy acquisition adequately captured observed variation in colony shape for *Turbinaria mesenterina* across a depth gradient. These results confirm that energy balance has a strong and measurable effect on growth and reproduction of corals in their natural environment.

6.2   Robustness of results

The environmental thresholds, or niche boundaries, identified in my thesis are derived from the principle that survival under a particular set of environmental conditions requires, at the minimum, sufficient energy uptake to meet cellular maintenance costs (Leibold 1995; Kooijman 2000; Kearney 2006). Energy budget models (e.g. Nisbet et al. 2000) are also based on this principle, and implicitly assume that above such environmental thresholds (i.e. within the fundamental niche), energy acquisition continues to influence performance. This assumption stems from the concept that a greater energy surplus (i.e. energy remaining once maintenance costs have been accounted for), translates to more rapid growth, or to greater reproductive output (e.g. Kooijman 2000). My results provide strong support for this assumption: energy balance was a strong predictor of colony morphology (Chapter 4), together with tissue biomass and reproductive output (Chapter 5). Nevertheless, corals acquire additional carbon through heterotrophic feeding (e.g. Ferrier-Pages et al. 1998a, 2003) and this potentially influences energy balance. Secondly, some of the carbon acquired through photosynthesis is excreted as mucus and is therefore not made available for growth and reproduction (e.g. Crossland et al. 1980a & b). In the following section I discuss the robustness of the light and flow niche boundaries defined for my study species to each of these processes individually.

6.2.1   Heterotrophy

Corals have the capacity to acquire carbon and nutrients from feeding on a variety of sources (Table 6.1). Originally, zooplankton feeding was considered to be the main alternative to carbon acquisition via symbiont photosynthesis (Muscatine & Porter 1977; Davies 1984). Several studies have explored how zooplankton density and/or water flow velocity influences plankton capture (e.g. Sebens & Johnston

1991; Sebens et al. 1998; Ferrier-Pages et al. 2003). Although these experiments have occasionally measured carbon uptake through zooplankton feeding at levels comparable to that obtained via photosynthesis (Table 6.1), they have generally been conducted at zooplankton densities much higher than observed in the field. The mean zooplankton concentration on coral reefs is approximately 1000 m^{-3} or one per litre (based on data in Heidelberg et al. 2004). However, Ferrier-Pages et al. (2003) used plankton concentrations of 1750 litre^{-1}, and Sebens et al. (1998) conducted feeding trials using a concentration of 100 litre^{-1}. Studies of corals under natural conditions estimate carbon acquisition through zooplankton feeding to be approximately 5μg C cm^{-2} d^{-1} (Table 6.1, Palardy et al. 2005). This suggests that zooplankton feeding makes a negligible contribution to overall carbon acquisition under typical field conditions, and is unlikely to affect the niche boundaries identified in my thesis.

In addition to feeding on zooplankton, corals consume bacteria and microplankton (Bak et al. 1998; Ferrier-Pages et al. 1998a), and take up dissolved carbon and nitrogen (Sorokin 1973; Muscatine & D'Elia 1978; Ferrier 1991; Grover et al. 2003). Although there is some evidence that this feeding mode is up-regulated in colonies from shaded habitats (where photosynthesis is reduced, Ferrier-Pages et al. 1998a; Hoegh-Guldberg & Williamson 1999), microplankton feeding and dissolved carbon uptake make a minor contribution to the total carbon acquisition for all coral species investigated to date (i.e. 2 – 30 μg C cm^{-2} d^{-1} from microplankton [Table 6.1] c.f. 200 – 3000 μg C cm^{-2} d^{-1} from photosynthesis [Table 1.3]). Therefore, this feeding mode is also unlikely to have a significant influence on the coral niche boundaries defined in my thesis.

Corals also have the potential to use suspended particulate matter (SPM) as a food source (e.g. Anthony 1999). Measurements of carbon acquisition through this

feeding mode vary between species by 2 orders of magnitude, ranging from

approximately 3 to 580 µg C cm^{-2} d^{-1} (Table 6.1). Species with larger polyps and/or a

Table 6.1: Summary of literature estimates of daily carbon and nitrogen acquisition

from various modes of heterotrophic feeding.

Prey	Species	Carbon (µg cm^{-2} d^{-1})	Nitrogen (µg cm^{-2} d^{-1})	Experimental conditions
Zoo-plankton	*Madracis mirabilis* (1)	529.2		100 Artemia l^{-1}
	Madracis decactis (2)	470.4		
	Porites porites (1)	604.8		100 Artemia l^{-1}
	Montastrea cavernosa (1)	85.7		100 Artemia l^{-1}
	Meandrina meandrites (3)	53.8		
	Meandrina meandrites (2)	33.6		
	Stylophora pistillata (4)	24.2		Up to 1750 plankters l^{-1}
	Pocillopora damicornis (5)	3.9		Field study
	Pocillopora damicornis (6)	268.8		
	Pavona clavus (5)	5.9		Field study
	Pavona gigantea (5)	6.0		Field study
Suspended particulate matter	*Diploria strigosa* (7)	152	13	[15 mg l^{-1}]
	Montastrea franski (7)	584	48	[15 mg l^{-1}]
	Siderastrea radians (7)	474	39	[15 mg l^{-1}]
	Madracis mirabilis (7)	118	9.6	[15 mg l^{-1}]
	Pocillopora damicornis (8)	9.9	0.81	Up to [30 mg l^{-1}]
	Montipora digitata (8)	5.4	0.44	Up to [30 mg l^{-1}]
	Acropora millepora (8)	4.4	0.36	Up to [30 mg l^{-1}]
	Porites cylindrica (8)	2.8	0.23	Up to [30 mg l^{-1}]
	Porites cylindrica (9)	5.4	0.44	Up to [30 mg l^{-1}]
	Goniastrea retiformis (9)	84	9.8	Up to [30 mg l^{-1}]
	Turbinaria mesenterina (10)	60	4.9	Up to [50 mg l^{-1}]
Micro-plankton	*Galaxea fascicularis* (11)	2.33	0.75	B, C, F
	Madracis mirabilis (12)	3.03		B
	Stylophora pistillata (13)	33.26		B, C
	Stylophora pistillata (11)	27.39	7.57	B, C, F
Dissolved compounds	*Agaricia fragilis* (14)	-	2.82	Amino acids
	Diploria strigosa (15)	-	1.68	Nitrate
	Favia fragum (14)	-	8.07	Amino acids
	Madracis mirabilis (14)	-	3.43	Amino acids
	Montastrea anularis (14)	-	16.74	Amino acids
	Pocillopora damicornis (16)	-	2.20	Ammonia
	Pocillopora damicornis (16)	-	0.24	Amino acids
	Stylophora pistillata (17)	-	0.15	Nitrate

Notes: Values converted into mg cm^{-2} d^{-1} based on the following: carbon content of zooplankton = 0.15µg C prey^{-1} (Ribes et al. 1998), carbon and nitrogen content of SPM = 5% and 0.41% respectively (Anthony & Fabricius 2000, same values used for carbon content of SPM in Mills et al. 2004). Zooplankton feeding rates per polyp were converted using polyp densities of: 14, 15, 1, 2 and 20 polyps cm^{-2} for *M. decactis*, *M. mirabilis*, *M. cavernosa*, *M. meandrites* (based on images in Veron 2000), and *P. porites* (Edmunds & Davies 1989) respectively. Microplankton feeding rates were converted using 360 and 1.2 polyps cm^{-2} for *S. pistillata* and *G. fascicularis* and biomass per polyp reported in (11). B, C and F represent feeding on bacteria, ciliates and flagellates respectively.

References: (1) Sebens et al. 1998, (2) Sebens & Johnson 1991, (3) Johnson & Sebens 1993, (4) Ferrier-Pages et al 2003, (5) Palardy et al. 2005, (6) Clayton & Lasker 1982, (7) Mills et al 2004, (8) Anthony 1999, (9) Anthony & Fabricius 2000, (10) Anthony & Connolly 2004, (11) Houlbreque et al 2004, (12) Bak et al. 1998, (13) Ferrier-Pages et al. 1998a, (14) Ferrier 1991, (15) Badgley et al 2006, (16) Hoegh-Guldberg & Williamson 1999, (17) Grover et al. 2003.

massive colony morphology (e.g. *Goniastrea retiformis* in Anthony & Fabricius 2000, and *Montastrea franksi* in Mills et al. 2004) tend to have higher SPM feeding capacity than species with smaller polyps and/or a branching morphology. There is also evidence that corals from reefs with high sediment loads have enhanced SPM feeding capacity compared with those from clear-water environs (Anthony 2000). Finally, SPM uptake increases in response to a reduction in symbiont photosynthesis and may potentially be sufficient to meet maintenance metabolism requirements for some species (Anthony & Fabricius 2000; Grottoli et al. 2006).

In the context of my thesis research, Anthony & Connolly (2004) showed that incorporating heterotrophic feeding on SPM into an energy budget model for *Turbinaria mesenterina* had an effect similar in magnitude to a 10% change in the maximum rate of photosynthesis. This indicates that inclusion of this feeding mode into the analyses presented in Chapters 3 through 5 of my thesis would have an effect similar in magnitude to the observed uncertainty in photophysiology (estimated uncertainty in photosynthesis parameters in my analyses was more than 10% of the best-estimate values of these parameters, Table 4.2 and Table 5.2). In other words, the shift in the position of the zero energy balance contour due to SPM feeding (e.g. Figure 5.5) would lie within the observed 95% confidence interval around this contour. Therefore, my results for *Turbinaria mesenterina* are likely to relatively insensitive to realistic levels of heterotrophic feeding. Similarly, SPM feeding is unlikely to influence the niche boundaries defined for the species investigated at One Tree Island. Firstly, there is no a priori reason to expect that heterotrophic feeding on SPM is a larger component of the energy budgets of *Acropora nasuta*, *Leptoria phrygia* and *Montipora foliosa/aequituberculata* than it is for *T. mesenterina*.

Secondly, due to its distance from the Australian mainland, the oceanic waters surrounding One Tree reef generally have low SPM concentrations (approximately 0.5 mg litre^{-1}, Devlin et al. 1997 compared with 20 mg litre^{-1} on nearshore reefs, Larcombe et al. 1995). Therefore, the energy available through SPM feeding is likely to be very limited at my One Tree Island study sites. One exception may be the One Tree Island lagoon, where water turbidity is generally higher than the surrounding waters (M. Hoogenboom, pers. obs.). However, the fact that energy acquisition model presented in Chapter 5 adequately captured variation in tissue quality suggests that light and flow are the primary drivers of variation in tissue properties, and indicates that any additional effect of sediment regimes on carbon acquisition is likely to be minor.

6.2.2 Carbon excretion

One factor that complicates the use of carbon acquisition as a framework for defining the fundamental niche is that not all of the carbon ingested by corals is assimilated into body mass. Indeed, corals have been shown to excrete between 8% and 70% of their daily carbon uptake as mucus or dissolved organic compounds (Crossland et al. 1980a; Bythell 1988; Davies 1991; Riegl & Branch1995). For some species, mucus production serves an important function in assisting sediment rejection (Stafford-Smith & Ormond 1992; Riegl & Branch 1995) and/or prey capture (Lewis & Price 1975). For other species, carbon excretion increases in response to nutrient limitation (e.g. Muscatine et al. 1984; Dubinsky & Jokiel 1994) or other stress factors. In a set of experiments conducted by Anthony & Connolly for two coral species (2004), carbon excretion increased 5- to 10-fold in response to increased sediment levels, and 3-fold in response to increased light intensity.

In the context of the research presented in this thesis, the observed increase in carbon excretion by corals exposed to high light intensities (Crossland et al. 1980a; Crossland 1987) indicates that the high-light region of the niche boundary would be more sensitive to changes in carbon excretion than the low-light region. Indeed, Anthony & Connolly (2004) showed this to be the case for *Turbinaria mesenterina* and *Acropora valida*. As mentioned above, these authors also found that carbon excretion increased linearly with growth irradiance for both of these species. Therefore, the upper niche boundary identified in Chapter 3 is likely to overestimate the range of conditions that allows a positive energy balance for *T. mesenterina*. This would tend to make my conclusions conservative with respect to the costs of high-light exposure for this species.

Despite the potential for carbon excretion to influence energy balance of corals, several aspects of my results indicate that the niche boundaries described throughout my thesis are not highly sensitive to these effects. Firstly, the geometric model developed in Chapter 4 predicted that the energetically optimal colony morphologies for *T. mesenterina* along a depth gradient were more vertically oriented than those that occur in the field. If carbon excretion incurs a significant energetic cost that increases with light intensity, then colonies in the field should be more vertically oriented than those predicted by the model. That is, the manifestation of additional costs that scale with light intensity should cause colonies to be more self-shading than predicted. The fact that the opposite was observed confirms that my results are robust to this effect. Similarly, in Chapter 5, I simulated the effects of changes in photophysiology on the light and flow niche boundaries calculated for *Acropora nasuta*, *Leptoria phrygia* and *Montipora foliosa*. These simulations were based on changes in energy balance parameters that mimic the effects of additional

costs of high-light exposure (see Chapter 5). Results of this analysis showed that the shape of the niche was relatively insensitive to these changes, except under a set of parameters that represented high-light acclimated colonies. Therefore, the niche boundaries calculated for my study species at One Tree Island are generally robust to the effects of light-enhanced carbon excretion on energy balance.

6.2.3   Nutrient limitation

Although heterotrophic feeding generally makes a minor contribution to carbon acquisition, the consensus in the literature is that uptake of nutrients such as nitrogen and phosphorus through heterotrophy is critical for tissue growth and reproduction (Muscatine & Porter 1977; Dubinsky & Jokiel 1994; Ferrier-Pages et al. 1998b). Based on models of carbon acquisition, the analyses presented in my thesis adequately captured variation in colony morphology for *Turbinaria mesenterina*, and variation in tissue quality and biomass for *Acropora nasuta* and *Leptoria phrygia*. However, for *T. mesenterina*, incorporating nutrient uptake may explain why colonies observed along a depth gradient in the field were flatter than predicted by the optimality model. For other foliose species, there is evidence that particle capture per polyp (and therefore nutrient acquisition) is generally greater for horizontal compared with vertical morphologies (e.g. Helmuth & Sebens 1993). This phenomenon would cause colonies to be flatter than predicted based on carbon acquisition. Therefore, incorporating nutrient acquisition into the model may improve the accuracy of model predictions. Nevertheless, the magnitude of the divergence between observed and predicted colony morphology is small relative to the magnitude of the change in colony morphology with depth. This is evident from the fact that the maximum distance between mean observed and predicted

morphology (i.e. between dashed and solid lines in Figure 4.5A) was 15º compared

to a change in morphology of approximately 70º across the depth gradient (Figure

4.5A). This indicates that nutrient acquisition has a smaller influence on the optimal

colony morphology for *T. mesenterina* than does carbon acquisition.

The potential effects of nutrient acquisition on fundamental niche boundaries

of corals are less clear for the species investigated at One Tree Island. Because

nutrients are required for tissue synthesis, it may be expected that nutrient limitation

would set an upper threshold on tissue quality that was not related to carbon

acquisition. For the analyses presented in Chapter 5 of my thesis, this would cause a

bias in model predictions toward over-estimating tissue quality when carbon

acquisition was high. That is, if nutrients were strongly limiting, the model would

predict tissue quality and reproductive output to be higher than observed because

nutrient uptake was in fact controlling how much carbon was assimilated into tissue.

The fact that my analyses showed good agreement between observed and predicted

tissue quality may indicate that the effects of nutrient uptake on tissue properties are

small relative to the effects of carbon acquisition. Alternatively, these results may

indicate that nutrient availability was sufficiently high at all sites such that no

constraint on carbon assimilation was apparent. Although nutrient concentration data

was not available for my study sites, this latter hypothesis is partially supported by

evidence that field concentrations of dissolved nitrogen in the lagoon at One Tree

Island are sufficient to meet the nitrogen requirements of one coral species

(*Pocillopora damicornis*, Hoegh-Guldberg & Williamson 1999). Overall, it is

unlikely that incorporating nutrient uptake into the models developed in this thesis

would have a strong effect on my results. Nevertheless, within the boundaries of the

fundamental niche, nutrient availability may influence how carbon is allocated

between tissue growth, energy storage and reproduction (e.g. Muller et al. 2001).

Extending the energy balance models developed herein to models of population

growth requires quantification of energy allocation (Kooijman 2000) and the effect

of nutrient uptake on these patterns therefore warrants further investigation.

6.3   Directions for future research

The physiological models developed in this thesis demonstrate that

environmental effects on energy balance fundamentally affect the capacity of

different coral species to grow, survive and reproduce. Under field conditions, where

factors such as competition and predation additionally influence coral performance,

physiology and energetics remain strong predictors of colony growth and

reproduction. From a broader ecological perspective, these findings suggest that the

fundamental niche (as predicted from energy balance) is not greatly different from

the realised niche (*sensu* Hutchinson 1957), or that effects of competition and

predation have a lesser influence on performance than do environmental factors.

Quantifying the relative effects of biotic and abiotic processes on the performance of

different coral species would be a useful extension to the models presented here.

This thesis focused on light intensity and water flow velocity as the dominant

environmental gradients on coral reefs (see Chapter 1). In addition to these

variables, temperature is known to influence coral physiology in general (e.g. Howe

& Marshall 2001) and photo-physiology in particular (Jones et al. 2000). Indeed,

elevated temperature is recognised to be the primary cause of coral bleaching (Jones

et al. 1998). Due to the predicted increase in the frequency and severity of bleaching

events (Hoegh-Guldberg 1999), an important extension of the physiological models

developed in this thesis would be to investigate how temperature influences the

shape to the fundamental niche.

6.4   Conclusions and Implications

Coral reefs are spatially complex ecosystems within which variation in light

and flow generates a mosaic of habitats with very different physical conditions.

Elucidating the processes that delineate the niche for different coral species requires

a mechanistic understanding of how these physical gradients influence coral

physiology. In this thesis, I have developed and calibrated process-based models that

link environmental gradients and physiological processes to ecological patterns. Such

models provide a framework for delineating the range of conditions under which an

organism can survive, grow and reproduce. In the broader context of general

ecological theory, establishing this framework is beneficial because it provides both

a means by which performance of different species can be compared, and a robust

platform from which the effects of environmental changes can be predicted.

REFERENCES

Adolf, J.E., D.K. Stoecker & L.W. Harding. 2003. Autotrophic growth and photoacclimation in *Karlodinium micrum* (Dinophyceae) and *Storeatula major* (Cryptophyceae). J. Phycol. 39: 1101-1108.

Al-Horani, F.A., S.M. Al-Moghrabi & D. de Beer. 2003. Microsensor study of photosynthesis and calcification in the scleractinian coral *Galaxea fascicularis*: active internal carbon cycle. J. Exp. Mar. Biol. Ecol. 288:1-15

Alpert, P. & E.L. Simms. 2002. The relative advantages of plasticity and fixity in different environments: when is it good for a plant to adjust? Evol. Ecol. 16: 285-297.

Anderson, J.M., W.S. Chow & Y.I. Park. 1995. The grand design of photosynthesis: Acclimation of the photosynthetic apparatus to environmental cues. Photosyn. Res., 46: 129-139.

Anthony, K.R.N. 1999. Coral suspension feeding on fine particulate matter. J. Exp. Mar. Biol. Ecol., 232: 85-106.

Anthony, K.R.N. 2000. Enhanced particle-feeding capacity of corals on turbid reefs (Great Barrier Reef, Australia). Coral Reefs, 19: 59-67.

Anthony, K.R.N. 2006. Enhanced energy status of corals on coastal, high-turbidity reefs. Mar. Ecol. Prog. Ser., 319: 111-116.

Anthony, K.R.N., & S.R. Connolly. 2004. Environmental limits to growth: physiological niche boundaries of corals along turbidity-light gradients. Oecologia 141:373-384.

Anthony, K.R.N., & K.E. Fabricius. 2000. Shifting roles of heterotrophy and autotrophy in coral energetics under varying turbidity. J. Exp. Mar. Biol. Ecol. 252: 221-253.

Anthony, K.R.N., & O. Hoegh-Guldberg. 2003a. Variation in coral photosynthesis, respiration and growth characteristics in contrasting light microhabitats: an analogue to plants in forest gaps and understoreys. Funct. Ecol. 17: 246-259.

Anthony, K.R.N., & O. Hoegh-Guldberg. 2003b. Kinetics of photoacclimation in corals. Oecologia 134:23-31.

Anthony, K.R.N., P.V. Ridd, A.R. Orpin, P.Larcombe & J. Lough. 2004. Temporal variation of light availability in coastal benthic habitats: Effects of clouds, turbidity and tides. Limnol. Oceanogr. 49:2201-2211.

Anthony, K.R.N., M.O. Hoogenboom & S.R. Connolly. 2005. Adaptive variation in coral geometry and the optimisation of internal colony light climates. Funct. Ecol. 19:17-26.

Antoine, M.E. & B. McCune. 2004. Contrasting fundamental and realized ecological ciches with epiphytic lichen transplants in an old-growth pseudotsuga forest. Bryologist, 107: 163 173.

Austin, M.P., A.O. Nicholls & C. R. Margules. 1990. Measurement of the realized quantitative niche: Environmental niches of five Eucalyptus species. Ecol. Monogr., 60: 161-177.

Ayre, D.J. & T.P. Hughes. 2004. Climate change, genotypic diversity and gene flow in reef-building corals. Ecol. Lett., 7: 273-278.

Babcock, R.C. 1991. Comparative demography of three species of scleractinian corals using age- and size-dependent classifications. Ecol. Mono. 61, 225-244.

Babin, M., A. Morel, H. Claustre, A. Bricaud, Z. Kolber & P.G. Falkowski. 1996. Nitrogen- and irradiance-dependent variations of the maximum quantum yield of carbon fixation in eutrophic, mesotrophic and oligotrophic marine systems. Deep-Sea Res. I – Oceanogr. Res. Papers, 43: 1241-1272.

Bachok, Z., P. Mfilinge & M. Tsuchiya. 2006. Characterisation of fatty acid composition in healthy and bleached corals from Okinawa, Japan. Coral Reefs 25:545-554.

Badgley, B.D., F. Lipschultz & K.P. Sebens. 2006. Nitrate uptake by the reef coral Diploria strigosa: effects of concentration, water flow and irradiance. Mar. Biol. 149: 327-338.

Bailey, S., R.G. Walters, S. Jansson & P. Horton. 2001. Acclimation of *Arabidopsis thaliana* to the light environment: the existence of separate low light and high light responses. Planta, 213: 794-801.

Baird, A. H., M. S. Pratchett, D. Gibson, N. Koziumi & C. P. Marquis. 2001. Variable palatability of coral eggs to a planktivorous fish. Mar. Freshwater Res. 52:865-868.

Baird, A.H. & P.A. Marshall. 2002. Mortality, growth and reproduction in scleractinian corals following bleaching on the Great Barrier Reef. Mar. Ecol. Prog. Ser., 237: 133-141.

Bak, R.P.M., M. Joenje, I. de Jong, D.Y.M. Lambrechts & G. Nieuwland. 1998. Bacterial suspension feeding by coral reef benthic organisms. Mar. Ecol. Prog. Ser., 175: 285-288.

Bak, R.P.M., G. Nieuwland, E.H. Meesters. 2005. Coral reef crisis in deep and shallow reefs: 30 years of constancy and change in reefs of Curacao and Bonaire. Coral Reefs, 24: 475-479.

Behrenfeld, M.J., O. Prasil, Z.S. Kolber, M. Babin & P.G. Falkowski. 1998. Compensatory changes in Photosystem II electron transport rates protect photosynthesis from photoinhibition. Photosynth. Res., 58: 259-268.

Behrenfeld, M.J., E. Maranon, D.A. Siegel & S.B. Hooker. 2002. Photoacclimation and nutrient-based model of light-saturated photosynthesis for quantifying oceanic primary production. Mar. Ecol. Prog. Ser., 228: 103-117.

Bradshaw, A.D. 1965. Evolutionary signficance of phenotypic plasticity in plants. Adv. Genet. 13: 115-155.

Brakel, W.H. 1983. Depth-related changes in the colony form of the reef coral *Porites astreoides*. The Ecology of Deep and Shallow Reefs, Symposia for Undersea Research 1: 21-26.

Brown, B.E., M.D.A. Le Tissier & J.C. Bythell. 1995. Mechanisms of bleaching deduced from histological studies of reef corals sampled during a natural bleaching event. Mar. Biol., 122: 655-663.

Brown, B.E., I. Ambarsari, M.E. Warner, W.K. Fitt, R.P. Dunne, S.W. Gibb & D.G. Cummings. 1999. Diurnal changes in photochemical efficiency and xanthophyll concentrations in shallow water reef corals: Evidence for photoinhibition and photoprotection. Coral Reefs, 18: 99-105.

Bruno, J.F. & P.J. Edmunds. 1997. Clonal variation for phenotypic plasticity in the coral *Madracis mirabilis*. Ecology 78: 2177-2190.

Bruno, J.F. & P.J. Edmunds. 1998. Metabolic consequences of phenotypic plasticity in the coral *Madracis mirabilis* (Duchassing & Michelotti): the effect of morphology and water flow on aggregate respiration. J. Exp. Mar. Biol. Ecol., 229: 187-195.

Bythell, J. 1988. A total nitrogen and carbon budget for the elkhorn coral Acropora palmata (Lamarck). Proc. 6th Int' Coral Reef Sym., Australia, 2:535-540.

Carpenter, R.C. & S.L. Williams. 2007. Mass transfer limitation of photosynthesis of coral reef algal turfs. Mar. Biol. 151: 435-450.

Chalker, B.E., W.C. Dunlap & J.K. Oliver. 1983. Bathymetric adaptations of reef-building corals at Davies reef, GBR, Australia II Light saturation curves for photosynthesis and respiration. J. Exp. Mar. Biol. Ecol. 73:37-56.

Chamberlain, J.A. & R.R. Graus. 1975. Water flow and hydromechanical adaptations of branched reef corals. Bull. Mar. Sci., 25: 112-125.

Chang, S.S., B.B. Prezelin & R.K. Trench. 1983. Mechanisms of photoadaptation in three strains of the symbiotic dinoflagellate *Symbiodinium microadriaticum*. Mar. Biol., 76: 219-229.

Clark, S. & A.J. Edwards. 1995. Coral transplantation as an aid to reef rehabilitation: evaluation of a case study in the Maldive Islands. Coral Reefs 14:201-213.

Clayton, W.S. & H.R. Lasker. 1983. Effects of light and dark treatments on feeding by the reef coral *Pocillopora damicornis*. J. Exp. Mar. Biol. Ecol. 63:269-279.

Connell, J.H. 1973. Population ecology of reef-building corals. In O.A. Jones & R. Endean (Eds). Biology and geology of coral reefs. Academic Press, New York, pp. 205-245

Crossland, C.J. 1987. *In situ* release of mucus and DOC-lipid from the corals *Acropora variabilis* and *Stylophora pistillata* in different light regimes. Coral Reefs, 6: 35-42.

Crossland, C.J., D.J. Barnes & M.A. Borowitzka. 1980a. Diurnal lipid and mucus production in the staghorn coral *Acropora acuminata*. Mar. Biol. 60:81-90.

Crossland, C.J., D.J. Barnes, T. Cox & M. Devereux. 1980b. Compartmentation and turnover of organic carbon in the staghorn coral *Acropora formosa*. Mar. Biol. 59:181-187.

Custodio, H.M. & H.T. Yap. 1997. Skeletal extension rates of *Porites cylindrica* and *Porites rus* after transplantation to two depths. Coral Reefs 16:267-268.

Danaher, D.G. 1998. Environmental plasticity in the Caribbean coral genus *Mycetophyllia* (Milne-Edwards & Haime 1848): Depth and flow effects on taxonomic characters. Am. Zool. 38: 97A.

Davies, P.S. 1984. The role of zooxanthellae in the nutritional energy requirements of *Pocillopora eydouxi*. Coral Reefs 2:181-186.

Davies, P.S. 1991. Effect of daylight variations on the energy budgets of shallow-water corals. Mar. Biol. 108:137-144.

de Kroon, H. & M.J. Hutchings. 1995. Morphological plasticity in clonal plants: the foraging concept reconsidered. J. Ecol., 83: 143-152.

de Witt, T.J., A. Sih & D.S. Wilson. 1998. Costs and limits of phenotypic plasticity. Trends Ecol. Evol., 13: 77-81.

Demmig-Adams, B. & W.W. Adams. 1992. Photoprotection and other responses of plants to high light stress. Ann. Rev. Plant Physiol. & Plant Molec. Biol. 43: 599-626.

Denny, M.W. 1988. Biology and the mechanics of the wave-swept environment. Princeton University Press, Princeton.

DeVantier, L.M., G. De'Ath, E. Turak, T.J. Done & K.E. Fabricius. 2006. Species richness and community structure of reef-building corals on the nearshore Great Barrier Reef. Coral Reefs, 25: 329-340.

Devlin, M., M. Lourey, H. Sweatman & D. Ryan. 1997. Water quality. In H. Sweatman (Ed). Long-term monitoring of the Great Barrier Reef Status Report No. 2. Australian Institute of Marine Science, Townsville, Australia.

Done, T. 1982. Patterns in the distribution of coral communities across the central Great Barrier Reef. Coral Reefs, 1: 95-107.

Dong, M. 1995. Morphological responses to local light conditions in clonal herbs from contrasting habitats, and their modification due to physiological integration. Oecologia, 101: 282-288.

Dove, S. 2004. Scleractinian corals with photoprotective host pigments are hypersensitive to thermal bleaching. Mar. Ecol. Prog. Ser., 272: 99-116.

Dove, S., J.C. Ortiz, S. Enriquez, M. Fine, P. Fisher, R. Iglesias-Prieto, D. Thornhill & O. Hoegh-Guldberg. 2006. Response of holosymbiont pigments from the scleractinian coral *Montipora monasteriata* to short-term heat stress. Limnol. Oceanogr., 51: 1149-1158.

Dubinsky, Z. & P. Jokiel. 1994. Ratio of energy and nutrient fluxes regulates symbiosis between zooxanthellae and corals. Pac. Sci., 48: 313-324.

Dubinsky, Z., P.G. Falkowski & K. Wyman. 1986. Light harvesting and utilization by phytoplankton. Plant Cell Physiol. 27: 1335 - 1349.

Dudley, S.A. 1996. Differing selection on plant physiological traits in response to environmental water availability: a test of adaptive hypotheses. Evolution 50: 92-102.

Dudley, S.A. & J. Schmitt. 1996. Testing the adaptive plasticity hypothesis: density-dependent selection on manipulated stem length in *Impatiens capensis*. Am. Nat., 147: 445-465.

Dustan, P. 1975. Growth and form in the reef building coral *Montastrea annularis*. Mar. Biol. 33: 101-107.

Dustan, P. 1982. Depth-dependent photoadaptation by zooxanthellae of the reef coral *Montastrea annularis*. Mar. Biol., 68: 253-264.

Eagle, J.V., M.J. Kingsford & G. P. Jones. In Press. Experimental evaluation of spatio-temporal variation in water flow near the substratum of a coral reef. Mar. Biol.

Edmunds, P.J. 2005. The effect of sub-lethal increases in temperature on the growth and population trajectories of three scleractinian corals on the southern Great Barrier Reef. Oecologia 146: 350-364.

Edmunds, P. 2006. Temperature-mediated transitions between isometry and allometry in a colonial, modular invertebrate. Proc. Roy. Soc. London Ser. B. 273: 2275-2281.

Edmunds, P.J. & P.S. Davies. 1986. An energy budget for *Porites porites* (Scleractinia). Mar. Biol. 92:339-347.

Edmunds P.J. & P.S. Davies. 1988. Post-illumination stimulation of respiration rate in the coral *Porites porites*. Coral Reefs 7: 7-9.

Edmunds, P.J. & P.S. Davies. 1989. An energy budget for *Porites porites* (Scleractinia) growing in a stressed environment. Coral Reefs 8:37-43.

Eichelmann, H., V. Oja, B. Rasulov, E. Padu, I. Bichele, H. Pettai, P. Mand, O. Kull & A. Laisk. 2005. Adjustment of leaf photosynthesis to shade in a natural canopy: reallocation of nitrogen. Plant Cell Env., 28: 389-401.

Elahi. R. & P.J. Edmunds. 2007a. Determinate growth and the scaling of photosynthetic energy intake in the solitary coral *Fungia concinna* (Verrill). J. Exp. Mar. Biol. Ecol., 349: 183-193.

Elahi. R. & P.J. Edmunds. 2007b. Tissue age affects calcification in the scleractinian coral *Madracis mirabilis*. Biological Bulletin, 212: 20-28.

Enriquez, S., E.R. Mendez & R. Iglesias-Prieto. 2005. Multiple scattering on coral skeletons enhances light absorption by symbiotic algae. Limnol. Oceanogr., 50: 1025-1032.

Fadallah, Y.H. 1983. Sexual reproduction, development and larval biology in Scleractinian corals. Coral Reefs, 2: 129-150.

Falkowski, P.G. & T.G. Owens. 1980. Light-shade adaptation - 2 strategies in marine-phytoplankton. Plant Physiol., 66: 592-595.

Falkowski P.G. & J.A. Raven. 1997. Aquatic photosynthesis. Blackwell Science, Massachusetts.

Falkowski, P.G., T.G. Owens, A.C. Ley & D.C. Mauzerall. 1981. Effects of growth irradiance levels on the ratio of reaction centers in 2 species of marine-phytoplankton. Plant Physiol., 68: 969-973.

Falster, D. S. & M. Westoby. 2003. Leaf size and angle vary widely across species: what consequences for light inteception. New Phytol. 158:509-525.

Falter, J. L., M. J. Atkinson, R. J. Lowe, S. G. Monismith & J. R. Koseff. 2007. Effects of non-local turbulence on the mass transfer of dissolved species to reef corals. Limnol. Oceanogr., 52: 274-285.

Fan, T.Y. & C.F. Dai. 1998. Sexual reproduction of the scleractinian coral *Merulina ampliata* in southern Taiwan. Bull. Mar. Sci., 62: 897-904.

Ferrier, M. D. 1991. Net uptake of dissolved free amino acids by four scleractinian corals. Coral Reefs, 10: 183-187.

Ferrier-Pages, C., D. Allemand, J.-P. Gattuso & J. Jaubert. 1998a. Microheterotrophy in the zooxanthellate coral *Stylophora pistillata*: Effects of light and ciliate density. Limnol. Oceanogr. 43:1639-1648.

Ferrier-Pages, C., J.-P. Gattuso, G. Cauwet, J. Jaubert & D. Allemand. 1998b. Release of dissolved organic carbon and nitrogen by the zooxanthellate coral *Galaxea fascicularis*. Mar. Ecol. Prog. Ser. 172: 265-274.

Ferrier-Pages, C., J. Witting, E. Tambutte & K.P. Sebens. 2003. Effect of natural zooplankton feeding on the tissue and skeletal growth of the scleractinian coral *Stylophora pistillata*. Coral Reefs, 22: 229-240.

Figueroa, F.L., R. Conde-Alvarez & I. Gomen. 2003. Relations between electron transport rates determined by pulse amplitude modulated chlorophyll fluorescence and oxygen evolution in macroalgae under different light conditions. Photosyn. Res., 75: 259-275.

Fitt W.K. & C.B. Cook. 2001. Photoacclimation and the effect of the symbiotic environment on the photosynthetic response of symbiotic dinoflagellates in the tropical marine hydroid *Myrionema amboinense*. J. Exp. Mar. Biol. Ecol. 256:15-31

Fitt,W.K., F.K. McFarland, M.E. Warner & G.C. Chilcoat. 2000. Seasonal patterns of tissue biomass and densities of symbiotic dinoflagellates in reef. Limnol. Oceanogr. 45: 677–685.

Flameling I.A. & J. Kromkamp. 1997. Photoacclimation of *Scenedesmus protuberans* (Chlorophyceae) to fluctuating irradiances simulating vertical mixing. J. Plankton Res. 19: 1011-1024.

Forster, R.M. & J.C. Kromkamp. 2004. Modelling the effects of chlorophyll fluorescence from subsurface layers on photosynthetic efficiency measurements in microphytobenthic algae. Mar. Ecol. Prog. Ser., 284: 9-22.

Foster, A.B. 1979. Phenotypic plasticity in the reef corals *Montastrea annularis* (Ellis & Solander) and *Siderastrea siderea* (Ellis & Solander). J. Exp. Mar. Biol. Ecol., 39: 25-54.

Foster, A.B. 1983. The relationship between corallite morphology and colony shape in some massive reef-corals. Coral Reefs, 2: 19-25.

Fryer, M.J., J.R. Andrews, K. Oxborough, D.A. Blowers & N.R. Baker. 1998. Relationship between CO_2 assimilation, photosynthetic electron transport, and active O_2 metabolism in leaves of maize in the field during periods of low temperature. Plant Physiol., 116: 571-580.

Fulton, C. & D.R. Bellwood. 2005. Wave-induced water motion and the functional implications for coral reef fish assemblages. Limnol. Oceanogr. 50: 255-264

Gardella, D.J. & P.J. Edmunds. 1999. The oxygen microenvironment adjacent to the tissue of the scleractinian *Dichocoenia stokesii* and its effects on symbiont metabolism. Mar. Biol., 135: 289-295.

Genty, B., J.M. Briantais & N.R. Baker. 1989. The relationship between the quantum yield of photosynthetic electron transport and quenching of chlorophyll fluorescence. Biochim. Biophys. Acta, 990: 87-92.

Gilmour, J. 1999. Experimental investigation into the effects of suspended sediment on fertilisation, larval survival and settlement in a scleractinian coral. Mar. Biol., 135: 451-462.

Gladefelter, E.H., R.K. Monahan & W.B. Gladefelter. 1978. Growth rates of five reef-building corals in the northeastern Caribbean. Bull. Mar. Sci. 28: 728-734.

Gleason, D. F. 1992. The adaptive significance of morphological plasticity in the reef coral *Porites astreoides*. Am. Zool. 32: 92A.

Glynn, P.W., J. Veron & G.M. Wellington. 1996. Clipperton Atoll (Eastern Pacific): oceanography, geomorphology, reef-building coral ecology and biogeography. Coral Reefs, 15: 71-99.

Glynn, P.W., S.B. Colley, J.H. Ting, J.L. Mate & H.M. Guzman. 2000. Reef coral reproduction in the eastern Pacific: Costa Rica, Panama and Galapagos Islands (Ecuador). IV. Agariciidae, recruitment and recovery of *Pavona varians* and *Pavona sp*. Mar. Biol., 136: 785-805.

Goiran, C., S.M. Al-Moghrabi, D. Allemand & J. Jaubert. 1996. Inorganic carbon uptake for photosynthesis by the symbiotic coral/dinoflagellate association I. Photosynthetic performance of symbionts and dependence on sea water bicarbonate. J. Exp. Mar. Biol. Ecol., 199: 207-225.

Gomez, E.D., A.C. Acala, H.T. Yap, L.C. Alcala & P.M. Alino. 1985. Growth studies of commercially important scleractinians. Proc. 5th Int'l Coral Reef Symp., Tahiti 6: 199-204.

Gorbunov, M.Y., Z.S. Kolber, M.P. Lesser & P.G. Falkowski. 2001. Photosynthesis and photoprotection in symbiotic corals. Limnol. Oceanogr., 46:75-85.

Gordillo, F.J.L., C. Jimenez, J. Chavarria & F.X. Niell. 2001. Photosynthetic acclimation to photon irradiance and its relation to chlorophyll fluorescence and carbon assimilation in the halotolerant green alga *Dunaliella viridis*. Photosynth. Res., 68: 225-235.

Graus, R.R. & I.G. McIntyre. 1982. Variation in growth forms of the reef coral *Montastrea annularis* (Ellis & Solander): A quantitative evaluation of growth response to light distribution using computer simulation. Smithsonian Contr. Mar. Sci. 12: 441-464.

Green, T.G.A., B. Schroeter, L. Kappen, R.D. Seppelt & K. Maseyk. 1998. An assessment of the relationship between chlorophyll-a fluorescence and CO_2 gas exchange from field measurements on moss and lichen. Planta 206: 611-618.

Greulich, S., G. Bornette, C. Amoros & J.G.M. Roelofs. 2000. Investigation on the fundamental niche of a rare species: an experiment on establishment of *Luronium natans*. Aquat. Bot., 66: 209–224.

Grime, J.P. & J.M.L. Mackey. 2002. The role of plasticity in resource capture by plants. Evol. Ecol. 16: 299-307.

Grotolli, A.G., L.J. Rodrigues & J.E. Palardy. 2006. Heterotrophic plasticity and resilience in bleached corals. Nature 440: 1186 – 1189.

Grover, R., J-F. Maguer, D. Allemand & C. Ferrier-Pages. 2003. Nitrate uptake in the scleractinian coral Stylophora pistillata. Limnol. Oceanogr., 48:2266-2274.

Guzman, H.M. & J. Cortes. 1989. Growth rates of eight species of scleractinian corals in the eastern pacific (Costa Rica). Bull. Mar. Sci., 44: 1189-1194.

Hall, V.R. & T.P. Hughes. 1996. Reproductive strategies of modular organisms: comparative studies of reef-building corals. Ecology 77:950-962.

Harland, A.D., P.S. Davies & L.M. Fixter. 1992. Lipid content of some Caribbean corals in relation to depth and light. Mar. Biol., 113: 357-361.

Harriot, V.J. 1999. Coral growth in subtropical eastern Australia. Coral Reefs, 18: 281-291.

Harrison, P.L. & C.C. Wallace. 1990. Reproduction, dispersal and recruitment of scleractinian corals. In Dubinsky Z (Ed) Ecosystems of the World, Volume 25: Coral Reefs, Elsevier, Amsterdam, pp. 133-207.

Heidelberg, K.B., K.P. Sebens & J.E. Purcell. 2004. Composition and sources of near reef zooplankton on a Jamaican forereef along with implications for coral feeding. Coral Reefs, 23: 263–276.

Helmuth, B.S.T. and K.P. Sebens. 1993. The influence of colony morphology and orientation to flow on particle capture by the scleractinian coral *Agaricia agaricites* (Linnaeus). J. Exp. Mar. Biol. Ecol., 165: 251-278.

Helmuth, B.S., K.P. Sebens & T.L. Daniel. 1997a. Morphological variation in coral aggregations: branch spacing and mass flux to coral tissues. J. Exp. Mar. Biol. Ecol. 209: 233-259.

Helmuth, B.S.T., B.E.H. Timmerman & K.P. Sebens. 1997b. Interplay of host morphology and symbiont microhabitat in coral aggregations. Mar. Biol., 130: 1-10.

Helmuth, B.S., E.F. Stockwell & D.R. Brumbaugh. 1997c. Morphological and environmental determinants of mass flux to corals. Proc. 8th Int.l Coral Reef Symp. 2: 1103-1108.

Herzig, R. & Z. Dubinsky. 1992. Photoacclimation, photosynthesis, and growth in phytoplankton. Israel J. Bot., 41: 199-212.

Heyward, A.J. & J.D. Collins. 1985. Growth and sexual reproduction in the scleractinian coral *Montipora digitata* (Dana). J. Mar. Freshwater Res. 36: 441-446.

Heyward, A., K. Yamazato, T. Yeemin & M. Minei. 1987. Sexual reproduction of corals in Okinawa. Galaxea, 6: 331-334.

Hikosaka, K. & I. Terashima. 1996. Nitrogen partitioning among photosynthetic components and its consequence for sun and shade plants. Funct. Ecol., 10: 335-343.

Hill, R., U. Schreiber, R. Gademann, A.W.D. Larkum, M. Kuhl & P.J. Ralph. 2004. Spatial heterogenetity of photosynthesis and the effect of temperature-induced bleaching conditions in three species of corals. Mar. Biol. 144: 633-640.

Hirose, M., I.R. Kinzie & M. Hidaka. 2001. Timing and process of entry of zoozanthellae into oocytes of hermatypic corals. Coral Reefs, 20: 273-280.

Hoegh-Guldberg, O. 1999. Climate change, coral bleaching and the future of the world's coral reefs. Marine & Freshwater Research, 50: 839-866.

Hoegh-Guldberg, O. & R.J. Jones. 1999. Photoinhibition and photoprotection in symbiotic dinoflagellates from reef-building corals. Mar. Ecol. Prog. Ser. 183: 73-86.

Hoegh-Guldberg, O. & J. Williamson. 1999. Availability of two forms of dissolved nitrogen to the coral *Pocillopora damicornis* and its symbiotic algae. Mar. Biol. 133:561-570.

Hoogenboom, M.O. & S.R. Connolly. In Press. Defining fundamental niche dimensions of corals: synergistic effects of colony size, light and flow. Ecology.

Hoogenboom, M.O., K.R.N. Anthony & S.R. Connolly. 2006. Energetic cost of photoinhibition in corals. Mar. Ecol. Prog. Ser., 313: 1-12.

Hoogenboom, M.O., S.R. Connolly & K.R.N. Anthony. 2008. Interactions between morphological and physiological plasticity optimize energy acquisition in corals. Ecology, 89: 1144-1154.

Hoogenboom, M.O. 2003. Fitness implications of phenotypic plasticity in corals. Honours Thesis, James Cook University, Townsville, Australia, 96p.

Houlbreque, F., E. Tambutte, D. Allemand & C. Ferrier-Pages. 2004. Interactions between zooplankton feeding, photosynthesis and skeletal growth in the scleractinian coral *Stylophora pistillata*. J. Exp. Biol., 207: 1461-1469.

Houter N.C. & Pons T.L. 2005. Gap size effects on photoinhibition in understorey saplings in tropical rainforest. Plant Ecol. 179: 43-51.

Hughes, T.P. & J.B.C. Jackson. 1985. Population dynamics and life-histories of foliaceous corals. Ecol. Monogr. 55:141-166.

Hurd, C.L. 2000. Water motion, marine macroalgal physiology, and production. J. Phycol., 36: 453-472.

Hutchings, M.J. & H. De Kroon. 1994. Foraging in plants: the role of morphological plasticity in resource acquisition. Adv. Ecol. Res. 25: 159-238.

Hutchinson, G.E. 1957. Concluding remarks. Cold Spring Harbour Symposium on Quantitiative Biology. 22: 415-427.

Howe, S.A. & A. T. Marshall. 2001. Thermal compensation of metabolism in the temperate coral, *Plesiastrea versipora* (Lamark, 1816). J. Exp. Mar. Biol. Ecol., 259: 231-248.

Iglesias-Prieto, R. & R.K. Trench. 1994. Acclimation and adaptation to irradiance in symbiotic dinoflagellates. I. Responses of the photosynthetic unit to changes in photon flux density. Mar. Ecol. Prog. Ser. 113: 163-175.

Iglesias-Prieto, R., V.H. Beltran, T.C. LaJeunesse, H. Reyes-Bonilla & P.E. Thome. 2004. Different algal symbionts explain the vertical distribution of dominant reef corals in the eastern Pacific. Proc. Roy. Soc. London Ser. B., 271:1757-1763.

Jackson, J.B.C. 1979. Morphological Strategies of Sessile Animals. In G. Larwood &
B.B. Rosen (Eds). Biology and Systematics of Colonial Organisms. Academic
Press, London & New York, pages 499-555.

Jassby, A.D. & T. Platt. 1976. Mathematical formulation of the relationship between
photosynthesis and light for phytoplankton. Limnol. Oceanogr., 21: 540-547.

Jaubert, J. 1981. Variations of the shape and of the chlorophyll concentration of the
scleractinian coral *Synaraea convexa* Verrill: Two complementary processes to
adapt to light variations. Proc. Fourth Int'l Coral Reef Symp. 2: 55-58.

Jeffery, S.W. & G.F. Humphrey. 1975. New spectrophotometric equations for
determining chlorophylls a, b, c and c2 in higher plants, algae and natural
phytoplankton. Biochim. Biophys. Acta, 167: 191-194.

Johnson, A.S. & K.P. Sebens. 1993. Consequences of a flattened morphology:
effects of flow on feeding rates of the scleractinian coral *Meandrina
meandrites*. Mar. Ecol. Prog. Ser., 99: 99-114.

Jokiel, P.L. 1978. Effects of water motion on reef corals. J. Exp. Mar. Biol. Ecol., 35:
87-97.

Jokiel, P.L. & J.I. Morrisey. 1986. Influence of size on primary production in the reef
coral *Pocillopora damicornis* and the macroalga *Acanthophora spicifera.* Mar.
Biol. 91: 15-26.

Jokiel, P.L. & R.H. York Jr. 1982. Solar ultraviolet photobiology of the reef coral
Pocillopora damicornis and symbiotic zooxanthellae. Bull. Mar. Sci., 32: 301-
315.

Jones, M.M., P. Olivas Rojas, H. Tuomisto & D.B. Clark. 2007. Environmental and
neighbourhood effects on tree fern distributions in a neotropical lowland rain
forest. J. Veg. Sci.. 18: 13-24.

Jones, R.J. & O. Hoegh-Guldberg. 2001. Diurnal changes in the photochemical efficiency of the symbiotic dinoflagellates (Dinophyceae) of corals: Photoprotection, photoinactivation and the relationship to coral bleaching. Plant Cell Env., 24: 89-99.

Jones, R.J., O. Hoegh-Guldberg, A.W.D. Larkum & U. Schreiber. 1998. Temperature-induced bleaching of corals begins with impairment of the CO_2 fixation mechanism in zooxanthellae. Plant Cell Env. 21: 1219-1221.

Jones, R.J., S. Ward, A. Yang Amri & O. Hoegh-Guldberg. 2000. Changes in quantum efficiency of Photosystem II of symbiotic dinoflagellates of corals after heat stress, and of bleached corals sampled after the 1998 Great Barrier Reef mass bleaching event. Mar. Freshwater Res., 51: 63-71.

Kaandorp, J.A. & P.M.A. Sloot. 2001. Morphological models of radiate accretive growth and the influence of hydrodynamics. J. Theor. Biol., 209: 257-274.

Kaandorp, J.A., C.P. Lowe, D. Frenkel & P.M.A. Sloot. 1996. Effect of nutrient diffusion and flow on coral morphology. Physical Rev. Lett., 77: 2328-2331.

Kana, R., D. Lazar, O. Prasil & J. Naus. 2002. Experimental and theoretical studies on the excess capacity of Photosystem II. Photosyn. Res., 72: 271-284.

Karlson, R.H., H.V. Cornell & T.P. Hughes. 2004. Coral communities are regionally enriched along an oceanic biodiversity gradient. Nature, 429: 867-700.

Kearney, M. 2006. Habitat, environment and niche: what are we modeling? Oikos, 115: 186-191.

Kearney, M. & W.P. Porter. 2004. Mapping the fundamental niche: physiology, climate, and the distribution of a nocturnal lizard. Ecology, 85: 3119–3131.

Kenyon, J.C. 1992. Sexual reproduction in Hawaiian *Acropora*. Coral Reefs, 11: 37-43.

Kim, K. & H.R. Lasker. 1998. Allometry of resource capture in colonial cnidarians and constraints on modular growth. Funct. Ecol. 12: 646–654.

Kingsolver, J.G. 1995. Fitness consequences of seasonal polyphenism in Western White butterflies. Evolution, 49: 942-954.

Kingsolver, J.G., D.W. Pfennig & M.R. Servedio. 2002. Migration, local adaptation and the evolution of plasticity. Trends Ecol. Evol., 17: 540-541.

Kinzie, I.R. 1993. Spawning in the reef corals *Pocillopora verrucosa* and *P edyouxi* at Sesoko Island, Okinawa. Galaxea, 11: 93-105.

Kirk, J.T.O. 1994. Light and photosynthesis in aquatic ecosystems, 2nd Ed. Cambridge University Press, London.

Koch, E.W. 1994. Hydrodynamics, diffusion-boundary layers and photosynthesis of the seagrasses *Thallasia testudinum* and *Cymodocea nodosa*. Mar. Biol., 118: 767-776.

Kojis, B.L. 1986. Sexual reproduction in *Acropora* (*Isopora*) species 1. *A cuneata* and *A. palifera* on Heron Island reef, Great Barrier Reef. Mar. Biol., 91:291-309.

Kojis, B.L. & N.J. Quinn. 1981. Aspects of sexual reproduction and larval development in the shallow water hermatypic coral *Goniastrea australensis* (Edwards and Haime, 1857). Bull. Mar. Sci. 31:558-573.

Kojis, B.L. & N.J. Quinn. 1984. Seasonal and depth variation in fecundity of *Acropora palifera* at 2 reefs in Papua New-Guinea. Coral Reefs, 3:165-172.

Kojis, B.L. & N.J. Quinn. 1985. Puberty in *Goniastrea favulus*: age or size limited? Proc. 5th Int'l Coral Reef Sym., Tahiti, 4: 289-293.

Kooijman, S.A.L.M. 2000. Dynamic energy and mass budgets in biological systems, 2nd edition. Cambridge University Press, Cambridge.

Krall, J.P. & G.E. Edwards. 1992. Relationship between photosystem II activity and CO_2 fixation in leaves. Physiol. Plantarum, 86: 180-187.

Krause, G.H. 1988. Photoinhibition of photosynthesis. An evaluation of damaging and protective mechanisms. Physiol. Plantarum, 74: 566-574.

Kuhl, M., Y. Cohen & T. Dalsgaard. 1995. Microenvironment and photosynthesis of zooxanthellae in scleractinian corals studied with microsensors for O_2, ph and light. Mar. Ecol. Prog. Ser., 117: 159-172.

Laing, W.A., D.H. Greer & T.A. Schnell. 1995. Photoinhibition of photosynthesis causes a reduction in vegetative growth rates of dwarf bean (*Phaseolus vulgaris*) plants. Aust. J. Plant Physiol. 22: 511-520.

Larcombe, P., P.V. Ridd, A. Prytz & B. Wilson. 1995. Factors controlling suspended sediment on inner-shelf coral reefs, Townsville, Australia. Coral Reefs, 14: 163-171.

Larkum, A.W.D., E.-M.W. Koch & M. Kuhl. 2003. Diffusive boundary layers and photosynthesis of the epilithic algal community of coral reefs. Mar. Biol. 142:1073-1082.

Leibold, M.A. 1995. The niche concept revisited - mechanistic models and community context. Ecology, 76:1371-1382.

Leichter, J.L., B. Helmuth & A.M. Fischer. 2006. Variation beneath the surface: Quantifying complex thermal environments on coral reefs in the Caribbean, Bahamas and Florida. J. Mar. Res. 64:563-588.

Leichter, J.L., S.R. Wing, S.L. Miller & M.W. Denny. 1996. Pulsed delivery of subthermoclinic water to Conch Reef (Florida Keys) by internal tidal bores. Limnol. Oceanogr. 41: 1490-1501.

Lesser, M.P. 2004. Experimental biology of coral reef ecosystems. J. Exp. Mar. Biol. Ecol., 300: 217-252.

Lesser M.P. & M.Y. Gorbunov. 2001. Diurnal and bathymetric changes in chlorophyll fluorescence yields of reef corals measured *in situ* with a fast repetition rate fluorometer. Mar. Ecol. Prog. Ser. 212: 69-77

Lesser, M.P., V.M. Weis, M.R. Patterson & P.L. Jokiel. 1994. Effects of morphology and water motion on carbon delivery and productivity in the reef coral, *Pocillopora damicornis* (Linnaeus): Diffusion barriers, inorganic carbon limitation and biochemical plasticity. J. Exp. Mar. Biol. Ecol. 178: 153-179.

Lesser, M.P., C. Mazel, D. Phinney & C.S. Yentsch. 2000. Light absorption and utilization by colonies of the congeneric hermatypic corals *Montastrea faveolata* and *Montastrea cavernosa*. Limnol. Oceanogr. 45:76-86.

Leuzinger, S., K.R.N. Anthony & B.L. Willis. 2003. Reproductive energy investment in corals: scaling with module size. Oecologia, 136: 524-531.

Levy, O., Z. Dubinsky, K. Schneider, Y. Achituv, D. Zakai & M.Y. Gorbunov. 2004. Diurnal hysteresis in coral photosynthesis. Mar. Ecol. Prog. Ser. 268: 105-117.

Lewis, J.B. & W.S. Price. 1975. Feeding mechanisms and feeding strategies of Atlantic reef corals. J. Zool. Lond. 176:527-544.

Long, S.P., S. Humphries & P.G. Falkowski. 1994. Photoinhibition of photosynthesis in nature. Ann. Rev. Plant Physiol. Plant Molec. Biol., 45: 633-662.

MacIntyre, H.L., T.M. Kana, T. Anning & R.J. Geider. 2002. Photoacclimation of photosynthesis irradiance response curves and photosynthetic pigments in microalgae and cyanobacteria. J. Phycol., 38: 17-38.

Maragos, J.E. 1972. A study of the ecology of Hawaiian reef corals. Unpublished PhD dissertation, University of Hawaii, Honolulu, p. 292.

Marra, J. 1978. Effect of short-term variations in light intensity on photosynthesis of a marine phytoplankter: A laboratory simulation study. Mar. Biol., 46: 191-202.

Marsh, J.A. 1970. Primary productivity of reef-building calcareous red algae. Ecology 51: 255-263.

Marubini, F. & P.S. Davies. 1996. Nitrate increases zooxanthellae population density and reduces skeletogenesis in corals. Mar. Biol., 127: 319-328.

Mass, T., S. Einbinder, E. Brokovich, N. Shashar, R. Vago, J. Erez & Z. Dubinsky. 2007. Photoacclimation of *Stylophora pistillata* to light extremes: metabolism and calcification. Mar. Ecol. Prog. Ser., 334: 93-102.

Maxwell, K. & G.N. Johnson. 2000. Chlorophyll fluorescence - a practical guide. J. Exp. Bot. 51: 659-668.

Maxwell, K., M.R. Badger & C.B. Osmond. 1998. A comparison of CO_2 and O_2 exchange patterns and the relationship with chlorophyll fluorescence during photosynthesis in C3 and CAM plants. Aust. J. Plant Physiol. 25: 45-52.

Mercado, J.M., C. Jimenez, F.X. Niell & F.L. Figueroa. 1996. Comparison of methods for measuring light absorption by algae and their application to the estimation of the package effect. Scientia Mar., 60: 39-45.

Merks, R., A. Hoekstra, J.A. Kaandorp & P.M.A. Sloot. 2003. Models of coral growth: spontaneous branching, compactification and the Laplacian growth assumption. J. Theor. Biol., 224: 153-166.

Meyers, L.A. & J.J. Bull. 2002. Fighting change with change: adaptive variation in an uncertain world. Trends Ecol. Evol., 17: 551-557.

Miller, M.W. 1995. Growth of a temperate coral: effects of temperature, light, depth, and heterotrophy. Mar. Ecol. Prog. Ser., 122: 217-225.

Mills, M.M., F. Lipschultz & K.P. Sebens. 2004. Particulate matter ingestion and associated nitrogen uptake by four species of scleractinian corals. Coral Reefs, 23: 311-323.

Mobley, C.D. 1994. Light and water: Radiative transfer in natural waters. Academic Press, San Diego, pp 592.

Muko, S., K. Kawasaki & K. Sakai. 2000. Morphological plasticity in the coral *Porites sillimaniani* and its adaptive significance. Bull. Mar. Sci. 66: 225-239.

Muller, E.B., R.M. Nisbet, S. Kooijman, J.J. Elser & E. McCauley. 2001. Stoichiometric food quality and herbivore dynamics. Ecol. Lett., 4: 519-529.

Murchie, E.H. & P. Horton. 1997. Acclimation of photosynthesis to irradiance and spectral quality in British plant species: chlorophyll content, photosynthetic capacity and habitat preference. Plant Cell Env. 20: 438-448.

Muscatine, L. & C.F. D'Elia. 1978. The uptake, retention and release of ammonium by reef corals. Limnol. Oceanogr., 23: 725-734.

Muscatine, L. & J. Porter. 1977. Reef Corals: Mutualistic symbioses adapted to nutrient-poor environments. Bioscience, 27: 454-460.

Muscatine, L., L. R. McCloskey & R. E. Marian. 1981. Estimating the daily contribution of carbon from zooxanthellae to coral animal respiration. Limnol. Oceanogr., 26: 601-611.

Muscatine, L., P.G. Falkowski, J.W. Porter & Z. Dubinsky. 1984. Fate of photosynthetically-fixed carbon in light and shade-adapted colonies of the symbiotic coral *Stylophora pistillata*. Proc. Roy. Soc. London Ser. B, 222: 181-202.

Muthiga, N.A. & A.M. Szamant. 1987. The effects of salinity stress on the rates of aerobic respiration and photosynthesis in the hermatypic coral *Siderastrea siderea*. Biol. Bull., 173: 539-551.

Myers, J. & J.R. Graham. 1971. The photosynthetic unit in *Chlorella* measured by repetitive short flashes. Plant Physiol., 48: 282-286.

Nisbet, R.M., E.B. Muller, K. Lika & S. Kooijman. 2000. From molecules to ecosystems through dynamic energy budget models. J. Animal Ecol., 69: 913-926.

Nobel, P.S. 1983. Biophysical Plant Physiology and Ecology. WH Freeman & Co., San Francisco.

O'Connell, B.M. & M.J. Kelty. 1994. Crown architecture of understory and open-grown white pine (*Pinus strobus* L.) saplings. Tree Physiol., 14: 89-102.

Ogren E. & M. Sjostrom. 1990. Estimation of the effect of photoinhibition on the carbon gain in leaves of a willow canopy. Planta 181: 560-567.

Oku, H., H. Yamashiro, K. Onaga, K. Sakai & H. Iwasaki. 2003. Seasonal changes in the content and composition of lipids in the coral *Goniastrea aspera*. Coral Reefs 22: 83-85.

Oliver J.K., B.E. Chalker & W.C. Dunlap. 1983. Bathymetric adaptations of reef-building corals at Davies Reef, Great Barrier Reef, Australia. I. Long-term growth responses of *Acropora formosa* (Dana 1846). J. Exp. Mar. Biol. Ecol., 73: 11-35.

Oren, U., Y. Benahyahu, H. Lubinevsky & Y. Loya. 2001. Colony integration during regeneration in the stony coral *Favia favus*. Ecology 82: 802-813.

Pahl-Wostl C. 1992. Dynamic versus static models for photosynthesis. Hydrobiologia. 238:189-196

Palardy, J.E., A.G. Grottoli & K.A. Matthews. 2005. Effects of upwelling, depth, morphology and polyp size on feeding in three species of Panamanian corals. Mar. Ecol. Prog. Ser., 300: 79-89.

Patterson, M.R. 1992. A chemical engineering view of cnidarian symbioses. Am. Zool. 32: 566-582.

Patterson, M.R. & K.P. Sebens. 1989. Forced convection modulates gas exchange in cnidarians. Proc. Nat'l Acad. Sci USA 86: 8833-8836.

Patterson, M.R., K.P. Sebens & R.R. Olson. 1991. *In situ* measurements of flow effects on primary production and dark respiration in reef corals. Limnol. Oceanogr. 36: 936-948.

Patton, J., S. Abraham & A. Benson. 1977. Lipogenesis in the intact coral *Pocillopora capitata* and its isolated zooxanthellae: Evidence for a light-driven carbon cycle between symbiont and host. Mar. Biol., 44: 235-247.

Pearcy, R.W. & W. Yang. 1995. A three-dimensional crown architecture model for assessment of light capture and carbon gain by understory plants. Oecologia, 108: 1-12.

Permata, W.D. & M. Hidaka. 2005. Ontogenetic changes in the capacity of the coral *Pocillopora damicornis* to originate branches. Zoological Science, 22: 1197-1203.

Piersma, T. & J. Drent. 2003. Phenotypic flexibility and the evolution of organismal design. Trends Ecol. Evol., 18: 228-233.

Platt T., C.L. Gallegos & W.G. Harrison. 1980. Photoinhibition of photosynthesis in natural assemblages of marine phytoplankton. J. Mar. Res. 38: 687-701.

Porter, J.W. 1976. Autotrophy, heterotrophy, and resource partitioning in Caribbean reef-building corals. Am. Nat., 110: 731-742.

Potts, D.C. 1978. Differentiation in coral populations. Atoll Res. Bull., 220: 54-74.

Pulliam, H.R. 2000. On the relationship between niche and distribution. Ecol. Lett. 3: 349-361.

Raps, S., K. Wyman, H.W. Siegelman & P.G. Falkowski. 1983. Adaptation of the Cyanobacterium *Microcystis aeruginosa* to light-intensity. Plant Physiol., 72: 829-832.

Raven, J.A. 1976. The quantitative role of 'dark' respiratory processes in heterotrophic and photolithotrophic plant growth. Annals Bot., 40: 587-602.

Reidenbach, M.A., J.R. Koseff, S.G. Monismith, J.V. Steinbuck & A. Genin. 2006. The effects of waves and morphology on mass transfer within branched reef corals. Limnol. Oceanogr. 51:1134-1141.

Rex, A.F., F. Montebon & H.T. Yap. 1995. Metabolic responses of the scleractinian coral *Porites cylindrica* Dana to water motion. I. Oxygen flux studies. J. Exp. Mar. Biol. Ecol. 186: 33-52.

Reynaud-Vaganay, S., A. Juillet-Leclerc, J. Jaubert & J. P. Gatusso. 2001. Effect of light on skeletal 13C and 18O and interaction with photosynthesis, respiration and calcification in two zooxanthellate scleractinian corals. Palaeo. Palaeo. Palaeo. 175:393-404.

Ribes, M., R. Coma & J.M. Gili. 1998. Heterotrophic feeding by gorgonian corals with symbiotic zooxanthella. Limnol. Oceanogr., 43: 1170-1179.

Richardson, K., J. Beardall & J.A. Raven. 1983. Adaptation of unicellular algae to irradiance - an analysis of strategies. New Phytol. 93:157-191.

Riegl, B. & G.M. Branch. 1995. Effects of sediment on the energy budgets of four scleractinian and five alcyonacean corals. J. Exp. Mar. Biol. Ecol. 186:259-275.

Riegl, B., C. Heine & G. M. Branch. 1996. Function of funnel-shaped coral growth in a high-sedimentation environment. Mar. Ecol. Prog. Ser., 145: 87-93.

Robison, J.D. & M.E. Warner. 2006. Differential impacts of photoacclimation and thermal stress on the photobiology of four different phylotypes of *Symbiodinium* (Pyrrhophyta). J. Phycol. 42: 568-579.

Rodrigues, L.J. & A.G. Grottoli. 2007. Energy reserves and metabolism as indicators of coral recovery from bleaching. Limnol. Oceanogr. 52: 1874-1882.

Rodriguez-Roman, A., Z. Hernandez-Pech, P.E. Thome, S. Enriquez & R. Iglesias-Prieto. 2006. Photosynthesis and light utilisation in the Caribbean coral *Montastera faveolata* recovering from a bleaching event. Limnol. Oceanogr., 51: 2702-2710.

Rossi, S. & G. Tsounis. 2007. Temporal and spatial variation in protein, carbohydrate, and lipid levels in *Corallium rubrum* (Anthozoa, Octocorallia). Mar. Biol., 152: 429–439.

Roos, P.J. 1967. Growth and occurrence of the reef coral *Porites astreioides* Lamarck in relation to submarine irradiance distribution. Drukkerij Elinwijk.

Salih, A., A. Larkum & G. Cox. 2000. Fluorescent pigments in corals are photoprotective. Nature, 408: 850-853.

Sanford, L. P. & S. M. Crawford. 2000. Mass transfer versus kinetic control of uptake across solid-water boundaries. Limnol. Oceanogr., 45: 1180-1186.

Scharf, F.S., F. Juanes & R.A. Rountree. 2000. Predator size - prey size relationships of marine fish predators: interspecific variation and effects of ontogeny and body size on trophic-niche breadth. Mar. Ecol. Prog. Ser., 208: 229-248.

Schlichting, C.D. 1986. The evolution of phenotypic plasticity in plants. Ann. Rev. Ecol. Syst. 17: 667-693.

Seaton, G.G.R. & D.A. Walker. 1990. Chlorophyll fluorescence as a measure of photosynthetic carbon assimilation. Proc. Royal Soc. London – Ser. B, 242: 29-35.

Sebens, K.P. 1997. Adaptive responses to water flow: Morphology, energetics and distribution of reef corals. Proc. Eighth Int'l Coral Reef Symp. 2: 1053-1058.

Sebens, K.P. & A.S. Johnson. 1991. Effects of water movement on prey capture and distribution of reef corals. Hydrobiologia, 226: 91-101.

Sebens, K.P., J. Witting and B. Helmuth. 1996. Effects of water flow and aggregation on particle capture by the reef coral *Madracis mirabilis*. J. Exp. Mar. Biol. Ecol., 211: 1- 28.

Sebens, K.P., S.P. Grace, B. Helmuth, E.J. Maney Jr & J.S. Miles. 1998. Water flow and prey capture by three scleractinian corals, *Madracis mirabilis*, *Montastrea cavernosa* and *Porites porites* in a field enclosure. Mar. Biol., 131: 347-360.

Sebens, K.P., B. Helmuth, E. Carrington & B. Agius. 2003. Effects of water flow on growth and energetics of the scleractinian coral *Agaricia tenuifolia* in Belize. Coral Reefs, 22: 35-47.

Shashar, N., Y. Cohen & Y. Loya. 1993. Extreme diel fluctuations of oxygen in diffusive boundary layers surrounding stony corals. Biol. Bull. 185: 455-461.

Shick, J.M., M.P. Lesser, W.C. Dunlap, W.R. Stochaj, B.E. Chalker & J. Wu Won. 1995. Depth-dependent responses to solar ultraviolet radiation and oxidative stress in the zooxanthellate coral *Acropora microphthalma*. Mar. Biol., 122: 41-51.

Shlesinger, Y., T.L. Goulet & Y. Loya. 1998. Reproductive patterns of scleractinian corals in the northern Red Sea. Mar. Biol., 132: 691-701.

Smith, R.C. & W.H.J. Wilson. 1977. Photon scalar irradiance. <u>In</u> J. E. Tyler (Ed.) Light in the sea: Benchmark papers in optics. p. 312-316. Dowden Hutchinson & Ross Inc.

Sorokin, Y.I. 1973. On the feeding of some scleractinian corals with bacteria and dissolved organic matter. Limnol. Oceanogr., 18: 380-385.

Staehr, P.A. & M.J. Birkeland. 2006. Temperature acclimation of growth, photosynthesis and respiration in two mesophilic phytoplankton species. Phycologia 45: 468-656.

Stafford-Smith, M.G. & R.F.G. Ormond. 1992. Sediment-rejection mechanisms of 42 species of Australian scleractinian corals. Aust. J. Mar. Freshwater Res., 43: 683-705.

Stearns, S.C. 1989. The evolutionary significance of phenotypic plasticity. Bioscience, 39: 436-445.

Steinger, T., B.A. Roy & M.L. Stanton. 2003. Evolution in stressful environments II: adaptive value and costs of plasticity in response to low light in *Sinapis arvensis*., J. Evol. Biol., 16: 313-323.

Stimson, J. 1985. The effect of shading by the table coral *Acropora hyacinthus* on understory corals. Ecology 66: 40-53.

Stimson, J. S. 1987. Location, quantity and rate of change in quantity of lipids in tissue of Hawaiian hermatypic corals. Bull. Mar. Sci. 41:899-904.

Suggett, D.J., K. Oxborough, N.R. Baker, H.L. MacIntyre, T.M. Kana & R.J. Geider. 2003. Fast repetition rate and pulse amplitude modulation chlorophyll *a* fluorescence measurements for assessment of photosynthetic electron transport in marine phytoplankton. Eur. J. Phycol., 38: 371-384.

Sukenik, A., J. Bennett & P. Falkowski. 1987. Light-saturated photosynthesis - limitation by electron-transport or carbon fixation. Biochim. Biophys. Acta, 891: 205-215.

Sultan, S.E. & H.G. Spencer. 2002. Metapopulation structure favors plasticity over local adaptation. Am. Nat., 160: 271-283.

Sundberg, B., D. Campbell & K. Palmqvist. 1997. Predicting CO_2 gain and photosynthetic light acclimation from fluorescence yield and quenching in cyano-lichens. Planta, 201: 138-145.

Tanaka, Y., T. Miyajima, I. Koike, T. Hayashibara & H. Ogawa. 2007. Imbalanced coral growth between organic tissue and carbonate skeleton caused by nutrient enrichment. Limnol. Oceanogr., 52: 1139-1146.

Terashima I. & J.R. Evans. 1988. Effects of light and nitrogen nutrition on the organisation of the photosynthetic apparatus in spinach. Plant Cell Physiol. 29: 143 – 155.

Titlyanov E.A. 1991a. The stable level of coral primary production in a wide light range. Hydrobiologia 216/217: 383-387.

Titlyanov E.A. 1991b. Light adaptation and production characteristics of branches differing by age and illumination of the hermatypic coral *Pocillopora verrucosa*. Symbiosis 10: 249-261.

Todd, P.A., R.C. Sidle & N.J.I. Lewin-Koh. 2004. An aquarium experiment for identifying the physical factors inducing morphological change in two massive scleractinian corals. J. Exp. Mar. Biol. Ecol. 299: 97 113.

Torruco, D., A. Gonzalez & J. Ordaz. 2003. The role of environmental factors in the lagoon coral community structure of Banco Chincorro, Mexico. Bull. Mar. Sci., 73: 23-36.

Ulstrup, K.E., P.J. Ralph, A.W.D. Larkum & M. Kuhl. 2006. Intra-colonial variability in light acclimation of zooxanthellae in coral tissues of *Pocillopora damicornis*. Mar. Biol., 149: 1325-1335.

Valladares, F., & F.I. Pugnaire. 1999. Tradeoffs between irradiance capture and avoidance in semi-arid environments assessed with a crown architecture model. Annals Bot. 83: 459-469.

van Buskirk, J. 2002. A comparative test of the adaptive plasticity hypothesis: Relationships between habitat and phenotype in anuran larvae. Am. Nat., 160: 87-102.

van Kleuenen, M., & M. Fischer. 2001. Adaptive evolution of plastic foraging responses in a clonal plant. Ecology, 82: 3309-3319.

van Veghel, M.L.J. & R.P.M. Bak. 1994. Reproduction characterisics in the polymorphic Caribbean reef building coral *Montastrea annularis*. III. Reproduction in damaged and regenerating colonies. Mar. Ecol. Prog. Ser., 109: 229-233.

Vermeij, M.J.A. & R.P.M. Bak. 2002. How are coral populations structured by light? Marine light regimes and the distribution of *Madracis*. Mar. Ecol. Prog. Ser., 233: 105-116.

Veron, J.E.N. 2000. Corals of the World. Australian Institute of Marine Science, Townsville, Australia.

Via, S., R. Gomulkiewicz & G. De Jong. 1995. Adaptive phenotypic plasticity: consensus and controversy. Trends Ecol. Evol. 10: 212-217.

Villinski, J.T. 2003. Depth-independent reproductive characteristics from the Carribean reef-building coral *Montastrea faveolata*. Mar. Biol., 142: 1043-1053.

Wallace, C.C. 1985. Reproduction, recruitment and fragmentation in nine sympatric species of the coral genus *Acropora*. Mar. Biol., 88: 217-233.

Walters, R.G. 2005. Towards an understanding of photosynthetic acclimation. J. Exp. Bot., 56: 435-447.

Ward, S. 1995a. Two patterns of energy allocation for growth, reproduction and lipid storage in the scleractinian coral *Pocillopora damicornis*. Coral Reefs, 14: 87-90.

Ward, S. 1995b. The effect of damage on the growth, reproduction and storage of lipids in the scleractinian coral *Pocillopora damicornis* (Linnaeus). J. Exp. Mar. Biol. Ecol. 187: 193-206.

Ward, S. & P. Harrison. 2000. Changes in gametogenesis and fecundity of Acroporid corals that were exposed to elevated nitrogen and phosphorus during the ENCORE experiment. J. Exp. Mar. Biol. Ecol., 246: 179-221.

Warner, M.E., G.C. Chilcoat, F.K. McFarland & W.K. Fitt. 2002. Seasonal fluctuations in the photosynthetic capacity of photosystem II in symbiotic dinoflagellates in the Caribbean reef-building coral *Montastrea*. Mar. Biol., 141: 31-38.

Webb, C.O. & D.R. Peart. 2000. Habitat associations of trees and seedlings in a Bornean rain forest. J. Ecol. 88: 464-478.

Werner, C., R.J. Ryel, O. Correia & W. Beyschlag. 2001. Effects of photoinhibition on whole-plant carbon gain assessed with a photosynthesis model. Plant Cell Env., 24: 27-40.

West, G.B., J.H. Brown & B.J. Enquist. 1997. A general model for the origin of allometric scaling laws in biology. Science, 276: 122-126.

Whittaker, R.H., S.A. Levin & R.B. Root. 1973. Niche, habitat, and ecotope. Am. Nat. 107: 321-338.

Willis B.L. 1985. Phenotypic plasticity versus phenotypic stability in the reef corals *Turbinaria mesenterina* and *Pavona cactus*. Proc. 5th Int'l Coral Reef Symp., Tahiti. 4: 107-112.

Winters G., Y. Loya, R. Roettgers & S. Beer. 2003. Photoinhibition in shallow-water colonies of the coral *Stylophora pistillata* as measured *in situ*. Limnol. Oceanogr. 48: 1388-1393.

Wolanski, E., K.E. Fabricius, S. Spagnol & R. Brinkman. 2005. Fine sediment budget on an inner-shelf coral-fringed island, Great Barrier Reef of Australia. Estuarine Coastal Shelf Sci., 65: 153-158.

Wright, J.W., K.F. Davies, J.A. Lau, A.C. McCall & J.K. McKay. 2006. Experimental verification of ecological niche modeling in a heterogeneous environment. Ecology, 87: 2433–2439.

Wyman K.D., Z. Dubinsky & J.W. Porter. 1987. Light absorption and utilization among hermatypic corals: a study in Jamaica, West Indies. Mar. Biol. 84: 283-292.

Yentsch, C.S., C.M. Yentsch, J.J. Cullen, B. Lapointe, D.A. Phinney, S.W. Yentsch. 2002. Sunlight and water transparency: cornerstones in coral research. J. Exp. Mar. Biol. Ecol., 268: 171-183.

Zakai, D., O. Levy & N.E. Chadwick-Furman. 2000. Experimental fragmentation reduces sexual reproductive output by the reef-building coral *Pocillopora damicornis*. Coral Reefs 19:185-188.

Zonneveld, C. 1997. Modeling effects of photoadaptation on the photosynthesis-irradiance curve. J. Theor. Biol., 186: 381-388.

APPENDIX A: PULSE AMPLITUDE MODULATED

FLUOROMETER (PAM) SETTINGS

Instrument: Mini-PAM (Walz, Germany)

Measuring intensity (MI) = 12

Saturation pulse intensity (SI) = 8

Saturation pulse width (SW) = 0.8s

Actinic light intensity (AI) = 8

Actinic width (AW) = 30

Actinic light factor (AF) = 1

Gain (G)= 3

Damp (D) = 2

ETR Factor (EF) = 0.84

Light width (LW) = 5

Light intensity (LI) = 10

Induction curve (IC) = 15

Induction width (IW) = 40

APPENDIX B: THREE-DIMENSIONAL GEOMETRIC MODEL OF LIGHT INTERCEPTION BY FOLISE CORALS

B.1 Radiance and Irradiance

Radiance measures the intensity of light passing through a unit volume of air/water, where this volume is measured in units of a three-dimensional 'solid angle' or steradian, sr^{-1}. Irradiance measures the intensity of light incident upon a unit of area of a surface. Converting radiance to irradiance requires knowledge of the angle at which light approaches the surface. This is because light passing through a volume of space spreads out as it encounters a surface, with the degree of spreading proportional to the cosine of the angle of incidence (θ) between the beam of light and the surface (the so called 'cosθ' rule of optics, see Mobley 1994, Falkowski and Raven 1997). The angle of incidence of light to the surface (θ) is measured from perpendicular (normal) to the surface. Irradiance is equal to radiance when the beam of light approaches exactly perpendicular to the surface (cos 0° = 1) because the area of the surface that the light falls on is equivalent to the area of a slice of the volume of space that the beam passes through. When light approaches a surface at angles between 1° and 89°, irradiance is less than radiance because the area that the light spreads across is expanded and the greater the angle, the greater this expansion. When light approaches a surface at 90° (parallel to the surface) the beam of light does not encounter the surface and irradiance is zero (cos 90° = 0). These basic principles apply equally to direct and scattered irradiance. In this Appendix I use θ_S and θ_D to refer to the angles of incidence of scattered and direct light respectively, E_S and E_D to refer to scattered and direct irradiance, and I_S and I_D to refer to scattered and direct radiance (see Figure 4.2).

B.2: Calculating scattered radiance from scattered irradiance measurements

My light intensity measuring equipment provided a measure of total downwelling irradiance (i.e. the total light incident upon a horizontal surface – light sensor – comprised of both direct and scattered light). In the case of an un-shaded horizontally oriented light sensor, scattered radiance approaches the sensor from within a hemisphere of angles. However for complex colony morphologies, the range of angles from which light can approach a point on the surface is reduced due to self-shading. Therefore, calculating scattered irradiance for our model colonies requires both the range of angles from which scattered light approaches the surface (see B.4) and the intensity of scattered radiance to be known. The experimental calibration of the composition of the underwater light field (see Methods and Figure 4.3) allowed differentiation between direct and scattered irradiance. I here outline the conversion from scattered irradiance to radiance.

Total scattered irradiance incident to a surface at a given depth, z, and time of day, t, ($E_S(z,t)$, µmol quanta m^{-2} s^{-1}) is equal to the integral of scattered radiance (intensity of scattered light per unit solid angle, I_S, µmol quanta sr^{-1} s^{-1}) over all angles of incidence, multiplied by the cosine of those angles of incidence of radiance to the surface (Smith & Wilson 1977). For a horizontal light sensor, scattered light approaches from within a hemisphere of angles and therefore the integral is calculated over angles in the θ_S plane ('vertical' angles) and the ϕ_S plane ('horizontal' angles):

$$E_S(z,t) = \iint_{\theta \; \phi} I_S(z,t) \cos\theta_S \sin\theta_S \; d\phi_S d\theta_S \qquad \text{Eqn B.2.1}$$

Assuming equal intensity of scattered radiance from all angles (i.e. $I_S(z,t)$ is constant over all angles of θ_S and ϕ_S), and integrating over a hemisphere (note that $sin\theta_S \, d\phi_S \, d\theta_S$ is the surface area corresponding to the solid angle delimited by $d\phi_S \, d\theta_S$), gives:

$$E_S(z,t) = I_S(z,t) \int\limits_{\theta=0}^{\pi/2} \int\limits_{\phi=0}^{2\pi} \cos\theta_S \sin\theta_S \; d\phi_S d\theta_S \qquad \text{Eqn B.2.2}$$

Simplifying and solving for $I_S(z,t)$ gives:

$$I_S(z,t) = \frac{E_S(z,t)}{\pi} \qquad \text{Eqn B.2.3}$$

Therefore, given measurements of $E_S(z,t)$ from light logger data, scattered radiance is calculated from Eqn B.2.3.

B.3 Intensity of direct irradiance taking into account self-shading within colonies

Calculating the intensity of direct irradiance requires knowledge of both the angle of incidence and the intensity of direct radiance, with the angle of incidence measured from perpendicular to the surface (B.1). Therefore in this section I calculate the direction of the surface normal for points on the colony surface. Secondly, I calculate the direction of incident direct light based on the path of the sun across the sky, taking the refraction of light across the air/seawater interface into account. Using vector operations the cosine of the angle of incidence between these two directions (i.e. between the surface normal and the beam of direct light) can be calculated. Finally, the geometry of model colonies is used to determine the range of angles from which direct radiance may approach points on the colony surface without being obstructed (shaded) by other parts of the colony.

The direction of the surface normal can be calculated using the mathematical equation for a cone written as vector component equations in spherical coordinates (see Lang 1979):

$$X(\phi,l) = \left(l\sin\alpha\cos\phi, l\sin\alpha\sin\phi, l\cos\alpha \right) \qquad \text{Eqn B.3.1}$$

where l represents the distance between a point on the cone surface and the apex of the cone, ϕ represents the horizontal angle of a point on the surface, and α is the angle between vertical and the side of the cone. A plane tangent to a point on a cone lies over two tangent vectors which are the partial derivatives of $X(\phi,l)$:

$$\frac{\partial X}{\partial \phi} = \left(-l\sin\alpha\sin\phi, l\sin\alpha\cos\phi, 0\right)$$

$$\frac{\partial X}{\partial l} = \left(\sin\alpha\cos\phi, \sin\alpha\sin\phi, \cos\alpha\right)$$

Eqn B.3.2

A line normal to the tangent plane is found from the cross product of these tangent vectors.

$$\widetilde{n} = \frac{\partial X}{\partial \phi} \times \frac{\partial X}{\partial l} = \begin{bmatrix} \widetilde{i} & \widetilde{j} & \widetilde{k} \\ -l\sin\alpha\sin\phi & l\sin\alpha\cos\phi & 0 \\ \sin\alpha\cos\phi & \sin\alpha\sin\phi & \cos\alpha \end{bmatrix}$$

Eqn B.3.3

Expanding the determinant, Eqn B.3.3 becomes:

$$\widetilde{n} = l\sin\alpha\cos\phi\cos\alpha\,\widetilde{i} + l\sin\alpha\cos\alpha\sin\phi\,\widetilde{j} - l\sin^2\alpha\,\widetilde{k}$$

Eqn B.3.4

We require $\widetilde{n}$ to be a unit vector. Using the Pythagorean theorem the magnitude of $\widetilde{n}$ simplifies to:

$$\left|\widetilde{n}\right| = l\sin\alpha$$

Eqn B.3.5

Therefore, dividing B.3.4 by B.3.5 the unit vector of $\widetilde{n}$ is:

$$\hat{\widetilde{n}} = \cos\phi\cos\alpha\,\hat{\widetilde{i}} + \cos\alpha\sin\phi\,\hat{\widetilde{j}} - \sin\alpha\,\hat{\widetilde{k}}$$

Eqn B.3.6

At a given time, t, on a day of known duration, λ, the angle of incidence of direct light to the ocean surface, θ_1, can be found by:

$$\theta_1(t) = \frac{\pi t}{\lambda} \qquad\qquad \text{Eqn B.3.7}$$

where π (radians) is the angular change in the sun's location over a day. Based on Snell's Law of refraction, the angle at which light passes through the water column, θ_2, is:

$$\theta_2(t) = \sin^{-1}\left(\frac{\sin\theta_1(t)}{1.33}\right). \qquad\qquad \text{Eqn B.3.8}$$

Once θ_2 is known, the direction of direct light, $\hat{\tilde{I}}_d$, is found using vector operations. Assuming that the sun passes directly overhead, the x-component of $\hat{\tilde{I}}_d$ is equal to zero. The component of $\hat{\tilde{I}}_d$ in the direction of the y-axis is equal to the sine of θ_2, and the component in the direction of the z-axis is equal to the cosine of θ_2, giving:

$$\hat{\tilde{I}}_d = \sin\theta_2\,\hat{j} - \cos\theta_2\,\hat{k} \qquad\qquad \text{Eqn B.3.9}$$

The cosine of the angle between these two unit vectors (B.3.6 and B.3.9) is found by taking their dot (element by element) product:

$$\cos\theta(\phi,\alpha,\theta_2(t)) = -\sin\theta_2(t)\cos\alpha\sin\phi - \cos\theta_2(t)\sin\alpha \qquad \text{Eqn B.3.10}$$

Multiplying Eqn B.3.10 by the intensity of direct radiance obtained from light logger data allows the intensity of direct irradiance on the colony surface to be calculated.

At a given time of day, direct light may only approach a point on the surface of a colony if the angle of incidence of that light is not shaded by other regions on the colony surface. I here calculate the range of unshaded angles for points on the colony surface.

Figure B.3.1: Calculation of range of angles from which direct light may approach points on the surface of a cone-shaped coral colony. A) View from above a 2-tier model colony showing relevant geometry. B) Cross-section view of the point, p1, on the surface showing relevant geometry for measurements along the face of the cone. See text for explanation.

ϕ_P = angular coordinate of the point, p, radians

x_P = x-coordinate of the point p1 on Cartesian axes

y_P = y-coordinate of the point p1 on Cartesian axes

y_B = y-coordinate of the point on the circle C_B corresponding to x_P

r_A and r_B = radii of the circles C_A and C_B respectively.

α_B = angle of inclination of the tier (cone) corresponding to the circle C_B

Δr = distance along the radius r_B corresponding to a shift z' down the face of the tier. Using trigonometry $\Delta r = z\sin\alpha_B$

h = vertical distance corresponding to a shift z' down the face of the tier. Using trigonometry $h = z\cos\alpha_B$

When viewed from directly above, our model colonies appear as a set of concentric circles (Figure B.3.1). A point on the colony surface can only be shaded by other positions along its own tier, or by the tier immediately above it. The objective is to find the y-coordinate of the edge/s of the relevant cone/s that correspond/s to the point on the surface because the y-axis corresponds to the path of the sun across the sky and these coordinates therefore allow the range of unshaded angles to be calculated.

The concentric circles (C_A and C_B) can be described in Euclidean coordinates using the general equation of a circle centered at 0,0 (i.e. the apex of all nested cones falls at 0,0) given the appropriate radii (r_A and r_B), as:

$$C_A = x^2 + y^2 - r_A{}^2 \text{ and } C_B = x^2 + y^2 - r_B{}^2 \qquad\qquad \text{Eqn B.3.11}$$

The point p_1 has distance z' from the edge of the lower tier (outer circle in Figure B.3.1A). Given the angle of this tier (α_B), the distances in the horizontal and vertical planes (Δr and h respectively, see Figure B.3.1B) corresponding to the distance z' are given by:

$$\Delta r = z'\ \sin\alpha_B \text{ and } h = z'\ \cos\alpha_B \qquad\qquad \text{Eqn B.3.12}$$

If Δr is less than the difference between the radii of the two tiers (e.g. p1 in Figure B.3.1A) then the point can receive direct light from within a range of angles that depends upon the distances in the direction of the path of the sun (y-axis) between the point and the rim of the shading tier/s of the colony. The following calculations apply for points where $\Delta r < (r_B - r_A)$. Note that this condition applies for all points on the uppermost tier of the colony.

From basic trigonometry of a right-angled triangle, given the horizontal angle of the point p_1 (ϕ_{p1}), the x and y coordinates of p_1 are:

$$x_P = (r_B - \Delta r)\cos\phi_{p1} \quad \text{and } y_P = (r_B - \Delta r)\sin\phi_{p1} \qquad \text{Eqn B.3.13}$$

If the distance x_P is greater than the radius of the upper tier ($x_P > r_A$), p1 is not shaded by the upper tier (C_A) and can only be shaded by the curvature of its own tier (C_B). In this case, to determine the range of un-shaded angles for the point we require the (positive) y-coordinate (y_B) of the circle C_B corresponding to the x-coordinate of p_1 (see Figure B.3.2A). This can be found by solving Eqn B.3.11 for y given the values for x_P and r_B. Therefore, we have:

$$y_B = \left| \sqrt{r_B{}^2 - x_P{}^2} \right| \qquad\qquad \text{Eqn B.3.14}$$

If the distance x_P is smaller than the radius of the upper tier ($x_P < r_A$), then the point is also shaded by the upper tier (Figure B.3.2B). In this case, the y-coordinate (y_A) of

the upper tier (C_A) is also calculated by modifying Eqn B.3.14 using the equation for

the circle C_A in place of C_B.

$$y_A = \left| \sqrt{r_A{}^2 - x_P{}^2} \right|$$ \hfill Eqn B.3.15

Once these y-coordinates are known we have two side lengths for each of two

right-angled triangles (h and the lengths calculated from the y-coordinates) and can

therefore use trigonometry to resolve the angles (γ_1 and γ_2) within the triangles (see

Figure B.3.2). These angles are the angular limits for interception of direct light

($\theta_{p(MIN)}$ and $\theta_{p(MAX)}$), and are calculated for the two cases above as:

$$\gamma_1 = \arctan\left(\frac{y_B - y_P}{h} \right) \qquad \gamma_2 = \arctan\left(\frac{y_B + y_P}{h} \right) \quad \Delta r < (r_B - r_A), \text{ for } x > r_A \quad \text{Eqn B.3.16}$$

$$\gamma_1 = \arctan\left(\frac{y_B - y_P}{h} \right) \qquad \gamma_2 = \arctan\left(\frac{y_P - y_A}{h} \right) \quad \Delta r < (r_B - r_A), \text{ for } x < r_A \quad \text{Eqn B.3.17}$$

The final possibility for shading of direct light occurs if Δr is greater than the

difference between the radii of the two tiers and the point moves below the rim of the

upper tier (e.g. p_2 in Figure B.3.1A). In these cases, the point is shaded by both the

upper and lower tier and only angles to the east of the point can illuminate the point

(Figure B.3.2C). In this final case, the angular range for interception of direct light

becomes:

$$\gamma_1 = \arctan\left(\frac{y_B - y_P}{h} \right) \qquad \gamma_2 = \arctan\left(\frac{y_A - y_P}{h} \right) \quad \Delta r > (r_B - r_A) \hfill \text{Eqn B.3.18}$$

Figure B.3.2: Range of angles from which direct light can approach points on the surface of model colonies showing differences in equations defining angular limits for the three possible cases. In each case the geometry is shown from above (circles) and in cross-section (triangles), and the geometric conditions for each case are given. A) The point (p) is only shaded by the curvature of its own tier, B) the point (p) is shaded by its own tier and the upper tier, and C) the point (p) is shaded by both the upper and lower tier but only angles to the left of the point are possible. Terms are defined in text.
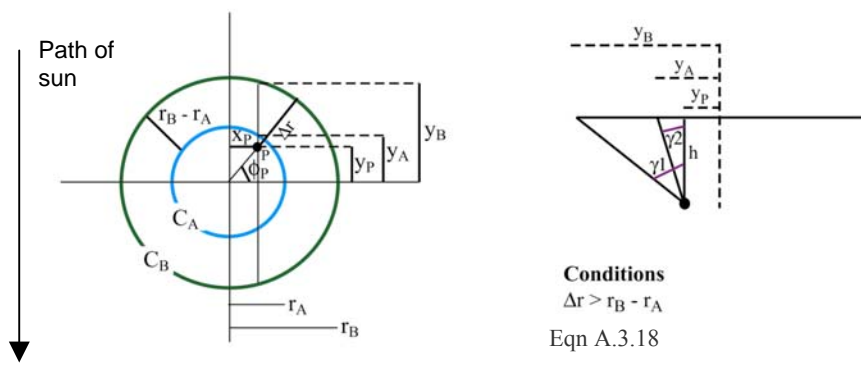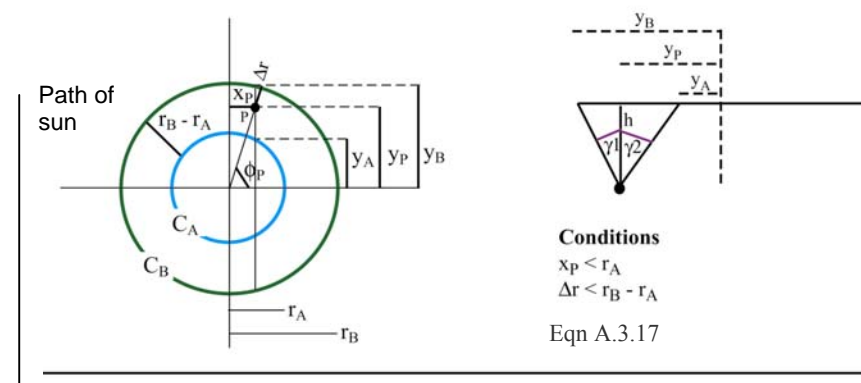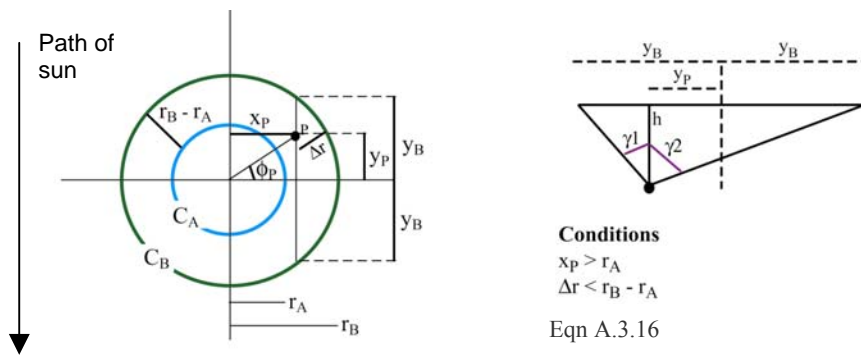
B.4 Intensity of scattered irradiance

As outlined in B.2, total scattered irradiance is equal to the integral of scattered radiance (intensity of scattered light per unit solid angle) over all angles of incidence, multiplied by the cosine of each angle. In this section, I define the range of angles over which scattered light can approach points on the surface of our model colonies. My general approach is to position a hypothetical hemisphere (with a total range of vertical angles, θ_S, between 0 and $\pi/2$ radians and a corresponding range of horizontal angles, ϕ_S, between 0 and 2π radians) over each point on the colony surface with its central axis along the normal to the point. I then calculate the angular ranges in both the vertical (θ_S) and horizontal (ϕ_S) directions that are not obstructed by either the upper or lower tiers. Because the ϕ_S range depends on the value of θ_S I calculate the range of vertical angles first. I first present equations relating to the uppermost tier of the colony, and then describe how those equations are modified for lower tiers. Because of the assumption of a diffuse scattered light field, scattered irradiance only varies from tier edge to center and is independent of horizontal position around the tier circumference. In addition, due to the construction of model colonies with equal angular spacing between tiers, scattered irradiance does not vary between tiers of the colony (except for the uppermost tier), because points that are the same distance from the tier edge on all lower tiers see the same sized 'window' of the total scattered irradiance field.

Uppermost tier

For each point on the upper tier of model colonies the un-shaded vertical angles range between the side of the tier and a line joining the point of interest to the opposite edge of the tier. Using trigonometry, the vertical line joining a point at

distance z' from the edge of the tier to the top face of the tier has length h = z'cos

α_A (where α_A is the angle of inclination of the tier, Figure B.4.1). This vertical line

makes a right-angled triangle with the side of the tier which has width r_α = z'sin α_A.

The distance (r_β) from the vertical line to the opposite edge of the tier can then be

calculated as the diameter of the tier ($2r_A$) minus the width r_α, and the angle between

the vertical line and a line joining the point of interest to the opposite edge of the tier

to be calculated from trigonometry as β = atan[($2r_A - r_\alpha$)/h]. Measured from the side

of the tier, the maximum angle through which scattered light can approach the point

is then equal to $\beta + \alpha_A$. Measured from normal to the surface, this angle becomes ε =

($\beta + \alpha_A - \pi/2$) and the range of vertical angles is [$\varepsilon > \theta_S > \pi/2$]. If ε is greater than 0

then the normal to the surface does not intercept the opposite edge of the tier and for

angles between 0 and ε, the range of horizontal angles ϕ_S is equal to 2π (360°). That

is, a line an angle between 0 and ε to the normal can rotate full circle without

encountering the sides of the tier (dashed ellipse in Figure B.4.1). For angles between

ε and $\pi/2$ (given the symbol κ) a line rotated in the same way will strike the sides of

the tier (dotted ellipse in Figure B.4.1). The range of horizontal angles corresponding

to each vertical angle can therefore be identified by determining the points of

intersection between lines at known angles within this range and the circle marking

the top face of the tier.

I then set the radius of the scattered light hemisphere equal to the length of

the line joining the point of interest to the opposite edge of the tier, with this length

found from the Pythagorean theorem as $h_N = (h^2 + r_\beta^2)^{0.5}$. Because the radius of the

scattered light hemisphere is known, the radius (d_κ) of any circle at angle κ to the

normal can be calculated from trigonometry as d_κ = $h_\beta$sinκ. Similarly, the height (h_κ)

along the normal to the surface where the line d_κ intercepts the normal is equal to $h_\kappa = h_\beta \cos\kappa$.

There are three possibilities as to where the rotation of d_κ about the normal is blocked/shaded (see Figure B.4.2), each of which requires a modification to the calculation of the range of horizontal angles. Firstly, d_κ may rotate past the normal until it reaches the plane at the top of the tier (Figure B.4.2A). Secondly, d_κ may rotate to precisely where the normal to the surface intercepts the top face of the tier (Figure B.4.2B), and thirdly, d_κ may encounter the plane at the top of the tier before it rotates to the normal (Figure B.4.2C). To determine which of these cases applies for each angle κ, I calculate the length of the line joining the point where d_κ intercepts the normal to the point where d_κ intercepts the top face of the tier, and determine whether the intercept of d_κ with the normal is above or below the top of the tier. To do this, I first define a right-angled triangle formed by the line h_κ, a line running along the side of the tier, and a line running parallel to the top of the tier (Figure A2.4.3A and B). This triangle has an inner angle equal to $(\pi/2 - \alpha_A)$, allowing the remaining side lengths to be calculated as $x_\kappa = h_\kappa / \sin(\pi/2 - \alpha_A)$ and $z_\kappa = (h_\kappa^2 - x_\kappa^2)^{0.5}$.

Because d_κ is parallel to z_κ, the distance between the top face of the cone and the point where d_κ intercepts the normal is equal to $d_{diff} = z' - z_\kappa$. Secondly, because x_κ is parallel to the top face of the cone, the length x_κ also measures the horizontal distance between the edge of the cone and the point where d_κ/d_{diff} intercept the top face of the cone. If d_{diff} is negative d_κ intercepts the normal before the top face of the tier and the range of ϕ_S is greater than π ($>180°$). If d_{diff} is equal to zero then the range of $\phi_S = \pi$, and if d_{diff} is positive then d_κ cannot rotate to the normal and $\phi_S < \pi$.

Figure B.4.1: Diagram showing the potential hemisphere of angles through which scattered light can approach a point on the surface and identifying the range of un-shaded vertical angles.
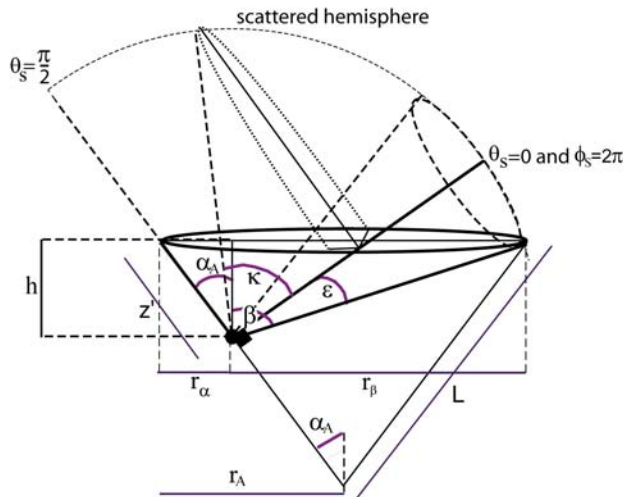
α_A = angle of inclination of the tier

z' = distance between point and edge of tier.

L = side-length of the tier

h = vertical distance between point and top face of tier, $h = z'\cos\alpha_A$

r_A = Tier radius, from trigonometry $r_A = L\sin\alpha_A$

r_α = distance between vertical line joining point to the top face of the tier and the adjacent side of the cone, from trigonometry $r_\alpha = z'\sin\alpha_A$

r_β = distance between vertical line joining point to the top face of the cone and the opposite side of the cone, $r_\beta = 2r_A - r_\alpha$

β = maximum vertical angle, from trigonometry $\beta = atan[2r_A - r_\alpha)/h]$

ε = maximum vertical angle measured from normal to the surface $\varepsilon = \alpha_A + \beta - \pi/2$

Figure B.4.2. The three possible intercepts between a circle made by rotating a line at angle κ around the normal and the upper tier of a cone shaped colony. In A) the line d_κ intercepts the normal above the top of the tier and $\phi_S > \pi$. In B) the line d_κ intercepts the normal at the top face of the tier and $\phi_S = \pi$. In C) the line d_κ intercepts the top face of the tier before intercepting the normal and $\phi_S < \pi$.
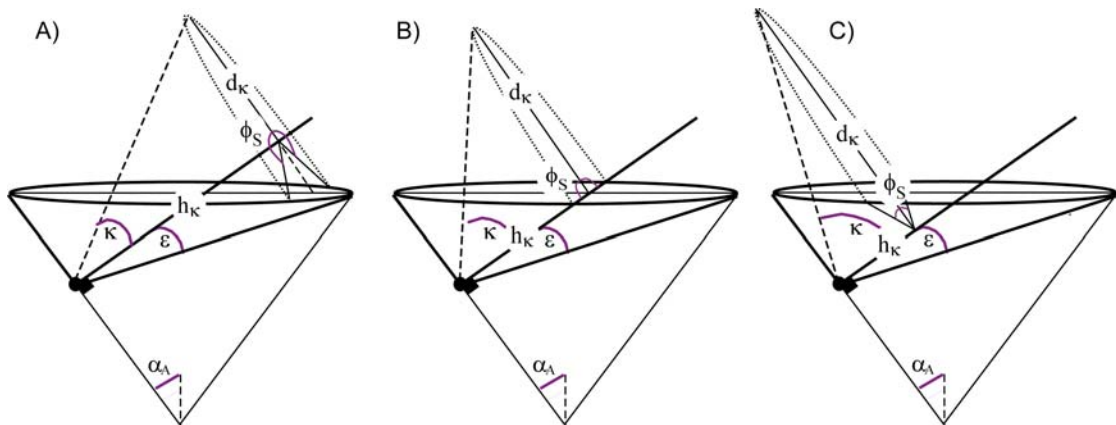
Figure B.4.3. Diagram showing the right-angled triangle used to calculate the distance, d_{diff}, between the intercepts of d_κ with the normal and the top face of the tier. In A) d_κ intercepts the normal above the top of the tier, $z_\kappa > z'$, $d_{diff} < 0$ and therefore $\phi_S > \pi$. In B) d_κ intercepts the top face of the tier before intercepting the normal, $z_\kappa < z'$, $d_{diff} > 0$ and therefore $\phi_S < \pi$. Terms are as defined in text. Panel A and B correspond to panels A and C in Figure B.4.2 respectively.
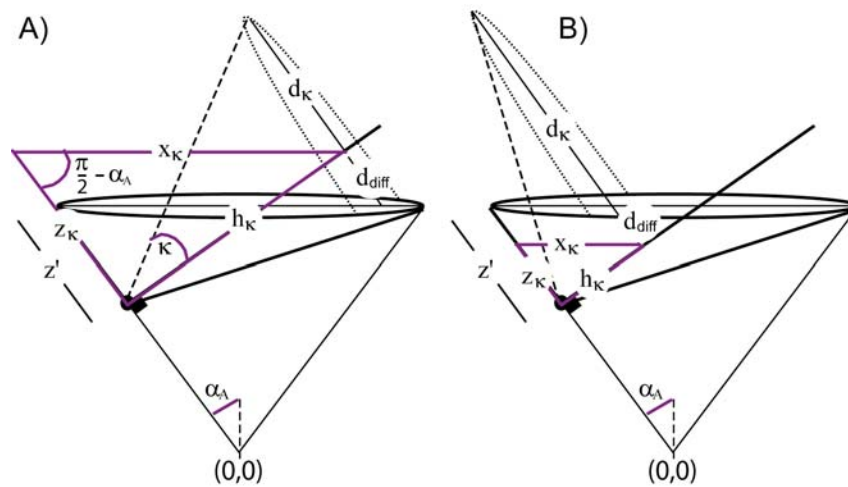
A further complication is that where d_κ encounters the top face of the tier, the range of horizontal angles may be set either by the diameter of the circle made as d_κ (circle C_κ) rotates around the normal or by the width of the tier (Figure B.4.4). That is, the rotation of a line of length d_κ around the normal may be obstructed either by the outer rim of the tier or at some point along the top face of the tier. Because the radius of the tier is known, I allow the circle made by the top rim of the tier to be centered at position (0,0) and use the value of x_κ calculated above to determine the x-coordinate (x_{co}) of the position on this circle where d_κ encounters to top of the tier as $x_{co} = -r_A + x_\kappa$. Substituting the values of x_{co} and r_A into the general equation for a circle (see Eqn. B.3.11) and solving for y gives the y-coordinate (y_κ) on the circle

corresponding to x_{co} and therefore, the width of the circle made by the top rim of the tier at that point. I then compare this value to the horizontal distance (d_C) covered by the line d_κ if it were able to rotate to the top face of the tier. This distance is found from trigonometry by drawing a right-angled triangle with height d_{diff} and hypotenuse d_κ, giving $d_C = (d_\kappa^2 - d_{diff}^2)^{0.5}$. If d_C is greater than y_{co} the rotation of d_κ around the normal is blocked by the rim of the tier (Figure B.4.4A.i and B.i). Conversely, d_κ rotates to the top face of the tier d_C is less than or equal to y_κ (Figure B.4.4A.ii and B.ii). Once these values are known, the range of horizontal angles (ϕ_S) is calculated from the inner angle (ϕ') of right-angled triangles created between d_{diff} and either d_k or y_k. Equations for calculation of ϕ_S under each condition are summarized in Figure B.4.4 below.

Lower tiers

To calculate the angular range from which beams of scattered light may approach a point on the surface of lower tiers of our model colonies, potential shading by both tiers must be taken into account. My calculations follow the same approach as for the upper tier except that there are additional possibilities as to which part of the colony blocks the rotation of a line at some vertical angle around the normal. In addition, the calculation of the range of vertical angles is modified to take the position of the upper tier into account (Figure B.4.5).

Figure B.4.4: Diagram showing the calculation of the range of horizontal angles (ϕ_S) corresponding to vertical angles (θ_S) between ε and $\pi/2$. Panels A and B correspond to panels A and B in Figure B.4.3 and terms are as defined in text. In both panels the rotation of d_κ around the normal may be blocked either at the rim of the tier (A.i and B.i if $y_\kappa < dC$) or at the top face of the tier (A.ii and B.ii if $y_\kappa > d_C$).

L – tier length

z' = distance between point and edge of tier

α_A = tier angle of inclination

r_A = tier radius ($r_A = L\sin\alpha_A$)

κ = vertical angle for which horizontal angle (ϕ_S) is calculated

h_N = radius of scattered light hemisphere (see text)

d_κ = radius of circle formed by rotating a line at angle k around the normal ($d_\kappa = h_N\sin\kappa$)

h_κ = distance between point and position where d_κ intercepts the normal ($h_\kappa = h_N\cos\kappa$)

x_κ and z_κ = sides in right-angle triangle formed with h_κ. $x_\kappa = h_\kappa\sin(\pi/2 - \alpha_A)$, and $z_\kappa = (x_\kappa^2 - h_\kappa^2)^{0.5}$

d_{diff} = distance between intercepts of d_κ with the normal and with the top face of the tier ($d_{diff} = z_\kappa - z'$)

x_{co} = x-coordinate of intercept between d_κ and top face of tier ($x_{co} = -r_A + x_\kappa$)

y_κ = y-coordinate corresponding to x_{co} ($y_\kappa = (r_A^2 - x_{co}^2)^{0.5}$)

d_C = horizontal distance corresponding to decrease in height over the length of d_κ ($d_C = (d_\kappa^2 - d_{diff}^2)^{0.5}$)

if $d_{diff} < 0$ and $d_C \geq y_\kappa$: $\phi' = \text{atan}(y_\kappa/d_{diff})$, $\phi_S = 2(\pi - \phi')$ (Ai)

if $d_{diff} < 0$ and $d_C < y_\kappa$: $\phi' = \text{acos}(d_{diff}/d_\kappa)$, $\phi_S = 2(\pi - \phi')$ (Aii)

In the above 2 conditions the absolute value of d_{diff} is used.

if $d_{diff} = 0$: $\phi_S = \pi$ (Figure B.4.2B)

if $d_{diff} > 0$ and $d_C \geq y_\kappa$: $\phi' = \text{atan}(y_\kappa/d_{diff})$, $\phi_S = 2\phi'$ (Bi)

if $d_{diff} > 0$ and $d_C < y_\kappa$: $\phi' = \text{acos}(d_{diff}/d_\kappa)$, $\phi_S = 2\phi'$ (Bii)

Figure B.4.5: Cross-section view of the upper two tiers of a model colony showing relevant radii and angles. B and C are enlarged diagrams of triangles within panel A.
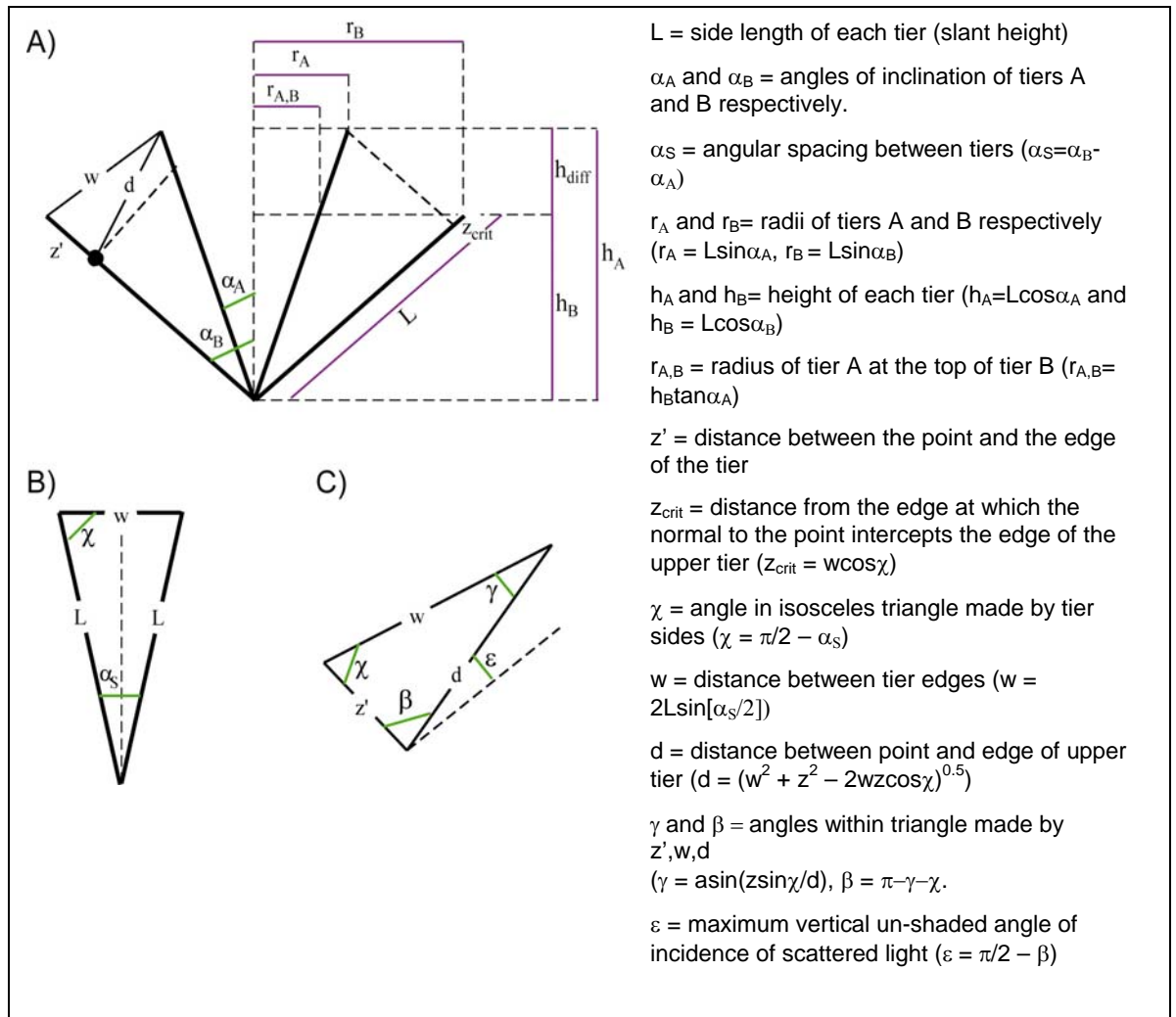
For points on the surface of the lower tiers, the maximum un-shaded vertical angle (ϵ) is calculated from the triangle formed by the distance between the point and the edge of the tier (z'), the line joining the point to the edge of the upper tier (d) and a line joining the edges of both tiers (w, Figure B.4.5A). The length w is calculated using trigonometry based on the isosceles triangle formed by the sides of both tiers that are inclined at angle $\alpha_S = (\alpha_B - \alpha_A)$ to each other, and the second inner angle of this triangle is found as $\chi = \pi/2 - \alpha_S$ (Figure B.4.5B). The length d is subsequently found using the rule of cosines as $d = (w^2 + z'^2 - 2wz\cos\chi)^{0.5}$. This allows the angle, β, between the side of the tier and the line joining the point to the edge of the upper

tier, and the angle ε to be calculated as $\varepsilon = \pi/2 - \beta$ (Figure B.4.5C). As for the upper

tier of the colony, if the value of ε is positive then the range of horizontal angles (ϕ_S)

is equal to 2π for vertical angles between 0 and ε. For vertical angles within the

range ε to $\pi/2$, the range of horizontal angles is restricted due to shading by either the

upper or lower tiers. To calculate this range for points on the lower tiers I set the

radius of the scattered light hemisphere equal to d (instead of h_β for the upper tier)

and calculate the values of d_κ, h_κ, z_κ, $x_{co,}$ d_{diff} and d_C exactly as for the upper tier, and

the value of y_κ using the same method as for the upper tier except using the radius of

the lower tier (r_B in place of r_A for the upper tier).

If the value of ε is positive, there are 8 possibilities as to which part of the

upper/lower tier obstructs the rotation of d_κ around the normal. Firstly, if d_{diff} is

positive or equal to zero (conditions 1 & 2) the rotation of d_κ is blocked at the top

face of the lower tier and the same equations as for the upper tier are used to

calculate ϕ_S. If d_{diff} is negative however (condition 3), the range of horizontal angles

may be set either by the top face of the lower tier, or by the radius of the upper tier at

some height above the top of the lower tier. Which one of these conditions applies

depends on the relative sizes of d_C, y_κ and the radius of the upper tier at the height

where d_κ intercepts it, and also on whether the value of x_{co} is positive or negative.

For small vertical angles, d_κ may be less than the radius of the upper tier at the height

where d_κ intercepts the normal to the point (condition 4). I calculate this height using

the right-angled triangle formed by $d_{diff,}$ the top face of the tier and a vertical line

joining the top face of the tier to the point where d_κ intercepts the normal (Figure

B.4.6A). This triangle has an inner angle α_B, allowing the distance between the top

of the lower tier and the intercept of d_κ with the normal to be calculated as $h'_\kappa =$

$|d_{diff}|\cos\alpha_B$. The corresponding height on the upper tier is then given by $h'_{A,\kappa} = h_B + h'_\kappa$ and the radius of the upper tier at this height is given by $r'_{A,\kappa} = h'_{A,\kappa}\tan\alpha_A$ (see Figure B.4.6A.i). If d_κ is less than or equal to $r_{A,\kappa}$ then d_κ may rotate past the normal to the line joining the point of interest to the edge of the upper tier, and the range of horizontal angles is calculated from $\phi' = a\sin(d_\varepsilon/d_\kappa)$ where $d_\varepsilon = h_\kappa\tan\varepsilon$ as $\phi_S = \pi+2\phi'$ (A.ii and A.iii of Figure B.4.6). The next possibility is that d_κ is greater than $r_{A,\kappa}$ but less than the magnitude of the length d_{diff}. In this case d_κ is shaded by the upper tier at some height between where d_κ intercepts the normal and the top face of the lower tier (d_κ cannot intercept the lower tier because $d_\kappa < d_{diff}$). The height on the upper tier at which this shading occurs depends on whether the x-coordinate (x_{co}) of the intercept between d_κ and the top face of the lower tier is positive or negative. If x_{co} is negative (condition 5, Figure B.4.6B), the height on the upper tier ($h'_{A,\kappa}$) is set by the decrease in height over the length of d_κ ($h' = d_\kappa\cos\alpha_B$, Figure B.4.6Bii) and $h'_{A,\kappa}$ is given by $h'_{A,\kappa} = h_B + (h'_\kappa - h')$. The radius of the upper tier at this height is recalculated as $r_{A,X} = h'_{A,\kappa}\tan\alpha_A$ and the range of horizontal angles is calculated from the isosceles triangle formed by d_κ and $r_{A,X}$ with $\phi' = a\sin(r_{A,X}/d_\kappa)$ and $\phi_S = 2(\pi - \phi')$ (Figure B.4.6Biii). If x_{co} is positive (Figure B.4.6C), the relevant height on the upper tier is calculated differently and also depends on whether d_κ extends past the central axis of the upper tier. I first calculate the height on the upper tier where d_{diff} intercepts the central axis (Figure B.4.6Ciii) as $h_2' = x_{co}\tan(\pi/2-\alpha_B)$ and use this height to calculate the distances along d_{diff} between the intercepts with the central axis of the upper tier and the top face of the lower tier ($d_A = [x_{co}^2 + h_2'^2]^{0.5}$, Figure B.4.6Ciii) and between the intercepts with the normal and the central axis of the upper tier ($d_{new} = d_{diff}-d_A$, Figure B.4.6Ciii).

Figure B.4.6: Diagram showing relevant angles and triangle lengths for calculation of range of horizontal angles for vertical angles between ε and π/2 for cases where $d_{diff} < 0$ and ε is positive. In A) the length d_κ is less than the radius of the upper tier at the height where d_κ intercepts the normal to the point. In B) d_κ is greater than the above radius but less than d_{diff} and the x-coordinate of the intercept of d_{diff} with the top face of the lower tier is negative. In C) the same conditions as in B are true except the x-coordinate is positive. Terms are defined in text.
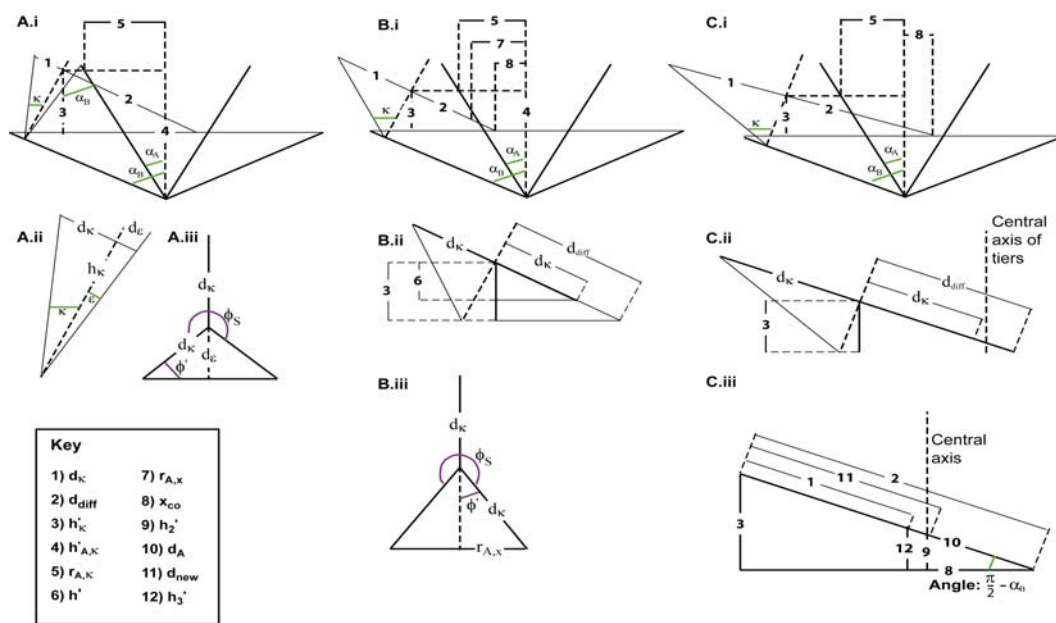
If d_κ is greater than or equal to d_{new} (condition 6) then the range of horizontal angles is set by the isosceles triangle formed by the radius of the upper tier corresponding to $h_2{}'$ and the side length of d_κ. If d_κ is less than d_{new} (condition 7) then the height on the upper tier is set by the decrease in height over the length of d_κ (as for condition 5) with this height calculated as $h_3{}' = |d_{diff}| - d_\kappa/\sin(\pi/2 - \alpha_B)$ (Figure B.4.6Ciii). For conditions 5, 6 and 7, the range of horizontal angles is calculated using exactly the same equations, the only difference is the value of the radius of the upper tier which sets the base-length of the isosceles triangle from which ϕ_S is

calculated. The final possibility (condition 8) occurs when d_κ is greater than the magnitude of d_{diff}. In this case, d_κ rotates to the top face of the (i.e. is not shaded by the upper tier), and the range of horizontal angles is calculated using the same procedure as for condition 1 & 2 (and for the upper tier when d_{diff} is negative).

For positions on the lower tiers where the value of ε is negative (i.e. the normal to the surface intercepts the side of the upper tier) condition 4 must be modified. Where this occurs, the rotation of d_κ is shaded by the radius of the upper tier not at the height where d_κ intercepts the normal (line 1 in Figure B.4.7) but instead at the height where d_κ intercepts a normal to the side of the tier that is tangent to the edge of the upper tier (Figure B.4.7). To determine the magnitude of this radius I first calculate the decrease in height (h'_c, Figure B.4.7 line 6) over the distance covered by z_{crit} (Figure B.4.7 line 5) where z_{crit} is as defined in Figure B.4.5 as $h'_c = z_{crit}\sin(\pi/2 - \alpha_B)$. I also calculate the heights corresponding to the distances d_κ and d_{diff} as $h'_\kappa = d_\kappa\cos\alpha_B$ and $h'_{diff} = |d_{diff}|\cos\alpha_B$ (Figure B.4.7 lines 7 and 8). The height on the upper tier ($h_{A,x}$) corresponding to the intercept of d_κ with the normal at z_{crit} is then given by $h_{A,x} = h_B + h'_{diff} + (h'_\kappa - h'_c)$ and the radius calculated as $r_{A,x} = h_{A,x}\tan\alpha_A$ as previously. If d_κ is less than or equal to $r_{A,x}$ then the range of horizontal angles is determined from $\phi' = \mathrm{acos}([z'-z_{crit}]/d_\kappa)$ as $\phi_S = 2\phi'$ (see Figure B.4.7B).

Figure B.4.7: Diagram showing modification of condition 4 (above) for cases where e < 0. Terms are defined in text.
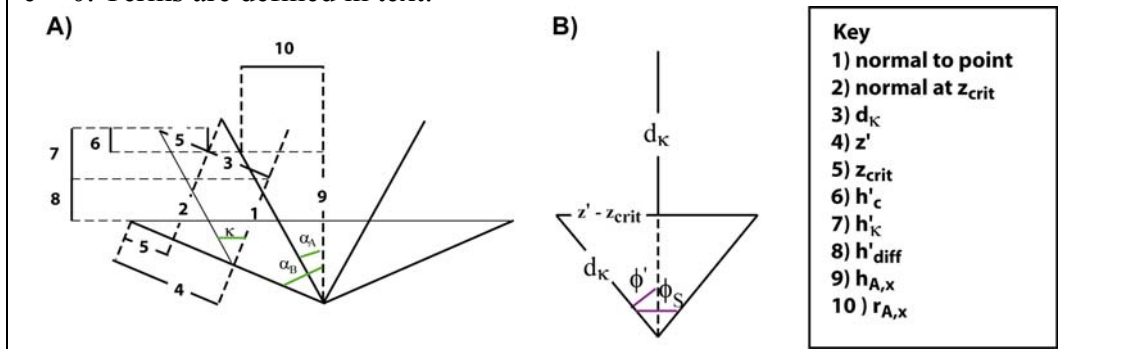
Table B.4.1: Summary of the range of horizontal angles from which scattered light can approach points on the lower tiers of model colonies. These ranges comprise the integral limits for the scattered irradiance equation (Eqn B.2.2). ϕ_S represents the upper bound of the range of horizontal angles which has lower bound at 0 in all cases.

Condition 1	Additional conditions	Horizontal angle range (ϕ_S)	Figure
$\varepsilon > 0$	$0 < \theta < \varepsilon$ $\varepsilon < \theta < \pi/2$	$\phi_S = 2\pi$	Same as upper tier
$\varepsilon > 0 \,\&\, \varepsilon < 0$	$d_{diff} > 0$	if $d_C \geq y_\kappa$ then $\phi' = \mathrm{atan}(y_\kappa/d_{diff})$ and $\phi_S = 2\phi'$	Same as upper tier
		if $d_C < y_\kappa$ then $\phi' = \mathrm{acos}(d_{diff}/d_\kappa)$ and $\phi_S = 2\phi'$	Same as upper tier
$\varepsilon > 0 \,\&\, \varepsilon < 0$	$d_{diff} = 0$	$\phi_S = \pi$	Same as upper tier
$\varepsilon > 0$	$d_{diff} < 0$	if $d_\kappa < r_{A,\kappa}$ then $\phi' = \mathrm{asin}(d\varepsilon/d_\kappa)$ and $\phi_S = \pi + 2\phi'$	A.4.6A
		if $d_{diff} > d_\kappa > r_{A,\kappa}$ and $x_{co} < 0$	A.4.6B
		$\quad \phi' = \mathrm{asin}(r_{A,\kappa}/d_\kappa)$ and $\phi_S = 2(\pi - \phi')$ $\quad$ with $r_{A,\kappa}$ calculated from h'	
		if $d_{diff} > d_\kappa > r_{A,\kappa}$ and $x_{co} > 0$ and $d_\kappa > d_{new}$	A.4.6C
		$\quad \phi' = \mathrm{asin}(r_{A,\kappa}/d_\kappa)$ and $\phi_S = 2(\pi - \phi')$ $\quad$ with $r_{A,\kappa}$ calculated from h_2'	
		if $d_{diff} > d_\kappa > r_{A,\kappa}$ and $x_{co} > 0$ and $d_\kappa < d_{new}$	A.4.6C
		$\quad \phi' = \mathrm{asin}(r_{A,\kappa}/d_\kappa)$ and $\phi_S = 2(\pi - \phi')$ $\quad$ with $r_{A,\kappa}$ calculated from h_3'	
$\varepsilon > 0 \,\&\, \varepsilon < 0$		if $d_\kappa > d_{diff}$ and $d_C \geq y_\kappa$, $\phi' = \mathrm{atan}(y_\kappa/|d_{diff}|)$ and $\phi_S = 2(\pi - \phi')$	Same as upper tier
$\varepsilon > 0 \,\&\, \varepsilon < 0$		if $d_\kappa > d_{diff}$ and $d_C < y_\kappa$, $\phi' = \mathrm{acos}(|d_{diff}|/d_\kappa)$ and $\phi_S = 2(\pi - \phi')$	Same as upper tier
$\varepsilon < 0$	$d_{diff} < 0$		A.4.7 A.4.6B
		if $d_\kappa < r_{A,X}$ then $\phi' = \mathrm{acos}([z'-z_c]/d_\kappa)$ and $\phi_S = 2\phi'$	
		if $d_{diff} > d_\kappa > r_{A,X}$ and $x_{co} < 0$	A.4.6C
		$\quad \phi' = \mathrm{asin}(r_{A,X}/d_\kappa)$ and $\phi_S = 2(\pi - \phi')$ $\quad$ with $r_{A,X}$ calculated from h'	
		if $d_{diff} > d_\kappa > r_{A,X}$ and $x_{co} > 0$ and $d_\kappa > d_{new}$	A.4.6C
		$\quad \phi' = \mathrm{asin}(r_{A,X}/d_\kappa)$ and $\phi_S = 2(\pi - \phi')$ $\quad$ with $r_{A,X}$ calculated from h_2'	
		if $d_{diff} > d_\kappa > r_{A,X}$ and $x_{co} > 0$ and $d_\kappa < d_{new}$	
		$\quad \phi' = \mathrm{asin}(r_{A,X}/d_\kappa)$ and $\phi_S = 2(\pi - \phi')$ $\quad$ with $r_{A,X}$ calculated from h_3'	

B.5 Surface area of segments of the colony surface

Colony surface area can be found using a multiple integration technique based on the component equations of a conical surface (as per Appendix B.3). In summary, the magnitude of the vector perpendicular to the surface is integrated over the three-dimensional range of the surface. In the case of a cone, the three-dimensional range of the surface is defined by the length of the side of the cone and the circle formed by the top of the cone.

The general formula for surface area for a surface expressed by component equations *X(t,u)* over a region *R*, when calculated in this way is:

$$S = \iint_R \left| \frac{\partial X}{\partial t} \times \frac{\partial X}{\partial u} \right| dt\,du \qquad \text{Eqn B.5.1}$$

where, $\left| \dfrac{\partial X}{\partial t} \times \dfrac{\partial X}{\partial u} \right|$ represents the magnitude (length) of the normal vector as found by the cross product of the two tangent vectors (see Appendix B.3, Eqn B.3.4 and Eqn B.3.5).

$$\left| \tilde{n} \right| = l \sin \alpha \qquad \text{Eqn B.5.2}$$

Here, the component equations are functions of L (colony side length), ϕ (horizontal angle) and α (angle of inclination of the cone). The surface area integral becomes:

$$S = \int_{\phi \min}^{\phi \max} \int_{l(\min)}^{l(\max)} l \sin \alpha \; dl \; d\phi \qquad \text{Eqn B.5.3}$$

This expression can be evaluated over any section of the ranges $0 < \phi < 2\pi$ and $0 < x < L$ to find the area of any portion of the surface of a cone of known angle α.

Literature cited

Falkowski P.G. & J.A. Raven. 1997. Aquatic photosynthesis. Blackwell Science, Massachusetts.

Lang, S. 1979. Calculus of several variables. Addison-Wesley, Massachusetts, pp 479.

Mobley, C.D. 1994. Light and water: Radiative transfer in natural waters. Academic Press, San Diego, pp 592.

Smith, R. C and W. H. Wilson. 1977. Photon scalar irradiance. <u>In</u> J. E. Tyler (Ed.) Light in the Sea, Benchmark Papers in Optics volume 3, pp 312-316. Dowden Hutchinson & Ross, Pennsylvania.

APPENDIX C: DIAGRAM OF FLOW CHAMBERS

Figure C.1: Diagram of flow chambers used for respirometry measurements.
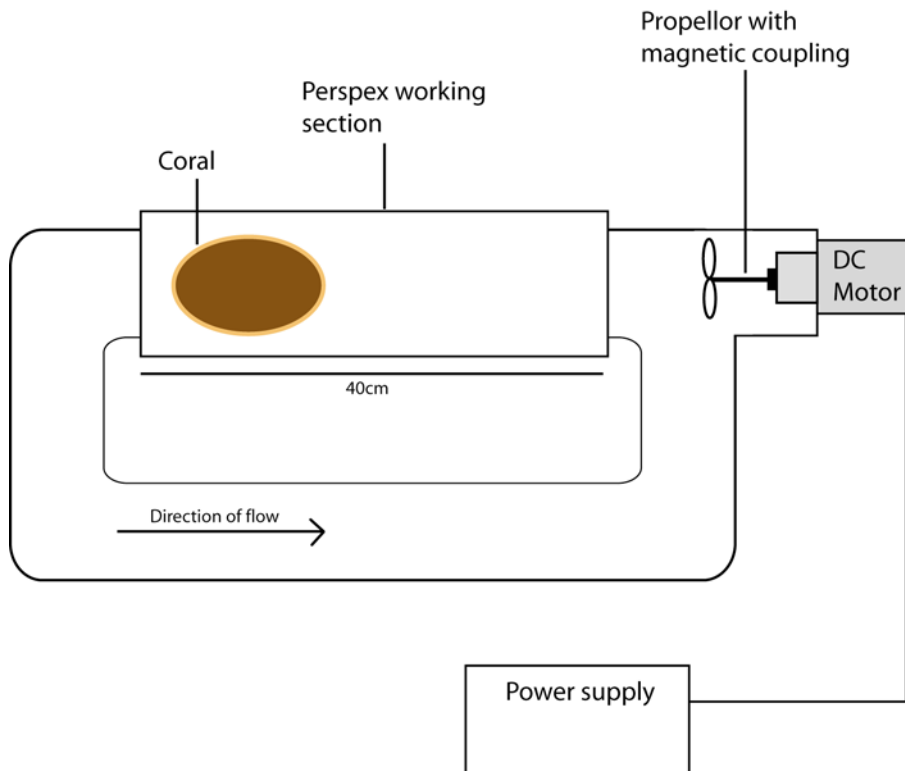
APPENDIX D: CHAMBER FLOW VELOCITY & TURBULENCE

For each chamber, and at each power setting, two-dimensional flow velocity was measured by particle tracking, using small, wooden beads as neutrally buoyant particles. To do this, multiple series' of still images were captured from video footage of particles circulating within chambers. These images were overlaid in a time series, and the distance moved by particles in horizontal (x) and vertical (y) directions over a known period of time was calculated using Image Tools software (UTHSCA, version 2). We first calculated the components of flow velocity in x- and y-directions ($\bar{x}$ and $\bar{y}$), and then calculated average flow velocity ($\bar{u}$, cm s^{-1}) from the linear distance between successive x- and y-coordinates of particles, as $\bar{u} = (\bar{x}^2 + \bar{y}^2)^{0.5}$. To account for any difference in water turbulence between our two flow chambers, we also calculated turbulence intensity, τ (dimensionless) for each flow speed as $\tau = q/\bar{u}$ where q is the root mean square of flow velocity in each of the component directions ($q = \frac{1}{2}(\bar{x}^2 + \bar{y}^2)^{0.5}$, after Falter et al. 2007). Flow within both of our chambers was uniformly turbulent across flow speeds and turbulence has therefore been excluded as a variable in our analyses (see Table B.1 below).

Table D.1: Average flow velocity (U) and turbulence intensity (τ) within respirometry chambers. U is found as the linear distance corresponding to the movement of 50 – 62 (n) particles in horizontal (x) and vertical (y) directions during a known period of time. τ is the ratio of the root mean square of two-dimensional velocity to average particle velocity (U). Values of τ lie between a minimum of 0.5 (precisely horizontal or vertical movement), and a maximum of 0.71 (equal movement in x- and y-directions).

Measurements	Volume (l)	Power setting (n)	U (cm s^{-1}, ± s.e.)	x (cm s^{-1}, ± s.e.)	y (cm s^{-1}, ± s.e.)	τ
Colony photosynthesis and respiration, broad flow range: • 6 – 38 cm s^{-1}	19.5	1 (51)	5.7 (0.4)	5.2 (0.4)	1.7 (0.2)	0.69
	19.5	2 (56)	10 (0.7)	9.6 (0.7)	2.5 (0.3)	0.68
	19.5	3 (52)	15 (1.0)	14 (1.0)	3.8 (0.4)	0.69
	19.5	4 (61)	30 (2.0)	28 (2.0)	7.1 (0.6)	0.70
	19.5	5 (62)	32 (1.6)	31 (1.6)	7.2 (0.7)	0.70
	19.5	6 (60)	38 (2.8)	36 (2.9)	8.9 (0.7)	0.70
Colony photosynthesis and tissue-level oxygen standing stock for calibration of Sh:Re	10	1 (50)	2.2 (0.1)	2.1 (0.1)	0.3 (0.03)	0.70
	10	2 (54)	4.2 (0.2)	4.0 (0.2)	0.8 (0.1)	0.70
	10	3 (55)	6.1 (0.2)	6.1 (0.2)	0.8 (0.1)	0.70
	10	4 (60)	9.7 (0.7)	9.4 (0.7)	1.5 (0.2)	0.70

Literature cited

Falter, J. L., M. J. Atkinson, R. J. Lowe, S. G. Monismith & J. R. Koseff. 2007. Effects of non-local turbulence on the mass transfer of dissolved species to reef corals. Limnol. Oceanogr., 52: 274-285.

APPENDIX E: REGRESSION ANALYSIS OF EFFECTS OF LIGHT AND FLOW ON BIOMASS & REPRODUCTION.

Table E.1: Regression analyses between tissue properties (total protein and egg number) with irradiance and flow conditions for each of *Acropora nasuta*, *Leptoria phrygia* and *Montipora foliosa*. * denotes statistically significant regression or partial correlation at $\alpha = 0.05$.

Acropora nasuta				
Protein content (mg cm^{-2})	Regression summary: R = 0.10, R^2 = 0.01, F(2,51) = 0.27, p = 0.76			
	β	Std. Error of β	t	p
Light intensity	-0.04	0.14	-0.28	0.79
Flow velocity	0.10	0.14	0.69	0.50
Reproduction (eggs polyp^{-1})	Regression summary: R = 0.16, R^2 = 0.02, F(2,51) = 0.64, p = 0.53			
	β	Std. Error of β	t	p
Light intensity	0.09	0.14	0.67	0.50
Flow velocity	0.12	0.14	0.89	0.38
				6.4.1.1
		6.4.1.2	*Leptoria phrygia*	
Protein content (mg cm^{-2})	Regression summary: R = 0.45, R^2 = 0.20, F(2,51) = 6.6, p < 0.01*			
	β	Std. Error of β	t	p
Light intensity	0.16	0.12	1.31	0.20
Flow velocity	-0.42	0.12	3.36	0.002*
Reproduction (eggs polyp^{-1})	Regression summary: R = 0.27, R^2 = 0.08, F(2,51) = 2.1, p = 0.13			
	β	Std. Error of β	t	p
Light intensity	0.10	0.13	0.76	0.45
Flow velocity	-0.25	0.13	-1.90	0.06
				6.4.1.3
		6.4.1.4	*Montipora foliosa*	
Protein content (mg cm^{-2})	Regression summary: R = 0.33, R^2 = 0.11, F(2,51) = 1.8, p =0.18			
	β	Std. Error of β	t	p
Light intensity	-0.33	0.17	-1.87	0.07
Flow velocity	-0.004	0.17	-0.02	0.98
Reproduction (eggs polyp^{-1})	Regression summary: R = 0.38, R^2 = 0.15, F(2,51) = 2.6, p =0.09			
	β	Std. Error of β	t	p
Light intensity	-0.38	0.17	-2.2	0.03*
Flow velocity	0.15	0.17	0.88	0.39